Design and Control of Supernumerary Robotic Limbs

by

Federico Parietti

B.S., Polytechnic University of Milan (2008)
S.M., Polytechnic University of Milan (2011)

Submitted to the Department of Mechanical Engineering
in partial fulfillment of the requirements for the degree of

Doctor of Philosophy in Mechanical Engineering

at the

MASSACHUSETTS INSTITUTE OF TECHNOLOGY

September 2016

Author ..... Signature redacted

Department of Mechanical Engineering
August 15, 2016

Certified by ..... Signature redacted

H. Harry Asada
Ford Professor of Mechanical Engineering
Thesis Supervisor

Accepted by ..... Signature redacted

Rohan Abeyaratne
Chairman, Department Committee on Graduate Theses

Design and Control of Supernumerary Robotic Limbs

by

Federico Parietti

Submitted to the Department of Mechanical Engineering
on August 15, 2016, in partial fulfillment of the
requirements for the degree of
Doctor of Philosophy in Mechanical Engineering

Abstract

Humans possess the remarkable ability to control their four natural limbs in a voluntary, accurate and independent manner. The simultaneous use of two or more limbs allows humans to learn and robustly perform a wide range of complex tasks. Since the use of multiple limbs enables humans to master advanced motor skills, it would be interesting to study whether having additional limbs would enable users to expand their skill set beyond its natural limits. Inspired by this vision, we propose a new form of human augmentation: a wearable robot that augments its user by providing him with an additional set of robotic limbs. We named this new device Supernumerary Robotic Limbs (SRL). However, humans have never had the possibility to control additional, powered limbs besides their natural arms and legs. The main theme of this thesis, besides realizing a prototype of the robot and proving its usefulness in real-world tasks, is demonstrating that humans can voluntarily control additional limbs as if they were a part of their own body.

We realized a lightweight (3.5 kg), comfortable prototype of the SRL that can be easily worn by an unassisted user. Two robotic limbs can assist the user in both manufacturing and locomotion tasks. We created control strategies that take advantage of the independence of the robotic limbs, enabling them to provide optimal assistance in specific tasks such as weight support, body stabilization, using powered tools, sitting/standing and dynamic walking. Finally, we developed an EMG-based control interface that enables users to voluntarily control the motion of the robotic limbs, without interfering with the posture of the rest of the body. The new augmentation technology presented in this thesis opens up new possibilities in the field of wearable robotics. The voluntary control of additional robotic limbs falls within the range of motor skills that humans can learn, and enables the acquisition of a new set of complex skills that would not be achievable using only the natural body.

Thesis Supervisor: H. Harry Asada
Title: Ford Professor of Mechanical Engineering

Acknowledgments

I would like to thank all of the people who, directly or indirectly, helped me during my doctoral studies. First, I would like to thank Prof. Asada for giving me the opportunity to work on this unique robotics project. Not many advisors have the courage and the vision to pursue research directions that are completely new and original, like this one. Prof. Asada has allowed and enabled me to implement my vision for this thesis, and there is no better thing than working on what you love and believe in.

I would like to thank MIT for giving me the opportunity of pursuing my highest degree. Studying here has always been a dream for me, and I have never nor will ever take it for granted. I still can't believe that I got in, and I hope that I worked hard enough to show everybody - including myself - that I deserved this opportunity.

I would like to thank all of the professors and teaching assistants in the classes that I took here at MIT. The challenges you gave me were always interesting and exciting to solve. From the problem sets to the tests to the Qualifying Exams, it has been a pleasure to fight through every question to prove that I got it. This level of challenge is exactly what I was expecting from an MIT education.

I would like to thank the members of my thesis committee for their support and advice during my doctoral studies. Together with Prof. Asada, they are the faculty members that I admire the most, and it has been a true honor to work with them on this research endeavor. In particular, I would like to thank Prof. Hogan for sharing his knowledge on the neural mechanisms at the base of the control of motion, Prof. Herr for his inspiring vision about the future of human augmentation, and Prof. Geyer for being an exceptional graduate research mentor and for believing in my research before anyone else.

I would like to thank my labmates, from the UROP students to the grad students, from the postdocs to the visiting engineers from Japan, for their incredible support in these years. You made this thesis possible not only with your knowledge and your advice, but also with your constant encouragement. And you also reminded me to

sleep and to go home from time to time, which I tend to forget too often. Your names are too many to be named here, but you already know that you are forever invited at all of my rooftop parties.

I would like to thank my friends in Cambridge and all over the world. Thank you for always being patient and supportive even if I disappeared from any form of communication for weeks at times, when I was working on a new prototype or experiment. I really appreciate what you did for me, and the fact that you always believed in me even if sometimes I didn't do it myself. I would also like to thank my girlfriend for understanding and supporting my vision, even when pursuing it meant working for insane amounts of time in the lab. Thank you for making the time we spend together always special, and for supporting my goals to the point of amplifying them.

I would like to thank my family for teaching me the value of education, and for supporting me in the darkest moments. I always knew that you had my back, even when you were in a different continent. And I know that I have been extremely privileged to be raised in an environment where I always had the luxury of putting my personal goals first, without worrying about anything else.

Finally, I would like to reserve special thanks to all of those who doubted me, or questioned my determination and my objectives. Thank you for providing additional motivation, and moral fuel to keep me awake during the long nights in the lab. I am proud of proving that you were wrong, with this document. And I cannot wait to continue the relentless pursuit of my goals. Enjoy the show, because there's much more to come!

Contents

List of Figures

List of Tables

Chapter 1

Introduction

The Supernumerary Robotic Limbs (SRL) is a novel kind of wearable robot. It augments the user by providing two additional robotic limbs, which can move independently from the natural human limbs. The SRL is worn through a harness, and the robotic limbs are attached to a rigid base that follows the shape of the user's hip. The workspace of the robotic limbs has been designed to allow them to act both as legs (reaching the ground) and as arms (reaching the space in front and above the user). They can also reach areas outside of the workspace of the human limbs (e.g. behind the user). The innovative features of the SRL are suitable for a wide range of applications. Many areas of human activity could benefit from the use of additional limbs, from manufacturing to rehabilitation. The challenge associated with the SRL is that humans are not used to have more than four limbs. They frequently learn to use tools of various complexity, but these tools always clearly separated from their body. The main research question, which will be explored in this doctoral thesis, is how to intuitively and effectively control the Supernumerary Robotic Limbs as if they were a part of the user's body.

One promising field of application for the SRL is the manufacturing of large size, high added-value products, such as planes and ships. These activities require human workers to perform extremely complicated and fatiguing tasks, such as assembling electromechanical systems, drilling holes, inspecting structures. Additionally, workers might also be required to operate on elevated platforms or on scaffolds, which expose

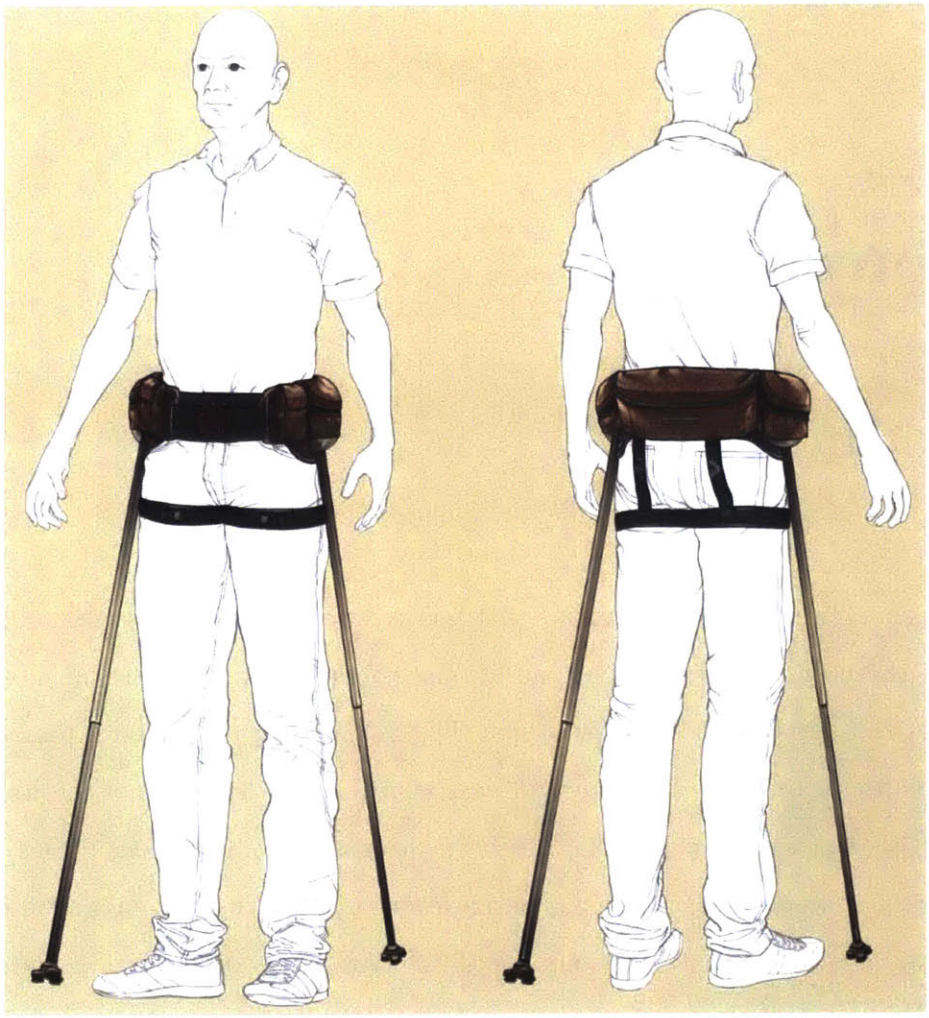

Figure 1-1: Vision for the Supernumerary Robotic Limbs (SRL) as an assistive device for the elderly. The SRL is a wearable robot that extends its user's body with two additional robotic limbs. In this case, the robot is worn above normal clothing and assists the users when walking or sitting down and standing up.

them to the risk of slipping or falling down [12]. If we also consider that specialized workforce has been rapidly aging - the median age in aircraft manufacturing is 48 years - there is a clear opportunity for the use of the SRL as an assistive tool to reduce fatigue and increase safety [58]. The building construction industry presents a similar opportunity, being the area of manufacturing with the most injuries caused by falls [1, 63].

Another area in which the SRL would be useful is mobility assistance for the elderly (Figure 1). The risk of losing balance and falling down is very high for the

population over 80 years old [83], and this demographic is in continuous growth in developed countries [16]. Loss of mobility for the elderly also includes difficulties in safely sitting down or standing up [59]. The conventional tools used to address these problems present significant limitations, and are not suitable for the active lifestyle that senior citizens expect in modern societies (Figure 2). Canes and crutches require the use of one or both arms to be operated, and significant forces must be exerted in order to avoid slips. Walkers are easier to operate but their wheels limit them to flat surfaces, mostly inside buildings. The SRL could be used in this context as an assistive tool that provides balance aid and weight compensation while keeping the user's arms free. The robotic limbs could also assist elderly subjects when sitting down or standing up [38], or as an emergency help in case of slips. Being wearable and not based on wheels, the SRL is able to follow and help users in any situations, including stairs and irregular terrain (streets, parks, etc.). Figure 2 shows how the use of the SRL could address the needs of large numbers of patients who currently can only use simple passive tools for locomotor assistance.

Finally, the field of rehabilitation robotics represents a new and promising research

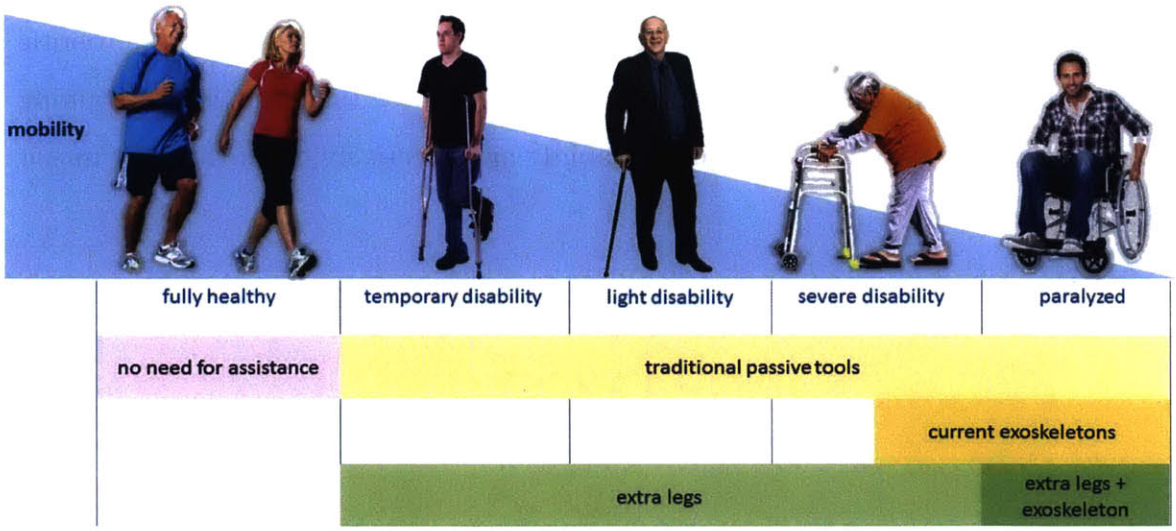

Figure 1-2: The SRL can assist the locomotion of patients that today are forced to use simple passive tools. The figure shows that current wearable robots (exoskeleton, orthoses) can assist only the most severe forms of locomotor impairment. It can also be observed that the combined use of SRL and exoskeletons could simultaneously assist locomotion and free the upper part of the body from the need of using crutches.

direction for the SRL. There is a large number of patients who need mobility assistance as a consequence of leg or spinal cord fractures, walking disabilities or neurological conditions such as strokes, Alzheimer's disease and Parkinson's disease [39, 81, 2]. Existing state-of-the-art wearable exoskeletons can provide these patients with the ability to stand and walk along a nominal gain cycle in the sagittal plane [32, 9, 23, 43, 54]. However, they do not have enough degrees of freedom to assist turning and balance. As a result, they can benefit only subjects who are fit enough to use crutches. The SRL can be used to assist these patients without requiring any arm effort, and leaving their legs free to move and exercise. Moreover, the SRL could provide targeted support along the walking gait, helping the user only when needed or generating forces to correct gait abnormalities.

Together with a wide range of practical applications, the SRL also offers a unique opportunity to study how the neuromuscular control system can adapt to additional limbs, and learn to use them as if they were natural. The ultimate goal of this project is for the SRL to become a natural extension of the human body. In order to achieve this goal, suitable control signals must be identified, measured and robustly employed in the robot control system. These signals must be independent from the motion of the natural limbs, and able to accurately control the motion of the robotic limbs. Since humans are not naturally provided with more than four limbs, training protocols must be developed in order to rapidly and effectively teach this new motor skill to SRL users.

Chapter 2

Voluntary, Independent Control of Extra Limbs

2.1 Introduction

Land-living vertebrates are capable of performing with apparent ease extremely complicated locomotion and manipulation tasks - ranging from flying to digging, from moving objects to modifying the surrounding environment. The simultaneous, coordinated use of multiple limbs is essential to perform such advanced behaviors. These tasks cannot be completed with a sequence of separate actions performed one after the other by a single limb. In animals with particularly evolved neuromuscular control systems - such as mammalians - the ability to simultaneously and voluntarily control independent limbs enables the acquisition of new, complex motor skills. This is particularly evident in humans, who can learn a vast array of coordinated skills that far exceed the capabilities of a single limb. Examples of advanced tasks involving two or more limbs include playing musical instruments, practicing sports, and executing complex locomotion patterns (e.g. climbing, swimming). Natural limbs are the result of evolution, and for humans - like in all tetrapods - their number is limited to four. This limits the complexity of the coordinated tasks that humans can perform. The ability to control additional limbs together with the natural ones would open up new possibilities, enabling the learning and execution of more advanced locomotion and

manipulation skills. The central question here is whether the neuromuscular system is capable of learning to control extra limbs as if they were a part of one's body, and which human-machine interface might enable this new form of augmentation.

Human limbs - especially the upper ones - possess remarkable flexibility, which enables them to be used for a wide range of different tasks. However, in numerous specific applications, technological progress has led to the development of artificial tools that vastly surpass the performance of natural limbs (e.g. sliding with skis, or cutting with a saw). The brain adapts to these tools, learning their kinematic and dynamic behavior and even incorporating them into the body schema - the brain's internal representation of the human body [48, 36, 52]. The use of a tool becomes intuitive and effortless after consistent training, in a process similar to the learning on new motor skills for the natural limbs [19]. Therefore, tools can be perceived and employed as an extension of the human body. In the last decade, research in neuroscience has shown that subjects can incorporate additional limbs in their body schema [10, 26, 30]. In the right hand illusion experiment, synchronous stimulation of a subject's hand and of a rubber hand placed besides it leads the subject to feel like the artificial hand is a part of their own body [11]. However, these experiments were performed using static extra limbs and deceiving the sensorimotor system with carefully designed stimuli. A promising research direction consists of developing additional robotic limbs which are wearable, powered and under the direct control of their user. Such systems provide both extra inputs (haptic and visual feedback) and extra outputs (new degrees of freedom) to the subject's sensorimotor system. Achieving voluntary control of powered extra limbs would show that humans can not only perceive them as parts of their body, but also incorporate them in the motion commands generated by the neuromuscular system.

The devices currently employed to increase the skills or performance of the human body can be divided into two broad categories: tools and wearable systems. Tools can be passive (e.g. hammer) or actuated (e.g. power drill), and are designed to be manipulated and controlled with the extremities of the natural limbs. Tools are not attached to the body, and when they are used they reduce the number of active

degrees of freedom available to the human. These active motions are employed to control the tool. For example, while operating a power drill the degrees of freedom of the arm and hand are devoted to positioning the tool, and (in the case of the index finger) to controlling the spinning speed of the drill bit. Wearable systems, on the other hand, are attached to the human body and provide direct assistance to natural joints. They can be unpowered (e.g. cushioned shoes, passive exoskeletons) or powered (e.g. active exoskeletons, exosuits) [32, 74, 42, 22, 64, 72, 47, 60]. They are designed to assist or enhance the function of specific joints, such as ankle, knee or hip flexion/extension in the case of leg exoskeletons [17, 57, 33, 85, 28, 27]. Wearable systems do not reduce nor increase the number of active degrees of freedom available to the human. Since they are focused on supporting the natural movements of the body, they tend to mimic its kinematic structure and control strategies. We proposed a third kind of augmentation device: a system that increases the number of active degrees of freedom available to the human user. Since the coordinated use of multiple limbs is essential for performing advanced tasks, the new active degrees of freedom should be provided through additional powered limbs under the direct control of the human. This augmentation strategy has the potential to expand the skill range of its users. However, human beings are not used to control more than four limbs. In this chapter, we will investigate whether it is possible for a human user to effectively control extra robotic limbs.

2.2 Experimental setup and control strategy

In this chapter, we will use a simplified version of the fourth prototype of the SRL, described in Chapter 8 (Figure 1). The motions of the extra limbs are controlled with muscle activation signals, measured by elecromyographic (EMG) sensors on the torso of the user [31, 20, 21]. Each of the two additional degrees of freedom is controlled by two torso muscles located on the same side of the human body (Figure 2). In particular, contracting the right pectoralis major originates an upward rotation (flexion) of the right robotic limb, while contracting the right rectus abdominis

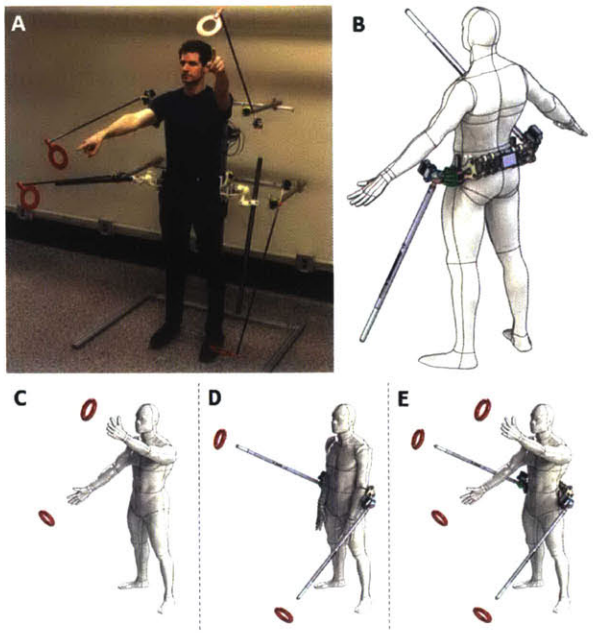

Figure 2-1: Subjects wearing the SRL and phases of the experiment to verify the possibility voluntary, independent control of the system. (A) A subject wearing the SRL. (B) The robot is worn at the hip of the user and the two extra limbs have one powered degree of freedom each, allowing them to rotate in the sagittal plane about their base (a movement analogous to the flexion/extension of the shoulder joint). (C) Phase 1 of the experiment, in which subjects do not wear the robot, and track the motions of two targets pointing at them with their natural arms. (D) In Phase 2 of the experiment, subjects track two moving targets with the robotic limbs. (E) Phase 3 requires subjects to control four limbs at once - two natural arms and two robotic limbs - in order to track the motion of four targets..

determines a downward rotation (extension) of the same robotic limb. An analogous relationship connects the left-side pectoral and abdominal muscles to the motions of the left robotic limb. The muscle activation signals are acquired with a 250Hz sampling rate, low-pass filtered (Butterworth filter, 2nd order, 10Hz cutoff frequency) and transformed into reference velocity commands for the robot's motors, according to the control law:

$$\begin{cases} \dot{\theta}_{ref} = (\alpha_{pec} - \alpha_{abs}) k_{vel} \\ \tau = (\dot{\theta}_{ref} - \dot{\theta}) k_p + \int_0^t (\dot{\theta}_{ref} - \dot{\theta}) k_i \, du \end{cases} \tag{2.1}$$

Where $\dot{\theta}_{ref}$ is the reference velocity for the robotic limb, and $\dot{\theta}$ is its actual velocity. α_{pec} and α_{abs} represent the normalized muscle activation values for the pectoral and

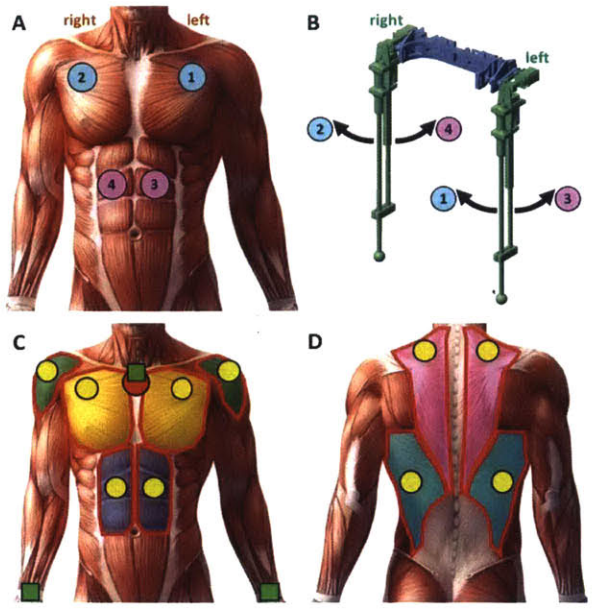

Figure 2-2: Control interface allowing the subjects to govern the motion of the robotic limbs, and sensors employed during the experiment. (A) Torso muscles used to control the extra limbs, and (B) the associated motions of the robot. Contracting the left pectoral muscle raises the left robotic limb, while contracting the left abdominal muscle lowers it. The same control scheme is replicated on the right side of the torso, for the right robotic arm. (C, D) Position of the sensors used on the front and on the back of the subjects. The yellow circles represent the locations of the EMG sensors used to measure the muscle activation signals of five couples of muscles. The area covered by each muscle is outlined in a different color (yellow: pectoralis major, blue: rectus abdominis, green: deltoid, pink: trapezius and light blue: latissimus dorsi). The red circle represents the location of the reference (ground) electrode, while the green squares indicate the position of the accelerometers employed to measure the inclination of arms and torso.

abdominal muscles respectively ($0\alpha_{pec}1$, $0\alpha_{abs}1$). k_{vel} is a constant converting muscle activation into a velocity reference, while k_p and k_i are the gains of the velocity PI controller that regulates the motion of the robotic limb. τ is the torque command sent to the motor. This control scheme is applied to each robotic limb, separately. It allows to extend the symmetric, independent organization of the left and right natural limbs to the additional limbs. The control law also shows that the muscle activation signals of the ipsilateral pectoral and abdominal muscles are subtracted. This is due to the fact that the two muscles control two different directions of motion for the same robotic joint, acting like antagonistic muscles for the new degree of freedom.

Muscle activation is converted into a velocity reference for the robotic joint, so that a burst in the EMG signal (the typical muscle activation pattern starts from zero, rises and then falls back to zero) generates a constant change in the position of the robotic limb. In other words, muscular activation is required to move the extra limbs - generating non-zero reference velocities - but not to hold them at a constant position - when the reference velocity is null.

We chose this control interface because it can enable the user to generate independent commands for the robotic limbs. The human torso comprises numerous superficial skeletal muscles (at least 10 pairs), whose activation can be measured with non-invasive EMG sensors [6]. In particular, we selected the pectoral and abdominal muscles for the control of the robot. These muscles are simple and comfortable to access with state-of-the-art EMG sensors, can be voluntarily contracted without effort, and are close to the physical location where the robot is worn. The reason why we focused on torso muscles is that they can activate in combinations that do not produce any motion of the body - for example, it is easy to contract the abdominal muscles without moving. These combinations of muscle activations belong to the null space of the torso. As long as the torso muscle activations lie in the null space, their forces will balance each others and there will not be any resulting motion. This is a higher-dimensional extension of the concept of co-contraction - the simultaneous activation of two antagonistic muscles that does not result in a movement for the joint that they control (e.g. biceps and triceps co-contracting without originating elbow flexion or extension). In the context of this chapter, the key consequence of the existence of a rich, multi-dimensional null space for the torso is that its muscles are able to generate independent activation signals that do not influence the posture of the human body. This has the potential to enable a human subject to control extra limbs without losing any natural degrees of freedom. Any other choice of control commands for the extra limbs (e.g. motion or muscle activation signals from the natural limbs, neck, face, tongue or eyes) would inevitably result in the loss of multiple natural degrees of freedom, re-directing them to the control of the robot [37, 4, 50].

2.3 Hypotheses

Based on these considerations, we formulate three main hypotheses. Hypothesis 1: it is possible to accurately control the extra robotic limbs, without influencing the posture of the human body. In particular, controlling the extra limbs does not require the loss of natural degrees of freedom - defined as preventing the motion of the natural limbs or forcing the subject to perform particular movements just to control the robot. As a consequence, we postulate that the coordinated control of natural and additional limbs allow subjects to perform a complex task better than just using the natural and artificial limbs separately, one after the other. Hypothesis 2: the direct, independent control of the robotic limbs is enabled by the use of torso muscle activation signals. The combinations of muscle activations used to generate control signals for the robot lie in the null space of the human torso. Moreover, these muscle activations are contained in a subspace that is different from the subspace of muscle combinations used to control the motion of the natural limbs. Hypothesis 3: there are natural limits to this approach, preventing it from being extended to an arbitrary number of extra limbs. More specifically, we expect the accuracy of the limbs (both natural and robotic) to decrease as we increase the number of limbs under the direct control of a human subject. However, we hypothesize that learning to control extra limbs is analogous to learning a new motor skill, and will therefore show performance improvement with consistent training.

2.4 Experiments

To test these hypotheses, we conducted experiments with healthy subjects (N=11). All of the subjects were male, right handed, in good physical shape (20âĽd'BMIâĽd'30) and between 23 and 37 years old. The participants to the experiment wore the extra robotic limbs, while standing in front of a set of four moving targets. The goal of the subjects was to track the motion of the targets by pointing at them with their natural arms and robotic limbs (Figure 1). Each limb was allowed only one degree of freedom

- the rotation about its base in the sagittal plane. In the case of the natural arms, this motion corresponded to the flexion/extension of the shoulder joint. Subjects were asked not to move the other degrees of freedom of the shoulder, extending their arms and keeping their elbows and wrists rigid. The targets were placed at the end of carbon fiber rods, whose rotation was actuated by servomotors. The targets moved to a new position every 15 seconds, and held it until the next movement. The trajectories of the four targets were different, randomly generated and independent. The experiment consisted of three phases (Figure 1). In Phase 1, subjects did not wear the robot and simply tracked the motion of two targets with their two natural arms. In Phase 2, subjects wore the robot and tracked the motion of two targets with the two robotic limbs. They were instructed to relax their natural arms. In Phase 3, subjects wore the robot and tracked the motion of 4 targets using both their natural arms and the robotic limbs. Each subject participated to two experimental sessions for Phase1, three for Phase 2 and three for Phase 3. Sessions were divided into tracking trials which lasted for 3 minutes each. Phase 1 and Phase 3 sessions contained 3 trials, while Phase 2 sessions consisted of 5 trials. Subjects could rest between trials, and could not participate in more than a session per day. In all of the phases, we measured the rotation of the human arms (with accelerometers held in the hands) and the extra limbs (with the actuator sensors) in the considered degree of freedom (Figure 2). We also measured the rotation of the subject's torso in the sagittal and frontal planes (using an accelerometer taped on the upper chest). Finally, we used EMG sensors (Figure 2) to record the activation signals of the 4 muscles used to control the robot (pectoralis major and rectus abdominis, left and right) and of 6 additional torso and shoulder muscles (trapezius, latissimus dorsi and deltoid, left and right).

All of the experiment subjects achieved accurate, voluntary control of the robotic limbs (Figure 3). The movements of the extra limbs are strongly correlated with the trajectory of the targets (Figure 4), both in Phase 2 ($r = 0.83$) and in Phase 3 ($r=0.77$). This implies that the subjects were able to efficiently track the motion of the targets with the two additional robotic limbs, and maintained that ability when

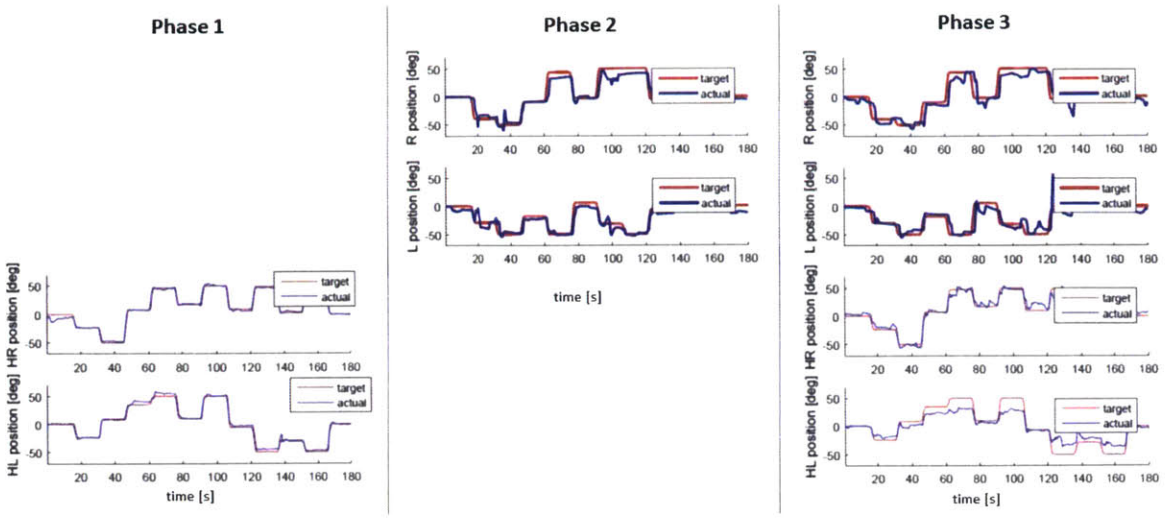

Figure 2-3: Examples of the tracking performance of the subjects during the experiment. The left column shows the best Phase 1 trial (tracking two targets with the human arms). The central column shows the best Phase 2 trial (tracking two targets with the robotic limbs). The right column shows the best Phase 3 trials (tracking four targets with the human arms and the robotic limbs).

they were tracking two additional targets with their natural arms. As expected, the correlation between the motion of the human arms and their target trajectories is very high in Phase 1 (r=0.93). Interestingly, this correlation remains high in Phase 3 (r=0.77). This confirms that learning to control additional robotic limbs did not affect the natural capacity of the subjects to control their own arms. Moreover, our data show that controlling the motion of the four limbs (both the robotic and the natural ones) did not affect the posture of the subjects' torso. Throughout the whole experiment, the correlation between the target trajectories and the motions of the torso was extremely low - never exceeding r=-0.31 in the case of the natural arms, and r=-0.10 in the case of the robotic limbs. In Phase 2, subjects actively controlled the motion of the robotic limbs, while relaxing their arms. There is no correlation between the target trajectories for the extra limbs and the motion of the natural arms (r=0.00). This indicates that direct control of the robotic limbs does not influence the posture of the natural arms. We also computed the target reaching time - the time required for a limb to reach its target with a tracking error smaller than 10deg. Our results show that the average reaching time in Phase 3 - when all four limbs were

used - is smaller than the sum of the average reaching times in Phase 1 and Phase 2 - when the two human arms and the two robotic limbs were used separately (Figure 5). This means that in Phase 3 subjects were able to execute the complicated tracking task by coordinating the four limbs. The direct, simultaneous control of four limbs yielded a better task performance (smaller reaching time) than simply executing a non-overlapping sequence of actions where the natural arms and the robotic limbs are activated one after the other.

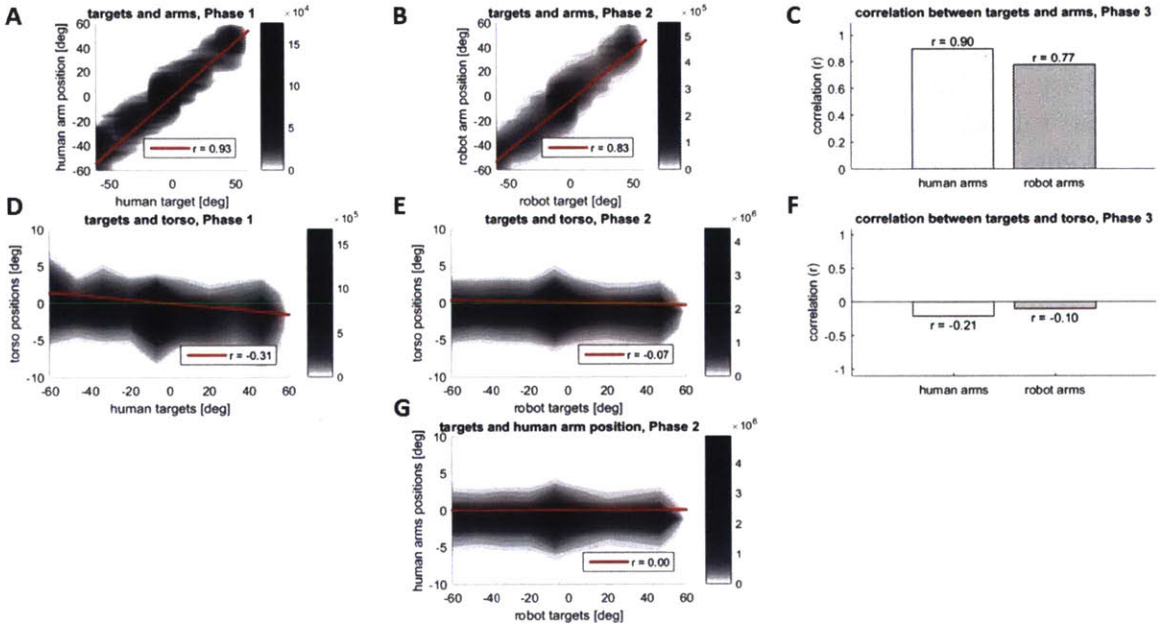

Figure 2-4: Correlation between the trajectories of the targets and the motion of limbs and torso. (A) Correlation between the position of the subjects' natural arms, and the position of their targets. The grayscale bar on the right indicates the number of data points in each location of the plot. The red line is a linear fit of the data, and Pearson's correlation coefficient is r=0.93. (B) Correlation between the position of the robotic limbs, and the position of their targets. (C) Correlation coefficients between the motion of the limbs (divided in natural arms and robotic limbs), and their targets. (D, E, F) Correlation between the trajectory of the targets, and the motion of the subject's torso. (G) Correlation between the motion of the robot targets, and the position of the human arm.

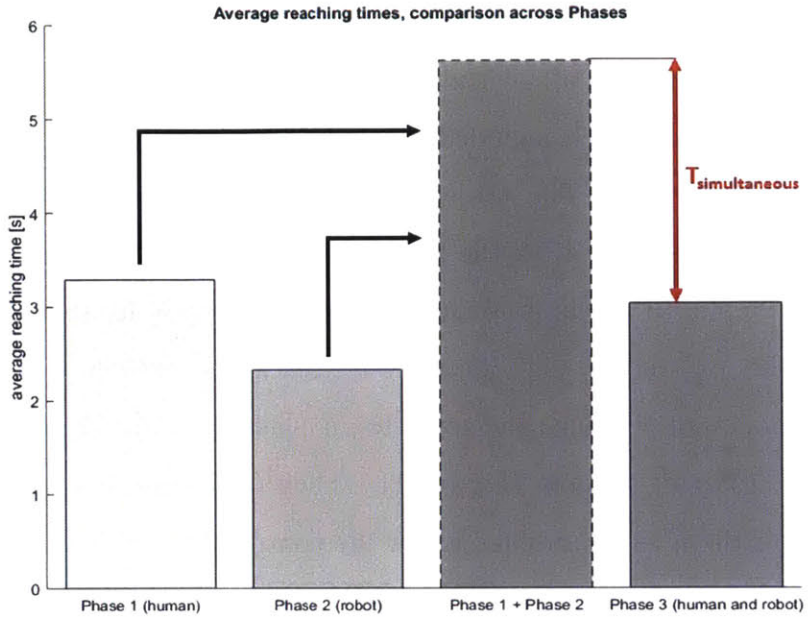

Figure 2-5: Average time to reach the targets in all of the phases of the experiment. Reaching time is computed as the time between the instant when a target reaches its position, and the instant when the corresponding limb reaches the target - within an interval of Âś10deg. For each trial, we calculated the average reaching time of every limb. The bars in the figure display the mean between the reaching times of all limbs and all trials for every phase of the experiment. The third column represents the sum of the average reaching times of Phase 1 and Phase 2. This is the average reaching time that we would expect in Phase 3, if the subjects controlled the four limbs sequentially (one after the other). The red arrow indicates the difference between this prediction and the actual average reaching time of Phase 3. Since subjects are faster in reaching the four targets, they are employing the two natural arms and the two robotic limbs in a coordinated, simultaneous manner.

2.5 Discussion

Direct control of the robotic limbs was enabled by several factors, including the simple control interface, the presence of sensory feedback, and the use of a velocity control strategy. The control interface for the robot (Figure 2) was based on torso muscles located on the same side of the body as the controlled extra limb, and in the same direction as the intended motion (pectorals to raise the limb, and abdominals to lower them). We also employed the smallest number of muscles (four) necessary to create an antagonistic control system for each of the two artificial degrees of freedom. Subjects got easily accustomed to the relationship between the contraction

of their torso muscles and the corresponding robot motions. An accurate tracking performance was achieved by all of the participants within the time frame of the experiment (Figure 3, 4), which included six daily sessions with control of the extra limbs (Phase 2 and Phase 3). The subjects' average tracking performance increased from trial to trial, consistently with the features of the first, fast stage of motor skill learning [24, 41, 25, 46, 51]. The presence of visual and haptic feedback was another key element of the experiment [44]. Sensory feedback has been proven to facilitate the learning of new motor skills, and even brain plasticity [71, 75]. Here, subjects tracked physical, rotating targets (Figure 1). They could also see the extra limbs moving in front of them as a consequence of the contractions of their torso muscles. And since the harness was securing the wearable system to the hip of the subjects, they were able to feel the reaction forces generated by the movements of the robotic limbs. Our data also confirm that employing muscle activations as velocity signals is an effective control strategy for tracking tasks where the goal is to accurately reach a position and then hold it. Subjects were able to track the targets both accurately and efficiently. The average muscular activation recorded in Phase 2 - when the natural arms were at rest - was 33% lower than in the other Phases. The reason is that this control scheme only requires muscle contractions to change the positions of the robotic limbs, but not to hold them in place. Conversely, when the natural arms were required to move the shoulder muscles had to be continually contracting in order to keep pointing at the targets in front of the subjects. This resulted in rapid fatigue symptoms for the deltoid muscles, and limited the number of tracking trials to three per session in Phase 1 and Phase 3 (the trials were 5 per session in Phase 2).

The motion of the robotic limbs did not influence the posture of the human body (Figure 4), because the subjects learned to use their muscles to generate independent control signals for the robot. The torso muscle activations associated with the movements of the extra limbs belonged to the null space of the torso. In fact, data from all of the three Phases of the experiment indicate that these combinations of muscle contractions did not influence the position of the torso. Moreover, subjects used different sets of muscles to control the robotic limbs and the natural arms (Fig-

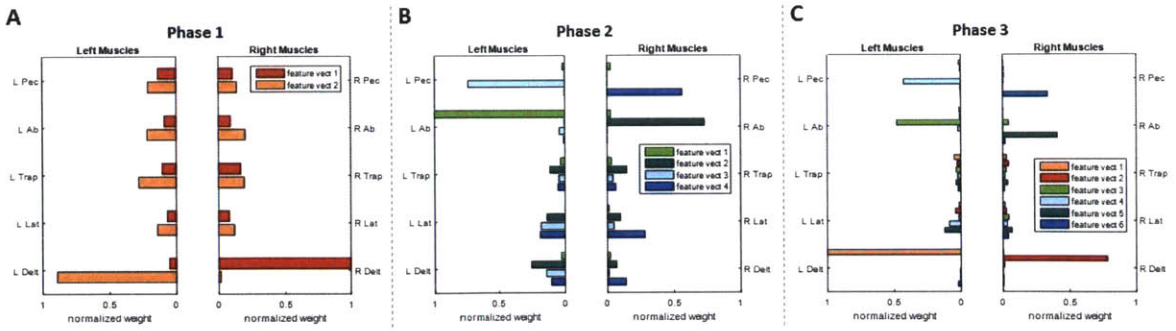

Figure 2-6: Main combinations of muscles activated during the different phases of the experiment. (A) The main muscle combinations used by subjects in Phase 1. These vectors have been extracted by applying non-negative matrix factorization (NMF) to the muscle activation data recorded in Phase 1 - considering all of the subjects. NMF outputs the feature vectors, displayed in the plot, that best approximate the signals under analysis. In this case, the right deltoid muscle dominates the first feature vector, while the left deltoid muscle dominated the second feature vector. This means that the natural arm movements - the only tracking movements present in Phase 1 - are dominated by the activation of the deltoid muscles. (B) The main muscle combinations used by subjects in Phase 2. The four feature vectors are dominated by the abdominal and pectoral muscles, one for each combination. This is consistent with the control scheme of the robotic limbs, which was based on those muscles. It also shows that there is minimal overlapping with the other torso muscles, and with the muscles employed to control the motion of the natural arms. (C) The main muscle combinations used by subjects in Phase 3. The feature vectors present in the two previous phases continue to dominate the muscular activation patterns of subjects. Since the muscle combinations used to control the natural arms and the robotic limbs do not overlap significantly, subjects combine the previously learned control strategies to achieve direct, coordinated control of four limbs.

ure 6). These sets of muscles have minimal overlapping, and can therefore be used independently. In particular, the pectoral muscles are involved both in the natural motion of the human arms, and in the control of the extra limbs. However, the levels of activations required by these two tasks are different - a much stronger activation is needed in order to generate a control signal for the robot. This explains why the same muscles could perform both functions without conflict, as a secondary component of the muscle combinations employed to move the natural arms and as a primary component of the muscle combinations employed to control the robotic limbs.

The main limit of this approach is that tracking accuracy decreases when adding active degrees of freedom under direct control of the subject (Figure 7). This reduction

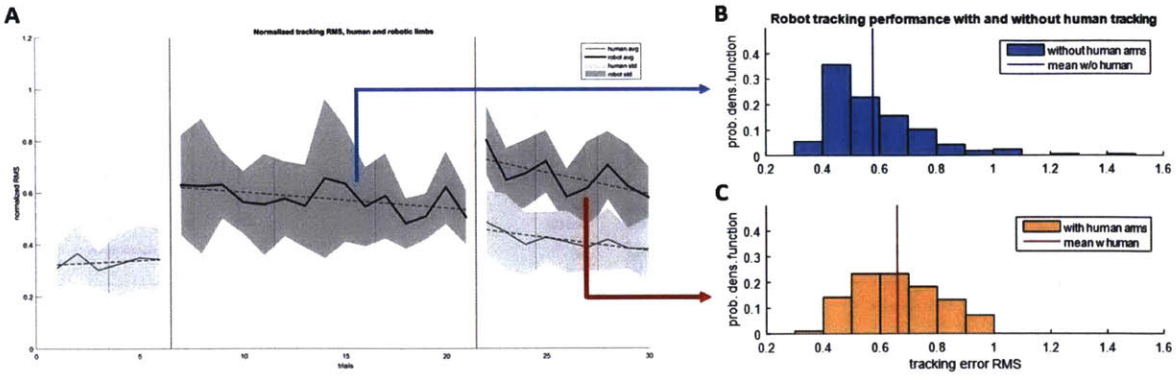

Figure 2-7: Normalized tracking performance in the different phases of the experiment. (A) Normalized root mean square (RMS) of the tracking error, as a function of the number of trials. Phase 1 consists of trials 1-6, Phase 2 consists of trials 7-21, and Phase 3 consists of trials 22-30. Solid lines represent the average RMS tracking error across all subjects, and the shaded areas indicate the standard deviation. Thin lines and light shades refer to the human arms, while thick lines and dark shades refer to the robotic limbs. The dotted lines indicate the linear fit on the data. The learning rate - the reduction of the tracking error from one trial to the next - is fast in Phase 3, intermediate in Phase 2, and absent in Phase 1. This confirms that learning to control extra limbs is analogous to learning a new motor skill. (B) Distribution of tracking errors for the robotic limbs in the Phase 2 trials. (C) Distribution of the tracking errors for the robotic limbs in the Phase 3 trials. The average tracking error increases as we add extra powered degrees of freedom to the human body.

in performance affects all of the limbs involved in the task. The average tracking error increases from Phase 1 to Phase 3 for the natural arms, and from Phase 2 to Phase 3 for the robotic limbs. At the same time, tracking accuracy gradually improves with training, confirming that subjects are adapting to the extra limbs as if they were learning a new motor skill. In particular, the learning rate (reduction of tracking error from trial to trial) is fastest in Phase 3, where both natural and robotic limbs are controlled by the subjects. While the learning rate is intermediate in Phase 2 (only robotic limbs), there is no significant learning in Phase 1 (only human arms). This is expected, because subjects have already refined the control performance of their natural arms over the years, and do not need to learn anything new to use them to track the target trajectories. Whenever we add the robotic limbs, though, subjects need to develop a new control strategy and the learning process is initiated.

2.6 Conclusions

We have demonstrated that humans can learn to accurately control additional powered limbs, without influencing the posture of their natural body. The human neuromuscular control system adapts to this new configuration in a few training sessions. The vast number of muscles in the human torso allows subjects to generate independent control signals. The combinations of muscles used to control the robotic limbs belongs to the null space of the torso, and does not significantly overlap with the set of muscles used to move the natural arms. The coordinated control of four limbs enables subjects to execute a tracking task faster than they would controlling single limbs or couple of limbs separately, one after the other. Tracking error increases with additional active joints, but consistent training leads to performance improvements analogous to learning a new motor skill. Adding powered degrees of freedom to the human body represents a new form of augmentation, capable of enabling the acquisition of new motor skills and the execution of new classes of complex, coordinated tasks.

Chapter 3

Design

3.1 Overview of the robot

Today's wearable robots closely mimic the structure of the human body. Wearable robots can be classified in exoskeletons, orthoses and prostheses [32]. Exoskeletons are employed to augment the performance (strength, endurance, etc.) of their user, orthoses restore or assist impaired motor functions, and prostheses replace missing limbs. All of these systems are designed to follow the kinematic organization of the human body, and to provide assistance to the natural joints. They focus on supporting existing degrees of freedom, and do not increase the number of active degrees of freedom available to the user.

We proposed a new kind of wearable robot that augments the user by providing additional robotic limbs. These extra limbs are independent from the natural human body. Therefore, the number of active degrees of freedom available to the user is increased, opening up new possibilities in terms of executing complex tasks and optimizing assistance. Humans have already evolved to take advantage of the simultaneous use of multiple limbs. We hypothesize that increasing the number of limbs will enable users to perform new, coordinated tasks that would not be possible - or would be significantly slower - using only the natural limbs. The increase in functionality brought about by extra limbs can be intuitively understood by trying to execute bimanual tasks (e.g. opening a bottle, carrying a large box) with only one

arm. We discussed this in detail in the previous chapter.

Another advantage of using independent robotic limbs is that their motions are not constrained to follow the motions of the user. This means that the robotic limbs are free to optimize their configuration to provide the best possible assistance, given the configuration of the user's body. Such optimal behavior is not available to traditional wearable robots, because their kinematic configuration must always follow the posture of the user joints to which they are attached. In Chapters 5, 6 and 7 we will take advantage of the independence of the robotic limbs to provide optimal weight support during static manufacturing tasks. In Chapter 8, the additional degrees of freedom of the robotic system will be employed to stabilize and assist quasi-static sitting/standing motions. In Chapter 9, the use of independent robotic limbs will enable a new balance augmentation strategy for dynamic walking.

The concept of the wearable robot is shown in Figure 1. The system is named Supernumerary Robotic Limbs (SRL) because of the new form of augmentation it provides. The robot is worn at the hip, through a harness composed of a belt and two leg straps. The base of the device follows the shape of the hip bone. The extra limbs extend outwards from the sides of the base. The range of motion of the robot is wide. For each robotic limbs, the workspace resembles a hemisphere centered on its base and extending outwards. The robotic limbs are able to reach up (like human arms), reach down (like human legs) and even reach areas that are outside of the workspace of the human limbs (e.g. behind the user). Each robotic limbs has three degrees of freedom (Figure 1). Two rotational degrees of freedom are located at the base of the limb, where it is attached to the base of the robot. The third degree of freedom is prismatic, and it is located axially in the limb itself.

In the following sections we will describe in detail the structure and the components of the latest SRL prototype (Figure 2). The harness and the base of the robot achieve a firm and comfortable fit with the human body, enabling the system to provide assistance without getting in the way of the user. The rotational degrees of freedom at the base of the robotic limbs have been realized with an innovative ball joint structure, able to bear the weight of the user without any heavy, conventional

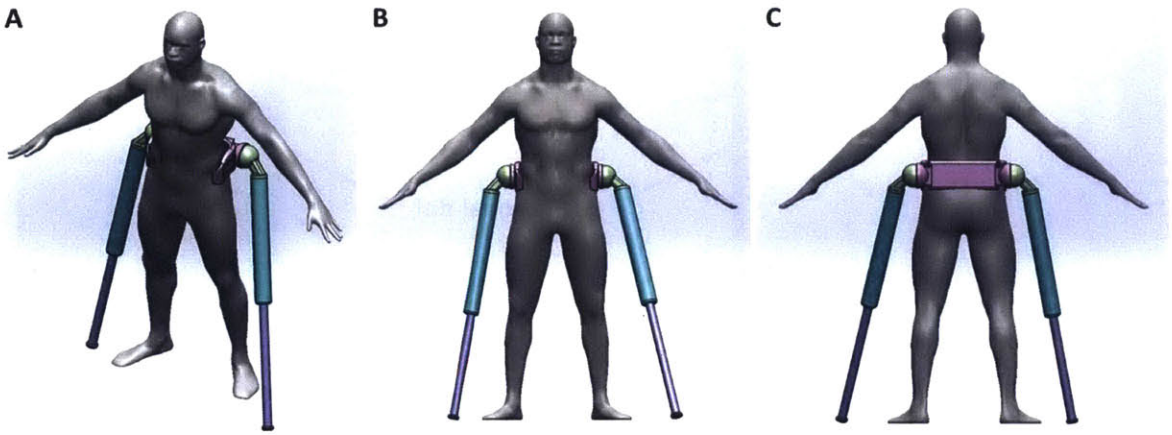

Figure 3-1: Concept of the Supernumerary Robotic Limbs (SRL), a wearable robot that extends its user's body with two additional robotic arms. A) Isometric view. B) Front view. C) Back view.

metal bearing or shaft. The prismatic joint in each limb is actuated by a pneumatic cylinder. This solution enabled us to realize a compliant, fast joint that is able to compensate for the whole weight of the user while keeping the system extremely light. Finally, we will describe the wide range of passive and active end effectors that have been developed for the SRL.

The final prototype of the SRL, presented in this chapter, combines its assistive capabilities with a small volume and weight (less than 3.5kg). This prototype has been employed to perform the experiments shown in Chapter 8 of this document. The other chapters show results obtained with earlier prototypes of the SRL, which were significantly different implementation of the same augmentation concept. In particular, Chapter 4 describes the realization and use of the first SRL prototype. The system had rotational elbow joints in both robotic limbs. These joints were actuated with series elastic actuators located in the base of the robot, and reaching the elbow through Bowden cable transmissions. The main limit of this approach, besides the overall weight, was the bulk and added stiffness of the Bowden cable sheaths. Chapters 5 and 6 detail the design and control of the second SRL prototype, which was equipped with elbow rotational joints, too. In this case, however, the Bowden cable transmission was substituted by a timing belt transmission that linked the elbow with an actuator in the base of the robotic limb. All of the actuators in this prototype were

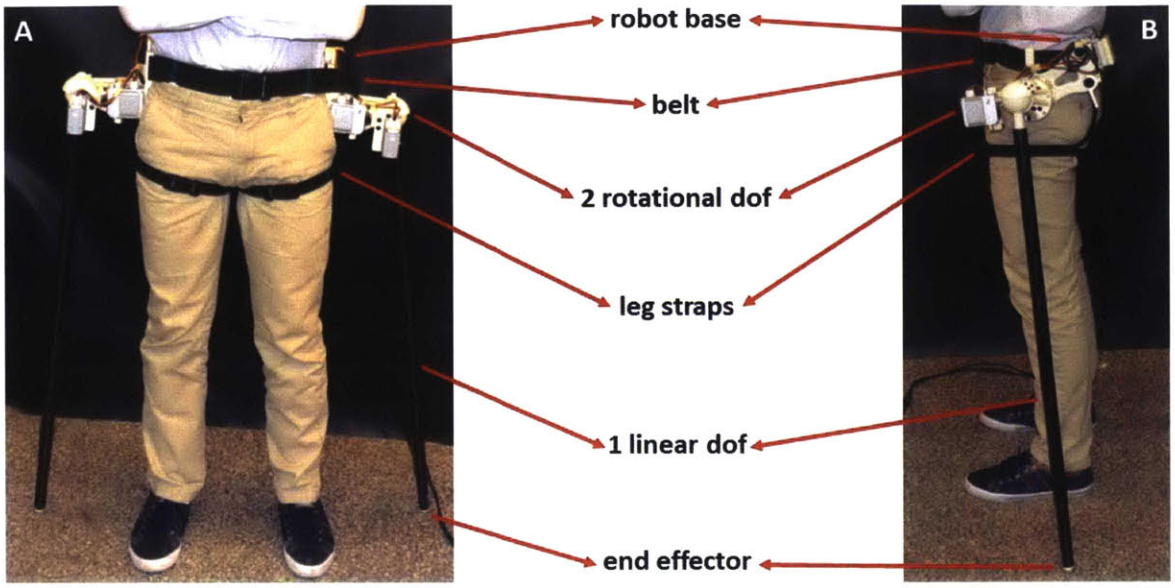

Figure 3-2: Main components of the Supernumerary Robotic Limbs (SRL). A) Front view. The robot is worn through a harness composed by a belt and two leg straps. The two robotic limbs are attached to the base of the robot, which follows the shape of the human hip. B) Side view. Each robotic limb has three degrees of freedom - two rotational ones in the base and a prismatic one in the limb itself.

series elastic. The performance of the actuators was very high in terms of maximum torque, sensing capabilities (position and torque) and built-in compliance. However, the weight and volume of the prototype remained significant limitations. Chapters 7 and 9 report the design and control details for the third SRL prototype. This system realized a significant weight and volume reduction, and greatly increased wearing comfort. It employed lighter rotational actuators, and an optimized structure with some composite components. The elbow joints were substituted with prismatic joints, actuated by linear electric actuators. Despite these improvements, the mass of the system and its weight distribution were still uncomfortable for users. Moreover, the linear actuators were slow and non-backdrivable, making it difficult for the robot to minimize impact while providing balance assistance during dynamic walking. All of the issues that have emerged in the development and testing of the three previous SRL prototypes have been addressed and solved in the fourth iteration of the robot, which is presented in this chapter.

3.2 Harness and base

The SRL is worn through a custom-built harness, enabling the robot to provide assistive forces in every direction. The harness is composed of two main parts: a belt and two leg straps (Figure 3). The belt is particularly wide (50 mm), and secures the robot to the hip of the user. The base of the robot follows the shape of the iliac crest, the edge of the hip bone. Between the base of the robot and the user, a wide (100 mm), thick (12.5mm) padding cushion ensures that the fit is comfortable. We designed the robot to be worn at the hip for two main reasons. First, the hip bone provides the most firm and comfortable physical interface between a rigid robot and the human body. Second, locating the base of the additional limbs close to the center of the human body allows them to reach the natural workspace of both arms and legs. This extends the potential assistive capabilities of the robot to manipulation and locomotion tasks. The second component of the harness are the leg straps. They are worn around the thighs of the user, half-way between the knee and the hip joint. These straps are connected to the belt with two additional straps, running vertically to the base of the robot on the back side of the user (Figure 3). The vertical straps and the thigh straps behave like a soft, wearable chair when the user bends his knees and shifts his weight on the robotic limbs. They ensure that the robot can transmit significant upward assistive forces to the wearer, maintaining comfort and without sliding up. The leg straps are padded, in order to distribute the loads on an area as wide as possible.

The harness is extremely simple to wear. There are only three buckles to secure (one for the belt and two for the leg straps). The whole process of wearing the robot takes only about 30 seconds, and can be carried out without any external assistance. The simplicity of the harness of the SRL differentiates it from the complexity of state-of-the-art exoskeletons (Figure 4). Exoskeletons are forced to employ numerous straps because they provide direct assistance to human joints. For example, a wearable system in parallel with a natural joint must have at least two straps (one proximal and one distal) in order to transmit torque to that joint. The SRL, on the other

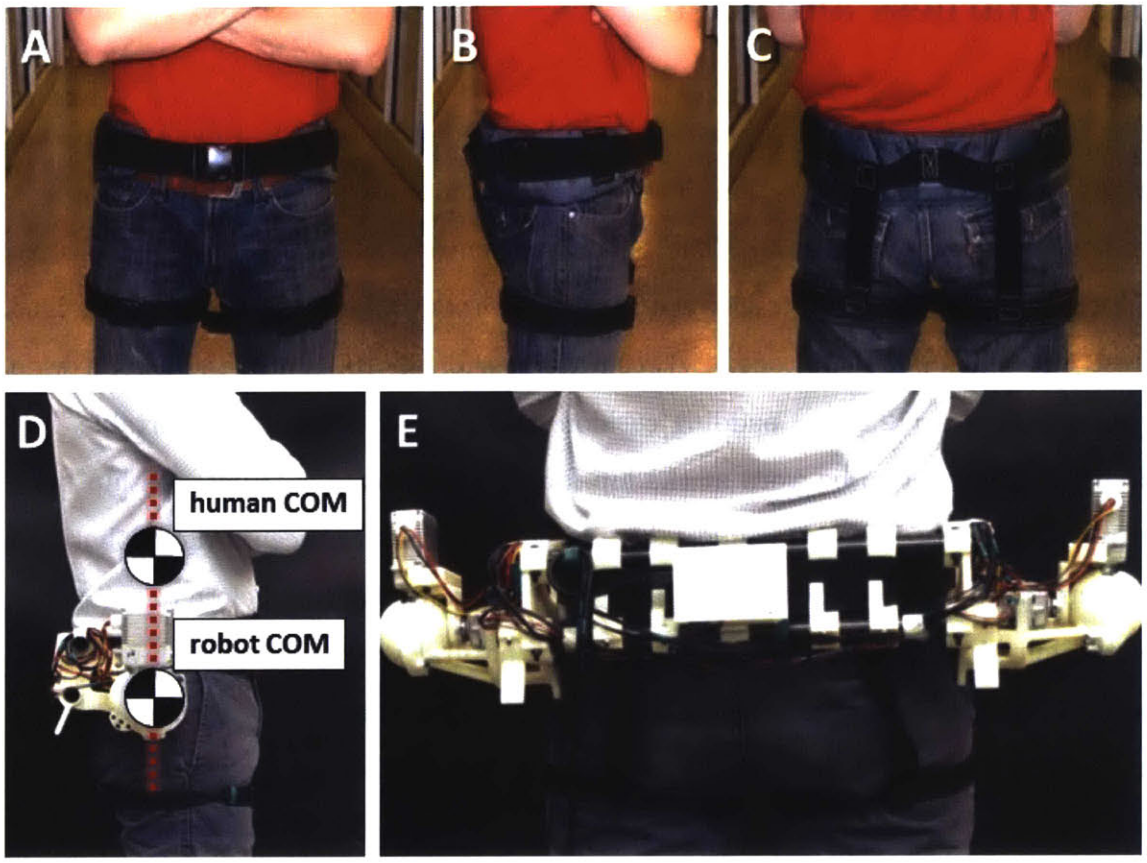

Figure 3-3: The SRL is worn through a custom harness. Views of the harness: A) front, B) side, and C) back. The harness is composed of a belt and two leg straps. Both belt and straps are provided with an internal padding layer to distribute loads on a wider surface. D) The center of mass (COM) of the robot is located below the human COM, in the direction of gravity. E) Back view of the SRL base worn by a user.

hand, is independent from the kinematic structure of the human body. This allowed us to reduce the size of the harness, employing only the minimum number of straps needed to ensure that the robot can be comfortably worn and is able to support the weight of the user. Another important feature of the harness is that it does not put any load on the upper part of the human body (torso, waist, shoulders, and arms). There are no shoulder straps, and the robot is not in contact with the user above its waist padding. This increases the comfort of the robot (it is tiring to bear loads above the waist), and ensures that the system does not get in the way of the natural movements of the user. The width of the base of the robot and the length of the straps can be adjusted to fit adult users of any body size within the 95th percentile.

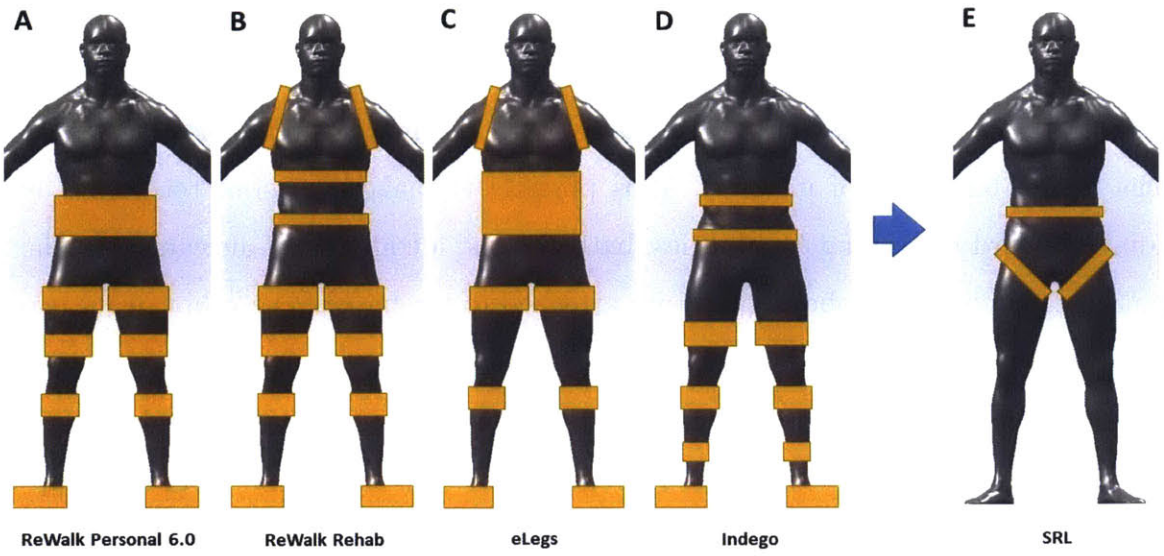

Figure 3-4: The SRL can be worn in under 30 seconds, because it has only three buckles to secure (one for the belt and two for the leg straps. A,B,C,D) Straps and harness components required by state-of-the-art exoskeletons. Each human joint needs at least a proximal and a distal strap in order to be assisted by a robotic system in parallel with it. E) Harness of the SRL. The SRL is easier to wear, because its limbs are independent from the human limbs.

The center of mass (COM) of the robot is very close to the center of mass of the human - their distance is about 0.15m for adult males. This ensures that the added metabolic cost due to carrying the weight of the robot is minimal [13]. Moreover, the mass distribution of the robot is balanced in the sagittal plane. In other words, the COM of the system is located below the COM of the human, in the direction of gravity. This ensures that the user does not need to generate any torque to compensate for a misalignment of the mass of the system. For example, when wearing a backpack the opposite is true: the wearer needs to generate a compensation torque with his shoulders, because the COM of the backpack is located far behind his back. The alignment of robot COM and human COM also means that, when standing at rest, the user discharges the weight of the robot to the ground through his leg bones, without requiring additional muscular contractions.

Besides providing the physical interface between the robot and the human, the base of the system also contains the control electronics that regulate the motion of

the actuators. This is accomplished through two boards that run low-level control loops in real time and receive reference commands from a remote computer. Control commands, power and pressurized air arrived to the robot through a tether that plugs in the back side of its base. It is possible to make the robot tetherless by adding onboard processing capabilities, batteries and a compressed air canister. The rotational joints of the robotic limbs are attached to the base of the robot at its two sides, and will be described in detail in the next section.

Lightweight was an essential requirement for the SRL, and one of the main drivers in the development of its prototypes. The current SRL system, presented in this chapter, has a mass of 3.5kg. Developing such a light wearable robot while maintaining the capability to bear the full weight of the human user (100kg is the average weight of adult men in the 95th percentile) was a significant technological challenge. This target was met by developing innovative design solutions and choosing unconventional actuation technologies (detailed in the following sections). Another important factor in the reduction of the weight of the SRL was the extensive use of custom composite parts. The majority of the structure of the robot is realized in carbon fiber and Kevlar composite parts, with a nylon filler (Figure 5). The rapid manufacturing of custom parts realized with composed materials was enabled by MarkForged, an MIT startup that developed a proprietary 3D printing technology for composite materials [53]. This manufacturing technique allowed us to realize composite parts that are able to bear the full weight of the human user with a 75% in weight with respect to analogous Aluminum parts. Additionally, MarkForged's 3D printing technology allowed us to quickly produce complex composite parts. These shapes could not have been easily realized in Aluminum using traditional subtractive manufacturing techniques.

3.3 Spherical load-bearing joints

The kinematic structure of the joint at the base of each robotic limb consists of two rotational degrees of freedom (Figure 6). The first rotation of the limb is within the sagittal plane, and is analogous to the flexion/extension movement of the human

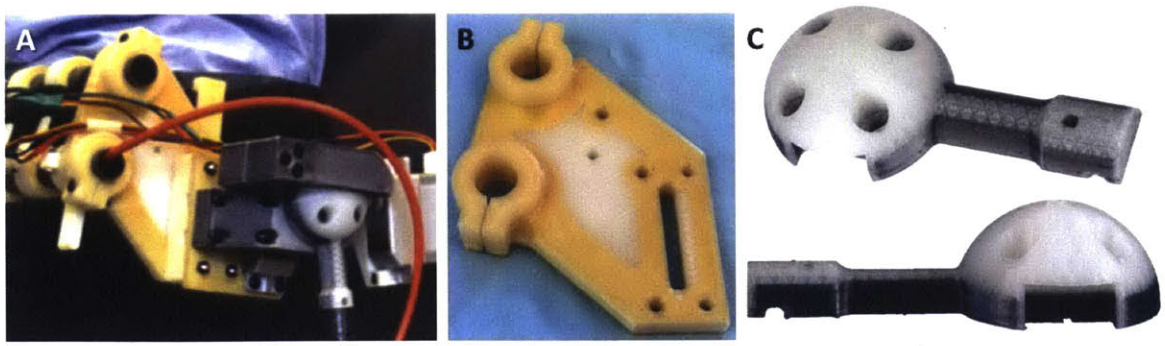

Figure 3-5: The structure of the SRL is realized with composite materials, printed using MarkForged's technology. A) Side view of the SRL base. The Kevlar parts (yellow) and carbon fiber parts (black) can be identified from their color. B) Detail of a Kevlar part (with nylon filler) in the SRL base. C) Detail of a carbon fiber part (with nylon filler) in the ball joint of the SRL.

shoulder. The second rotation is perpendicular to the first one, and is similar to the adduction/abduction movement of the human shoulder. If the robot is employed for assistance during locomotion (Chapters 8 and 9), the robotic limbs are always pointing downwards - their goal is to make contact with the ground in order to provide support to the user. In this case, the required range for the first rotational joint is $-60\,\text{deg} \leq \theta_1 \leq 60\,\text{deg}$, and the required range for the second rotational joint is $0\,\text{deg} \leq |\theta_2| \leq 45\,\text{deg}$ (the limit is 45 deg for the left robotic limb, and -45 deg for the right one, see Figure 6). The two joint angles θ_1 and θ_2 are zero when the robotic limbs are pointing downwards, aligned with the direction of gravity.

Besides this range of motion, there are numerous additional requirements for the base joint of the robotic limbs. The joint must be able to bear half of the weight of an adult user (this value is 50 kg for the 80th percentile), so that both robotic limbs together can fully support the human body. Moreover, the rotational degrees of freedom should be able to move at a speed compatible with the natural walking gait. When walking, humans can easily reach a stepping frequency of 1 Hz [14, 7, 73]. This implies that the sagittal plane rotational joints θ_1 for both robotic legs must be able to cover their whole range (120 deg) twice in 1 s, yielding a desired speed of at least 240 deg/s for the rotational actuators. The motors actuating the base joint should also be lightweight, as the rest of the robot. For actuators, this translates

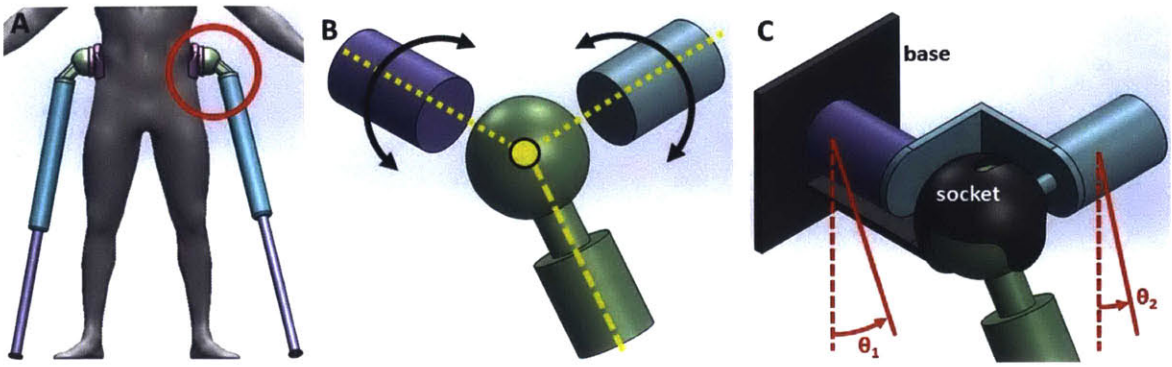

Figure 3-6: Design of the ball and socket joint at the base of the robotic limbs. A) Location of the ball and socket joint. B) Concept of the joint, showing the intersection of the axes of the rotational actuators and of the axis of the robotic limb. C) Concept of the joint, showing the angle conventions and the position and structure of the socket that absorbs the axial forces coming from the robotic limb.

into the requirement of a high torque density, which is usually achieved with motors employing significant gear ratios. Such actuators usually are non-backdrivable, which is not desirable for exoskeletons and robots that are worn in parallel with the human body. However, the independence of the SRL means that its limbs do not constrain the natural motions of the human limbs, and can therefore afford to be non-backdrivable without reducing the comfort of the user. The only joint of the SRL that needs to be compliant is the prismatic one, as will be explained in detail in the next section. In order to naturally coordinate with the motion of the human legs and to comfortably support the weight of the user, the base joints of the SRL need to be aligned with the hip joints of the wearer (Figure 6). Additional requirements for this joint are the proximity to the human hip and a small overall joint volume, so that the robotic limbs do not get in the way of the natural swinging motion of the user's arms.

In the human body, the joints at the base of the limbs are of the ball and socket type (shoulder and hip). In the SRL, we reproduce this kinematic configuration by having the axes of the two rotational actuators intersect in a single point (Figure 6). The axis of the robotic limb passes through the same point, too (Figures 6 and 7). As a consequence, axial forces coming through the robotic limb do not generate torques in the rotational joints at its base. The fact that ground reaction forces that are mostly directed along the axis of the robotic limb is a consequence of the

design of the limbs and their end effectors (see following sections), and of the control algorithms that optimize their use (see Chapters 5, 6 and 7). Since the structure of the ball joint can absorb these linear forces without requiring the rotational motors to generate torques, we are able to select smaller actuators for this joint. The two degrees of freedom of the ball joint are actuated by two Hitec SGT-1000 servomotors (weight: 363 g, max torque: 10Nm, max speed: 350 deg/s). These actuators have the highest torque density among commercially available servomotors, and a mass and maximum speed that are compatible with our requirements. Their maximum torque is lower than the one that the human hip joint can exert [29]. However, this torque is enough for the SRL, because the structure of its ball and socket joint absorbs most of the forces coming from the robotic limbs. Therefore, the servomotors are only used to move the robotic limbs (when they are not in contact with the ground) and to compensate for disturbances (when they are in contact with the ground).

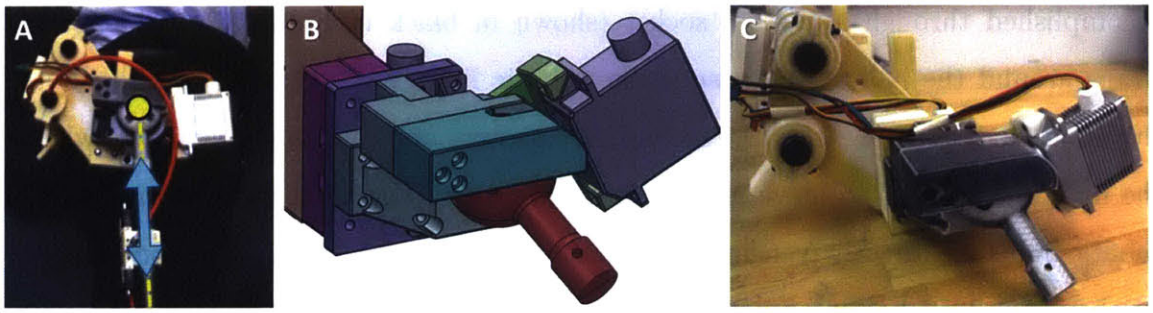

Figure 3-7: Implementation of the ball and socket joint at the base of the robotic limbs. A) Scheme showing that forces oriented as the axis of the robotic limb pass through the center of the ball joint and are absorbed by the socket, without originating torques on the servomotors. B) Design of the ball and socket joint, optimized for the composite 3D printing process. C) Implementation of the composite ball and socket joint.

Another important feature of the ball joints of the SRL is that they are actuated by commercially available servomotors. In the human body, ball and socket joints are controlled by a complex set of muscles that are activated in different combinations according to the desired movement and the current position of the limb. Replicating this architecture in the SRL would have required the use of multiple linear actuators, pulling and pushing on the robotic limb through a system of cables or rods. Such

a system would be extremely nonlinear and difficult to design, manufacture, maintain and control. On the contrary, the SRL ball joint design enables two standard rotational actuator to easily control the motions of the robotic limbs (Figures 6 and 7). The first actuator (colored in purple in Figure 6) is stationary - fixed to the base of the robot. The second actuator (colored in light blue in Figure 6) is attached to the output of the first actuator through a bracket. Finally, the output of the second actuator is attached to the ball at the base of the robotic limb. This configuration enables the two servomotors to directly control both rotations of the joint. It requires only two moving parts (the bracket and the ball), and it is easy to assemble and maintain.

The main advantage of this ball joint is that its structure bears the large axial forces coming from the robotic limb, allowing the robot to support the weight of the user without overloading the output shafts of its small servomotors. This is accomplished through a custom socket (shown in black in Figure 6). The socket wraps around the ball at the base of the robotic limb, and is carved to allow both the input shaft (coming from the second servomotor) and the output cylinder (where the limb is attached) to move within their full range. The axial forces borne by the robotic limbs are directly transmitted from the ball to the socket. The servomotors do not have any load bearing function. In this configuration, the 3D printed composite ball and socket system (realized in carbon fiber, Kevlar and nylon) replaces the much heavier and bulkier set of bearings and metal shafts that would have been used in a conventional design.

As a consequence of the design choices detailed in this section, the ball and socket joint employed in the SRL is extremely lightweight and compact. It also enables the use of small servomotors, because its structure absorbs most of the forces coming from the robotic limbs. It is easy to manufacture, assemble and maintain, and its composite materials make it particularly suitable to bear the loads and impact forces associated with human walking. Figure 7 shows the implementation of the ball joint in the SRL prototype. Besides the actuators and the bolts, there no metal parts in the lightweight composite structure.

3.4 Pneumatic legs

In order to be able to assist the user during locomotion and compensate for its weight, the robotic limbs must satisfy several requirements. First, their prismatic joints must be able to exert enough force to bear the full weight of the user (max force: 500 N for each robotic limb). Moreover, the range and speed of the extension and retraction movements of the prismatic joints must be compatible with the most common locomotion modes of adult humans. In order to clear the ground during walking and to follow the user during sitting/standing (see Chapters 8 and 9), the prismatic joint needs a range of 0.3m and a maximum speed of at least 0.5 m/s. The weight and mass distribution of the robotic limbs are essential, too. The target weight for the whole limb assembly is 0.75 kg, and its center of mass should be as close as possible to its base in order to minimize the moment of inertia.

The actuation solutions most commonly adopted for linear motions in robotic systems have limitations that prevent them from being employed in the SRL. Linear electric actuators require extremely high gear ratios to generate enough support forces and maintain a light weight. This makes them too slow to effectively assist a human user during normal locomotion activities. For example, a typical high-performance linear motor (model: FA-05-12-18; manufacturer: Firgelli, USA) can provide enough force and range of motion, but has a maximum speed of only 0.02 m/s and an excessive weight (1.7 kg). Additionally, the high gear ratio of the ball screw transmission makes the actuator non-backdrivable. As a consequence, when the robotic limbs contact the ground the impact force is directly transmitted to the hip of the user through the rigid structure of the actuator. Therefore, compliant linear actuators are necessary to ensure the comfort of the user when providing walking assistance. Other common solutions such as hydraulic actuators are not suitable for the SRL, because they require pressurized oil lines and noisy, heavy pumps that would exceed the weight and volume requirements of the robot. Substituting the prismatic joint with a rotational elbow joint actuated by an electric motor is not feasible, because when the elbow is significantly flexed the torque required to bear the user's weight vastly exceeds the

capabilities of standard lightweight servomotors (see Chapter 5).

Choosing a pneumatic cylinder to actuate the prismatic joint of the robotic limbs allowed us to meet all of the above mentioned requirements. The custom cylinder (manufacturer: Numatics, USA) is realized in aluminum and steel, and has an internal diameter of 25mm and a stroke of 0.3m (Figure 8). With a pressure of 10 bar, it is able to generate the required force and to move at the target speed. The mass of the cylinder is 0.306 kg. For testing purposes we used an external pressurized air source to power the pneumatic actuators. However, the cylinders could be easily made tetherless by providing the robot with a compressed air canister.

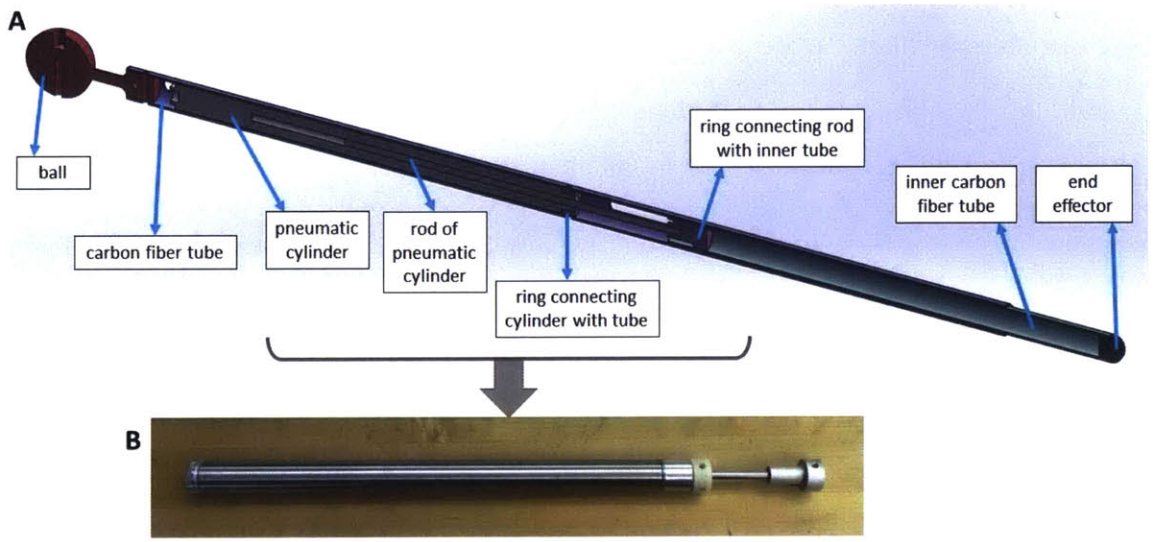

Figure 3-8: Structure of a robotic limb. A) Components of the robotic limb, displayed through a section view. B) Pneumatic cylinder actuating the prismatic degree of freedom.

The structure of the robotic leg is outlined in Figure 8. The pneumatic cylinder is placed inside a carbon fiber tube. The rod of the cylinder is fixed to a second carbon fiber tube, sliding inside the first one. This way, the external tube acts both as a structural element for the limb, and as a linear guide for the prismatic joint. Two slots at the side of the outer tube ensure that the output tube cannot rotate about the axis of the limb. The screws securing the output tube to the rod of the cylinder slide inside the slots, preventing any rotation. The extension and retraction movements of the pneumatic cylinder are controlled with a 5/3 valve (manufacturer:

Festo). The valve is fixed to the outer side of the larger carbon tube, weighs only 0.2 kg and requires a single input pressure line. Finally, the end effector of the robot is bolted at the end of the output carbon tube. The weight of the complete leg assembly is 0.670g, and its center of mass is located less than 0.2 m away from the center of the ball joint.

The robotic limb is equipped with a magnetic potentiometer sensor, which measures the position of the output tube along the stroke of the joint. This sensor is robust to misalignment, vibration and impacts, and its light weight makes it an ideal choice for the SRL. We also tested a compliant force sensor mounted between the output carbon tube and the end effector. The sensor (model: OMD-30-FE-450N, manufacturer: Optoforce) is realized in polyurethane and has a 200% overload tolerance, making it suitable to resist to the impacts that characterize human locomotion [15]. These impacts would easily break conventional, rigid load cells.

We developed a control algorithm that employs the 5/3 pneumatic valve to regulate the position of the cylinder. The algorithm is described more in detail in Chapter 8. For now, it suffices to specify that the valve does not have pressure regulation. It can only operate in one of three states: in the default configuration, the output rod is locked in place and the cylinder behaves like a spring-damper. When opening the valve on one side of the cylinder, the rod extends. When opening the other valve, the rod retracts. When one of the two valves is open, the other discharges the compressed air in the atmosphere, through a silencer. The operation noise of the robot is very quiet if a compressed air canister is used to power the cylinders. The control algorithm for the position of the linear degree of freedom first checks the current location of the output, and compares it with the desired position. It then checks on a lookup table what the desired opening time for the corresponding valve is. The valve opening time required to achieve a particular displacement is a function of the pressure inside the cylinder, and of the location of the output rod along within its range. We recorded these values with extensive experiments (see Chapter 8), and interpolate the valve commands starting from the measured values. Once the algorithm determines which valve has to open and for how long, it sends the command. After the valve has

executed the commands, the algorithm repeats the cycle. The sampling frequency of the control loop is variable, because the algorithm is repeated after the (variable) valve opening time has passed. The minimum sampling frequency, however, is 50 Hz. This algorithm is able to track the desired position with an accuracy of about $\pm$ 5 mm, which is enough for locomotion tasks (Chapter 8).

In conclusion, the choice of a pneumatic actuation system for the prismatic joint enabled us to realize a robotic limb which is lightweight, strong and fast. Its built-in physical compliance - the cylinder behaves like a spring-damper - allows the robot to avoid large impacts when contacting the ground, and increases the comfort of the user. Moreover, the standard locked configuration of the pneumatic valve does not consume any energy. This means that the robotic limb is able to efficiently compensate for a constant force, increasing the system's autonomy when running on a limited supply of compressed air.

3.5 End effectors

The end effectors of the SRL are mounted on the carbon tube actuated by the output of the pneumatic cylinder (Figures 8 and 9). The end effector is the most distal part of the wearable robot, and therefore it is essential to minimize its mass in order to limit the metabolic cost of wearing the robot [13]. This component of the system must also be small, in order not to interfere with the natural movements of the user as the robotic limbs provide assistance. Since the SRL is used in many tasks - from locomotion to heavy industry - that require the robot to bear significant loads, its end effectors should be able to withstand large forces and periodic impacts. As we will see in the rest of this section, achieving these goals while respecting our tight weight constraints often requires the use of underactuated or passive mechanisms.

The end effector used for locomotion tasks (Figure 9) is a typical example of this simplification. It is composed of a passive rubber joint, connected with a triangular base that makes contact with the ground. The presence of the passive joint allows the end effector to adapt to any inclination of the ground when pressed against it.

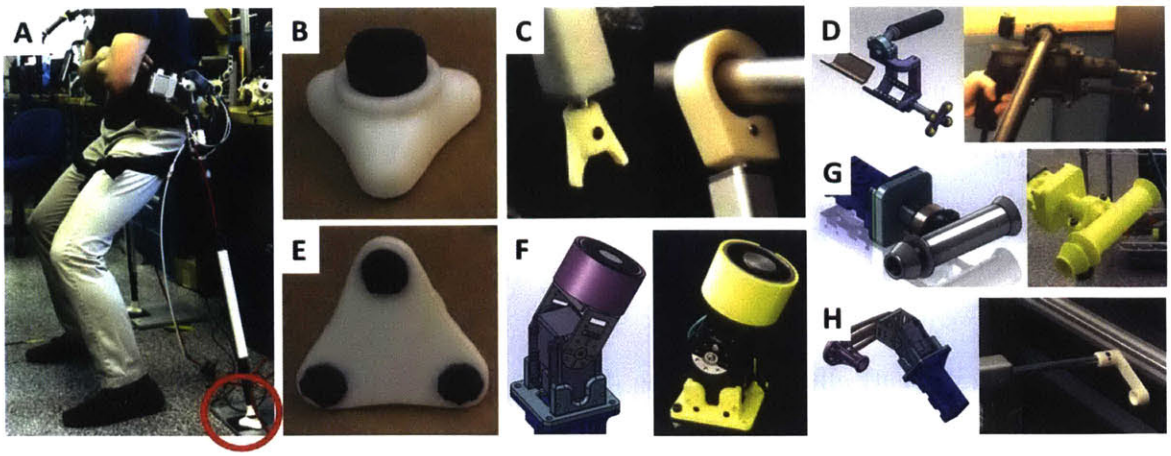

Figure 3-9: End effectors developed for the SRL. A) The SRL provides assistance to the user during sitting/standing motions. The end effectors adapts to the ground and makes full contact with it thanks to the deformation of its passive rubber joint. B,E) Passive end effector employed in locomotion tasks, suck as waking and sitting/standing assistance. C) Passive hooks used to secure the SRL to scaffolds or truss structures. F) End effector composed of an electromagnet and a powered wrist with one actuated degree of freedom. D,G,H) Task-specific end effectors developed for assisting aircraft manufacturing workers (power drill support, vacuum cleaner, drill bit support).

At the same time, the absence of active motors reduces the weight of this component to the minimum (less than 100g). The base of the end effector is triangular in order to extend the surface of contact with the ground, while maintaining a small overall volume. Additionally, three rubber cylinders located at the corners of the triangular base increase friction with the ground and limit the risk of slipping.

Other types of end effectors can be designed in order to secure the robotic limb to the environment. This is useful when the robot stabilizes the user when executing complex tasks, provides assistive forces to avoid fatigue, or increases safety by anchoring the human to a structure (Chapters 4, 5, 6 and 7). Some designs and prototypes of these end effectors are displayed in Figure 9. The simplest models consist of passive hooks, designed in shapes that adapt to the kind of support offered by a particular environment. For example, semi-circular hooks are easily anchored to scaffolds and truss structures. When the environment does not offer obvious attachment features but is made of ferromagnetic material, an electromagnet represents a good end ef-

fector solution for the SRL. Electromagnets can quickly generate significant contact forces, but they must be approximately aligned with the surface where the robots is making contact. For this reason, it is useful to add at least one active degree of freedom to the wrist of the robotic limb. If the surface where the robot must attach its end effector is not ferromagnetic, a vacuum gripper could be used as a simple general-purpose solution.

Finally, specific end effectors can be developed to execute particular tasks. This is common in the manufacturing environment, where workers need robotic assistance while using specialized tools or performing specific actions (Chapter 6). Figure 9 shows some end effectors that have been designed to provide assistance during aircraft manufacturing. The drill bit guide provide support during a drilling task, and helps a worker locate and maintain the correct drilling position (Chapter 6). The power drill support compensates for the weight of the heavy tool, and the vacuum cleaner helps the worker by automatically removing dangerous dust and drilling chips when operating on composite materials.

Chapter 4

State Estimation

4.1 Introduction

In this chapter, we present the mechanical design of the first prototype of the Supernumerary Robotic Limbs (SRL). This system is characterized by the use of rotational elbow joints in the robotic limbs. These joints are actuated through a bowden cable transmission, connecting them with series elastic actuators located in the backpack structure of the device. This solution allows us to reduce the mass and the moment of inertia of the robotic limbs, while still using actuators with significant maximum torque specifications.

We then introduce the aircraft manufacturing scenario, an area of application where extra robotic limbs could bring significant benefits to human workers, reducing their fatigue and increasing their precision. In order to provide these assistive capabilities, the SRL must accurately estimate the state of the human, despite the presence of several user-induced disturbances. In the following sections, we will model the dynamics of the human-robot system and develop a Kalman filter approach to estimate the state of the SRL despite the involuntary wearerâĂŹs motion, and a method for improving the accuracy and stabilizing the human body and the SRL. This technique - named the "bracing strategy" - will be a central theme of this thesis.

4.2 Using additional limbs to assist aircraft assembly tasks

Aircraft assembly is a complex process, requiring both highly skilled human workers and specialized automatic machines. As aircraft technology advances and market demand increases, enhancing the productivity and the quality standards of this skilled labor force becomes central for the industry's success. The work reported in this chapter was motivated by the need for assisting human workers in aircraft manufacturing.

Aircraft assembly personnel is challenged by several factors: (1) the continuous aging of the workforce, (2) the increasing complexity of assembly tasks, and (3) the fatiguing nature of many operations. This industry sector has been characterized by a particularly sharp increase in the age of its employees, even in the context of an overall aging workforce [58]. Moreover, productivity is limited by several assembly operations requiring the coordination of multiple workers. In these cases a single worker executes the main task (such as fastening a heavy part), with one or more colleagues acting as assistants (simply lifting the part). Therefore, multiple qualified workers must execute trivial or repetitive actions instead of making use of their trained skills. Another limiting factor is represented by fatiguing or dangerous situations. Among manufacturing workers, overexertion represents the most common nonfatal injury, accounting for 23% of the total injuries [12].

Industrial robots could be used to address these problems. Machines can easily execute repetitive or heavy tasks, and are not affected by fatigue or comfort issues. In addition, they are characterized by high positioning accuracy and high productivity. On the other hand, robots can hardly replicate human workers' adaptability to unforeseen situations, or capacity to quickly learn and execute new tasks. Workers are also able to move in the tight spaces within the hull of an aircraft under construction, and can flexibly modify their work plans depending on the particular situation. It is thus apparent that machines and humans possess two unique and complementary skill sets, both essential to the efficient execution of aircraft assembly operations. The

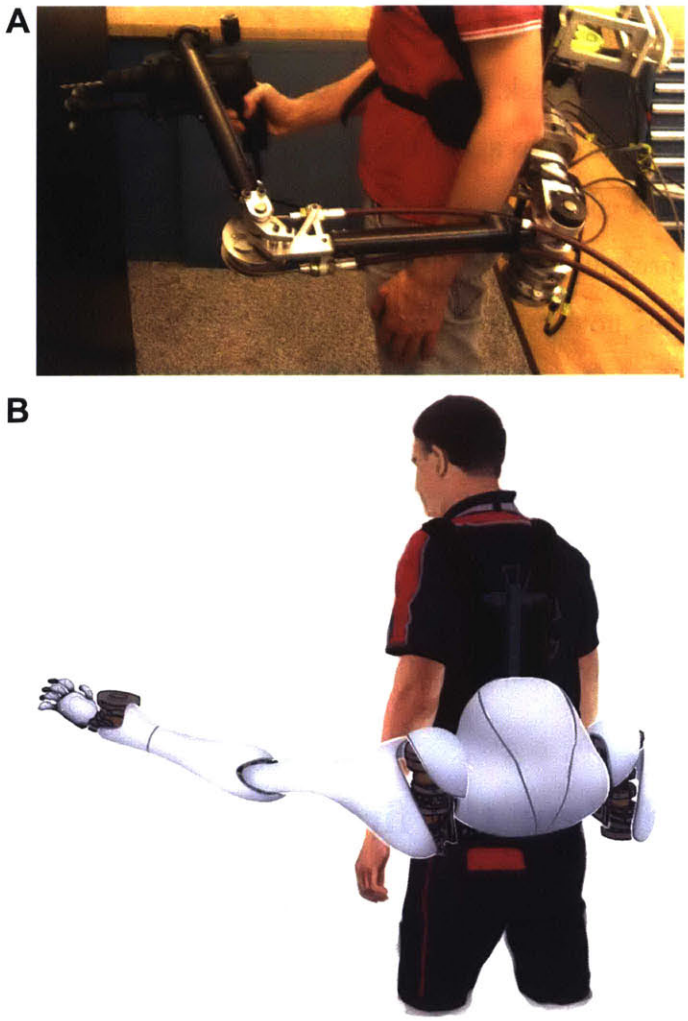

Figure 4-1: The initial Supernumerary Robotic Limbs (SRL) prototypes. A) First prototype. B) Concept of the second prototype.

solution that we propose is to provide the human workers with additional robot-like skills, by means of wearable robotic limbs.

Figure 1 illustrates the basic design concept of Supernumerary Robotic Limbs (SRL). The SRL have three main characteristics: they are wearable, independent, and multi-functional. Being wearable allows the robotic limbs to closely assist the worker at all times. They perform tasks together with the user, becoming almost an extension of the human body. Unlike an exoskeleton, which is attached directly to the human limbs, SRL is separated from the human limbs and thereby can take an arbitrary posture to best assist the wearer. Finally, the SRL can play multiple

roles, becoming extra legs as well as extra arms for supporting the human body and assisting in a manipulative task. They can exploit their large workspace to perform every action that is required to assist the user. Furthermore, they can also make use of interchangeable end effectors.

The SRL also presents several unique challenges. Unlike conventional robotic manipulators, it does not stand on a fixed base. And, unlike mobile robots, the movements of its base are not fully controllable or predictable. The SRL is worn by a human user who makes spontaneous movements and interacts with the environment. In consequence, the SRL is continuously disturbed by the human motion and interactions with the environment. This means that the robotic system must be capable of compensating for unpredictable disturbances. It is required to estimate its own state and attenuate the disturbances, providing the wearer with robot-like accuracy.

4.3 Robot design: the first SRL prototype

In this chapter, we present the first prototype of the SRL. The robotic system, consisting of a pair of robotic arms attached to a base unit, is worn with a backpack-like harness. The SRL base contains all the actuators and the main electronic components, and is located at the lower back, fixed to the iliac crest - the thick hip bone that provides the most stable base for the wearable robot. The robotic arms are attached to the SRL base at the level of the human hip, in order to maximize their workspace. They can interact with the environment in front and behind the wearer, and also reach the ground. The robot's weight is borne between the shoulder harness and the waist belt sitting on the iliac crest. The robot loads mainly the wearer's legs, without burdening the arms or the back [18]. Power is provided through a cable connected to the robot base. The tether is not a limitation in aircraft manufacturing, since workers usually operate tethered powered tools. The specifications of the robotic limbs have been inspired by the properties of the human arms in terms of torque, weight and joint series elasticity [49].

The robot has 6 degrees of freedom, 3 for each robotic arm - two in the shoulder

and one in the elbow. The shoulder flexion joint (range: 360 deg max torque: 69 Nm) is the most powerful and provides the torque necessary to lift objects in front of the user. The shoulder abduction and elbow flexion joints have identical specifications (range: 180 deg max torque: 39 Nm). The elbow actuator is placed in the SRL base, and its torque is transmitted to the joint via a cable system. This yields a significant reduction of the robotic arms mass and inertia [80]. Each axis is powered by a brushless DC pancake motor through a Harmonic Drive gearbox (1:50) and a series viscoelastic element (stiffness: 153 Nm/rad). The series elasticity at the drive train allows to a) decouple the load from the motor, b) robustly estimate the joint torque (measuring the spring deflection), and c) guarantee impact energy limits for the safety of the wearer [8]. The use of polyurethane (shear modulus: 0.003 GPa, elongation at break: 590%) allowed the realization of elastic elements smaller and lighter than conventional steel springs [18]. The behavior of viscoelastic materials can be effectively modeled and identified, enabling accurate force control [65].

4.4 Dynamic models

4.4.1 Equations of Motion of the Wearable Robotic System

The SRLs are worn by a human worker and thereby disturbed by involuntary movements of the wearer as well as by physical interactions with the environment. This section aims to analyze the dynamics of the human-SRL system, including a human model generating disturbances.

The reference scenario for this chapter is that a human worker standing in front of an aircraft fuselage, where some assembly operations requiring high accuracy must be completed. The worker is standing still, facing the hull, with the feet in contact with the ground. The worker is wearing the SRL, whose goal is to enhance the precision of the user. To achieve this goal, the wearable robot makes contact with the environment - in an aircraft assembly scenario, this could be achieved by grasping a structural beam - in order to attenuate the human-induced disturbances and improve

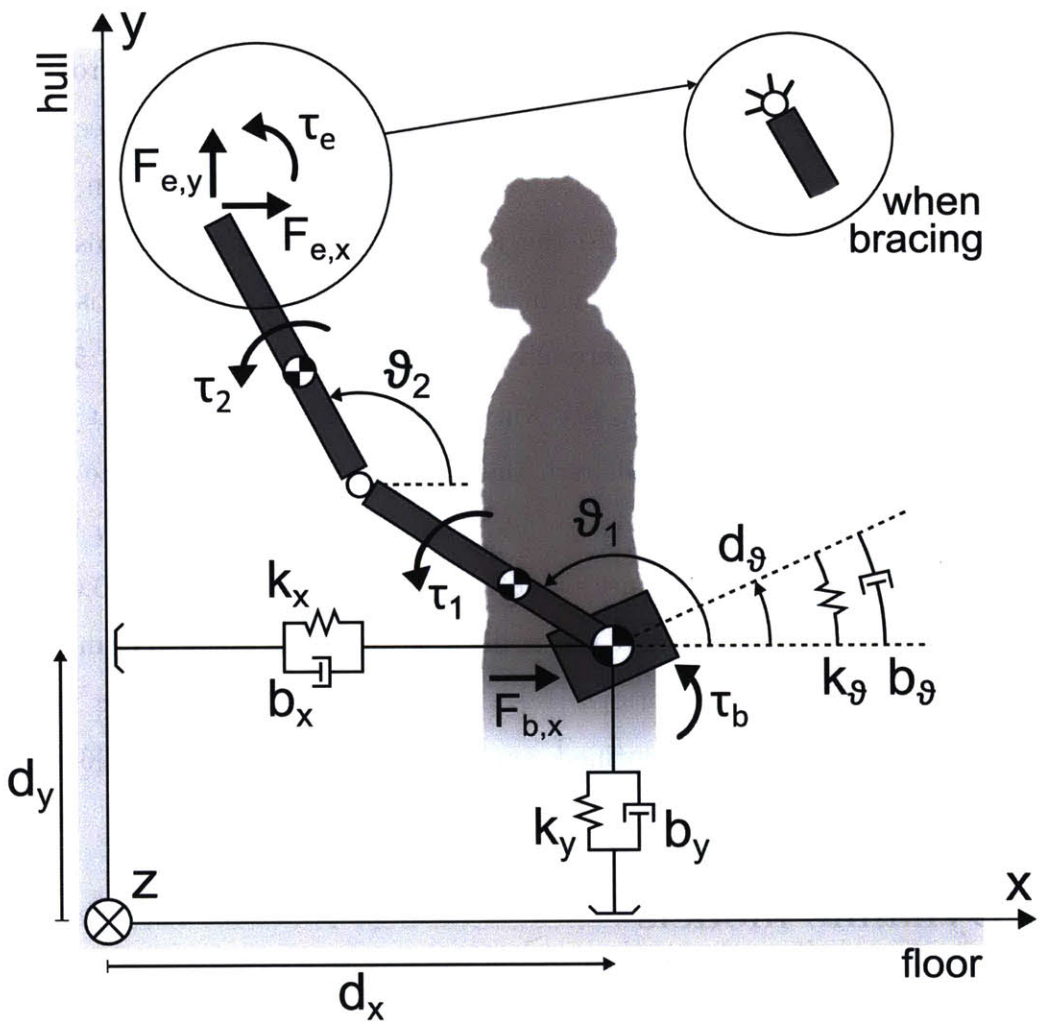

Figure 4-2: Dynamic model representing the user-SRL system.

the accuracy of state estimation. This is referred to as "bracing" of the human body with the SRL. When writing, humans often brace their hand on the desk to better position the pen. When taking a picture, photographers support their body by contacting the environment, or using a tripod. The SRLs can be used for bracing the wearer's body.

In order to create a complete but analytically tractable dynamic model of the reference scenario, it is necessary to make two main simplifying assumptions. First, the human-SRL system will be studied in 2D, considering the sagittal plane (see Figure 2). Although assembly operations require 3D actions, movements in the sagittal plane capture important aspects of the class of tasks considered in aircraft manufacturing.

The worker must often operate in very low or high segments of the fuselage (i.e. extending and contracting the body within the sagittal plane), which is ergonomically challenging. It is also difficult to perform an accurate task when working in uncomfortable postures. Furthermore, the human postural sway, which represents the major source of human involuntary disturbances, is more marked in the anterior/posterior direction (i.e. within the sagittal plane) [84].

The second assumption simplifies the modeling of the human legs and of the robot attachment to the human body. Instead of describing in detail the multi-dof dynamics of the legs and the deformable attachment mechanism, we lump their effects together about the hip equilibrium point with a three axis spring-damper system (two for x and y movements and the third one for rotation of the rigid robot base). For a single robotic limb attached to the human, the resulting model consists of three rigid bodies: two arm links and the base suspended by the three-axis spring-dampers, as shown in Figure 2. The model can be extended to describe a human arm. In this case, the values of the spring-dampers at the base will change to represent the human kinematic chain up to the shoulders.

The model has 5 generalized coordinates (d_x, d_y, $d\vartheta$, ϑ_1, ϑ_2). The inputs are the motor torques (τ_1, τ_2), the external forces at the end effector ($F_{e,x}$, $F_{e,y}$ and τ_e) and the human-induced disturbance force and moment at the robot base ($F_{b,x}$ and τ_b). Considering relatively slow movements, the Coriolis and centrifugal terms can be ignored and the equations of motion can be linearized as:

$$[M_T]\begin{bmatrix}\Delta\ddot{d}_x\\ \Delta\ddot{d}_y\\ \Delta\ddot{d}_\vartheta\\ \Delta\ddot{\vartheta}_1\\ \Delta\ddot{\vartheta}_2\end{bmatrix}+[B_T]\begin{bmatrix}\Delta\dot{d}_x\\ \Delta\dot{d}_y\\ \Delta\dot{d}_\vartheta\\ \Delta\dot{\vartheta}_1\\ \Delta\dot{\vartheta}_2\end{bmatrix}+[K_T]\begin{bmatrix}\Delta d_x\\ \Delta d_y\\ \Delta d_\vartheta\\ \Delta\vartheta_1\\ \Delta\vartheta_2\end{bmatrix}=[P_T]\begin{bmatrix}\Delta F_{b,x}\\ \Delta\tau_b\\ \Delta\tau_1\\ \Delta\tau_2\\ \Delta F_{e,x}\\ \Delta F_{e,y}\\ \Delta\tau_e\end{bmatrix} \tag{4.1}$$

The constant matrices M_T, B_T, K_T and P_T are reported in Appendix A. Among

the system inputs, only τ_1 and τ_2 are actuated. The other inputs are exogenous disturbances.

When the robotic arm grasps a solid structure in order to assist the user with the bracing strategy, the system loses two degrees of freedom. The end effector of the robot is not free to move anymore, and the whole robotic arm is hinged to the wrist (see Figure 2, insert). The linearized equation of motion of the bracing SRL (generalized coordinates: $d\vartheta$, ϑ_1, ϑ_2) are as follows

$$[M_B]\begin{bmatrix}\Delta\ddot{d}_\vartheta\\ \Delta\ddot{\vartheta}_1\\ \Delta\ddot{\vartheta}_2\end{bmatrix}+[B_B]\begin{bmatrix}\Delta\dot{d}_\vartheta\\ \Delta\dot{\vartheta}_1\\ \Delta\dot{\vartheta}_2\end{bmatrix}+[K_B]\begin{bmatrix}\Delta d_\vartheta\\ \Delta\vartheta_1\\ \Delta\vartheta_2\end{bmatrix}=[P_B]\begin{bmatrix}\Delta\tau_1\\ \Delta\tau_2\\ \Delta F_{b,x}\\ \Delta\tau_b\end{bmatrix} \tag{4.2}$$

The constant matrices M_B, B_B, K_B and P_B are omitted for brevity. This system is still disturbed by the human-induced forces $F_{b,x}$ and τ_b, but is not influenced anymore by the end effector forces (which are now ground reaction forces).

4.4.2 Human Disturbances Model

The SRL are worn by a human user, and their control strategies must therefore take into account the disturbances caused by involuntary human motions. When the user is standing still during the execution of an assembly task, these motions usually belong to two general groups: postural sway and physiological tremor [35]. Postural sway designates the center-of-mass oscillations resulting from the neuromuscular control of balance in quiet standing. An upright human can be modeled as an inverted pendulum. In order to keep this unstable standing position, the neuromuscular system exerts a restoring force which can be modeled as a spring, resulting in approximately undamped oscillations in the anterior/posterior direction [84]. This translational motion also produces an angular oscillation of the trunk. Therefore, the human-induced disturbances acting on the SRL base can be modeled as

$$\begin{cases} \Delta\ddot{F}_{b,x} = -\omega_s^2 \cdot \Delta F_{b,x} \\ \Delta\ddot{\tau}_b = -\omega_s^2 \cdot \Delta\tau_b \end{cases} \tag{4.3}$$

where ω_s is the sway frequency about which the expressions have been linearized. The sway frequency can be obtained from the literature [84], and is generally around 0.5 Hz. Incorporating the above human disturbance dynamics into the equations of motion yields an augmented state space system, which we will use for dynamic analysis.

Physiological tremor is a rapid, involuntary oscillatory movement of a body part with frequencies ranging from 10 to 15 Hz [56]. It characterizes all individuals and is caused by a variety of factors, ranging from central and peripheral nervous system activities to heart beat [5]. Tremor has been extensively studied for the development of surgical robots capable of rejecting user-generated disturbances [76]. Physiological tremor oscillations are smaller than postural sway, with a rms amplitude of 30 μm. It is thus possible to model tremor as white process noise acting on the three degrees of freedom of the SRL base.

4.5 Kalman filtering

The dynamic model developed above will be used for constructing a Kalman filter for estimating the state of the human-SRL system disturbed by the human and the environment. It will be shown that the state estimation accuracy depends on the SRL posture and that it can be significantly improved with bracing. We initially consider the state-space model describing the SRL when it is not making contact with the environment (Eq. 4.1). At the beginning of our analysis, the human-induced disturbances will be modeled as process noise, and the forces at the end effector will not be considered. The basic model will then be augmented to include the state equations of the external forces causing postural sway (Eq. 4.3), so that the disturbances can be estimated in real time.

4.5.1 Basic model of SRL and human-induced disturbances

The fundamental dynamics of the human-SRL system are described by the linearized equations of motion (Eq. 4.1), neglecting the external forces at the end effector and at the base. The state vector has dimension 10, and is composed by the generalized coordinates and their time derivatives: $x = [\Delta d_x, \Delta\dot{d}_x, \Delta d_y, \Delta\dot{d}_y, \Delta d_\vartheta, \Delta\dot{d}_\vartheta, \Delta\vartheta_1, \Delta\dot{\vartheta}_1, \Delta\vartheta_2, \Delta\dot{\vartheta}_2]^T$. The system has two inputs (τ_1, τ_2) and is controllable. Appendix B details the values of the constant parameters (the damping coefficient is set to 0.5, and originates from both the human soft tissues and the deformable backpack harness). The conversion of the system matrices from continuous-time to discrete-time allows the application of the discrete Kalman filter:

$$\begin{cases} x_{t+1} = A_t x_t + B_t x_t + G_t w_t \\ y_t = H_t x_t + v_t \end{cases} \tag{4.4}$$

w_t and v_t represent the process and measurement noises (zero-mean, white and uncorrelated, with covariance matrices Q_t and R_t respectively).

With this first basic system we do not intend to estimate the human-induced disturbance forces; instead we treat them as process noise. The noise characteristics may be obtained from published studies of involuntary human sway motion [84]. The typical values for the amplitude of the postural sway oscillations are denoted by $n_{x,nom}$, $n_{y,nom}$, $n_{\vartheta,nom}$. These oscillations affect the SRL base movement (Δd_x, Δd_y, Δd_ϑ and their derivatives). See Appendix B and [84]. We also take in account the variation of the postural sway oscillations as a function of the SRL base stiffness k_x, k_y and k_ϑ. These parameters have nominal values of $k_{x,nom}$, $k_{y,nom}$ and $k_{\vartheta,nom}$ (reported in Appendix B), but their values can be significantly increased when the human body is braced (see Section V). As the base stiffness increase, the human hip is more constrained and its oscillations decrease in amplitude, following the relations

$$\begin{bmatrix} n_x \\ n_y \\ n_\vartheta \end{bmatrix} = \begin{bmatrix} k_{x,nom}/k_x \cdot n_{x,nom} \\ k_{y,nom}/k_y \cdot n_{y,nom} \\ k_{\vartheta,nom}/k_\vartheta \cdot n_{\vartheta,nom} \end{bmatrix} \tag{4.5}$$

where the amplitude of the oscillations varies linearly with the base stiffness. The process noise on the SRL base velocity is derived from the conservation of energy in an undamped oscillator ($k_i n_i^2/2 = m_h v_i^2/2$). The resulting equations are

$$\begin{bmatrix} v_x \\ v_y \\ v_\vartheta \end{bmatrix} = \begin{bmatrix} \sqrt{k_x/m_h} \cdot n_x \\ \sqrt{k_y/m_h} \cdot n_y \\ \sqrt{k_\vartheta/J_a} \cdot n_\vartheta \end{bmatrix} \tag{4.6}$$

, where m_h and J_h are the mass of the human-SRL system and its inertia about the ankle (see Appendix B). Note that the process noise position and velocity amplitudes decrease if the stiffness parameters increase.

The process noise on the states representing the motion of the robotic arm ($\sigma_{\Delta\vartheta 1}$, $\sigma_{\Delta\dot{\vartheta} 1}$, $\sigma_{\Delta\vartheta 2}$, $\sigma_{\Delta\dot{\vartheta} 2}$) originates from the geometric tolerances of the manufacturing process, also reported in Appendix B. Process noise on these states is not influenced by the stiffness parameters. Assuming that all the extra-diagonal terms are null, matrix Q_t can be written as

$$\begin{aligned} Q_t = diag(&n_x^2\,,\, v_{x,n}^2\,,\, n_y^2\,,\, v_{y,n}^2\,,\, n_\vartheta^2\,,\, v_{\vartheta,n}^2\,, \\ &\sigma_{\Delta\vartheta 1}^2\,,\, \sigma_{\Delta\dot{\vartheta} 1}^2\,,\, \sigma_{\Delta\vartheta 2}^2\,,\, \sigma_{\Delta\dot{\vartheta} 2}^2) \end{aligned} \tag{4.7}$$

The diagonal elements are the variances of the process noise on the system states, which we conservatively assume to be equal to the squares of the amplitudes identified above. Matrix G_t, connecting the process noise on each state with the state equations, is equal to matrix A_t.

4.5.2 Effect of sensors choice on state estimation

The robotic limbs are equipped with quadrature encoders at the load side of every joint. A compact dual-camera motion capture system measures the position of the robot end effector. Additionally, the SRL base motion can be monitored with an inertial measurement unit (IMU) containing a 3-axis gyroscope and accelerometer,

which is capable of measuring absolute angular position and velocity (for the accuracy of the sensors, see Appendix B). Two different sensor sets can be considered. Set A uses only the encoders and the motion capture system:

$$y_A = \begin{bmatrix} \Delta\vartheta_1 - \Delta d_\vartheta & : \text{encoder} \\ \Delta\vartheta_2 - \Delta\vartheta_1 & : \text{encoder} \\ x_{end} & : \text{motion capture} \\ y_{end} & : \text{motion capture} \end{bmatrix} \tag{4.8}$$

Conversely, set B uses encoders, motion capture system, and IMU:

$$y_B = \begin{bmatrix} \Delta\vartheta_1 - \Delta d_\vartheta & : \text{encoder} \\ \Delta\vartheta_2 - \Delta\vartheta_1 & : \text{encoder} \\ \Delta d_\vartheta & : \text{IMU angle} \\ \Delta\dot{d}_\vartheta & : \text{IMU velocity} \\ x_{end} & : \text{motion capture} \\ y_{end} & : \text{motion capture} \end{bmatrix} \tag{4.9}$$

The linearized measurement matrices C_A and C_B corresponding to the two sensor sets are given in Appendix A. The measurement noise covariance matrix R_t is characterized by diagonal elements equal to the square of the accuracy of each sensor (a conservative estimate of the sensor noise variance). The off-diagonal elements are null.

The system is theoretically observable for both sensor sets A and B. In theory it is observable without the IMU. However, it is useful to quantify the difference between the two sensor configurations. A more informative evaluation of the observability can be performed by analyzing the evolution of the error covariance matrix P_t. The Kalman filter allows an off-line computation of the convergence of matrix P_t, which can be used to identify the optimal sensor set. Figure 3 shows the evolution of the diagonal elements of P_t, representing the a posteriori state estimation error variance for each state. It is evident that the error variance of $\Delta\dot{d}_\vartheta$ converges too slowly if the IMU is not used. Employing the full sensor set is therefore necessary to guarantee

the observability of the system in practice.

4.5.3 Effect of robot configuration on state estimation

When the robotic limbs move in their workspace, the system dynamics and the accuracy of state estimation vary as a function of the robot configuration. It is important to identify the areas of the workspace where the robot is most (or least) accurate, in order to evaluate if the assembly tasks accuracy requirements are met. It is well known that the trace of the covariance matrix P_t provides the mean squared error of a posteriori state estimation. Therefore, evaluating $trace(P_t)$ in every point of the workspace after a fixed number of iterations (100) provides a measure of the quality of state estimation corresponding to every robot configuration (Figure 4). The lower $trace(P_t)$, the smaller the state estimation error. From the estimation accuracy map in Figure 4, it can be observed that the quality of state estimation is worse in front

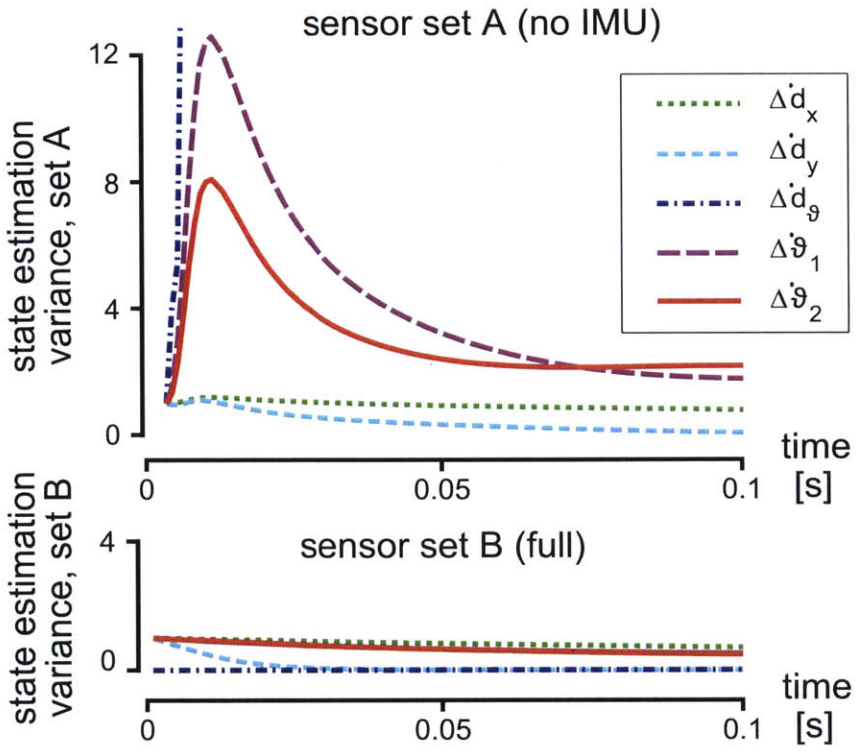

Figure 4-3: Sensor choice, based on error covariance. Above: sensor set A (without IMU). Below: sensor set B (encoders, IMU, motion capture).

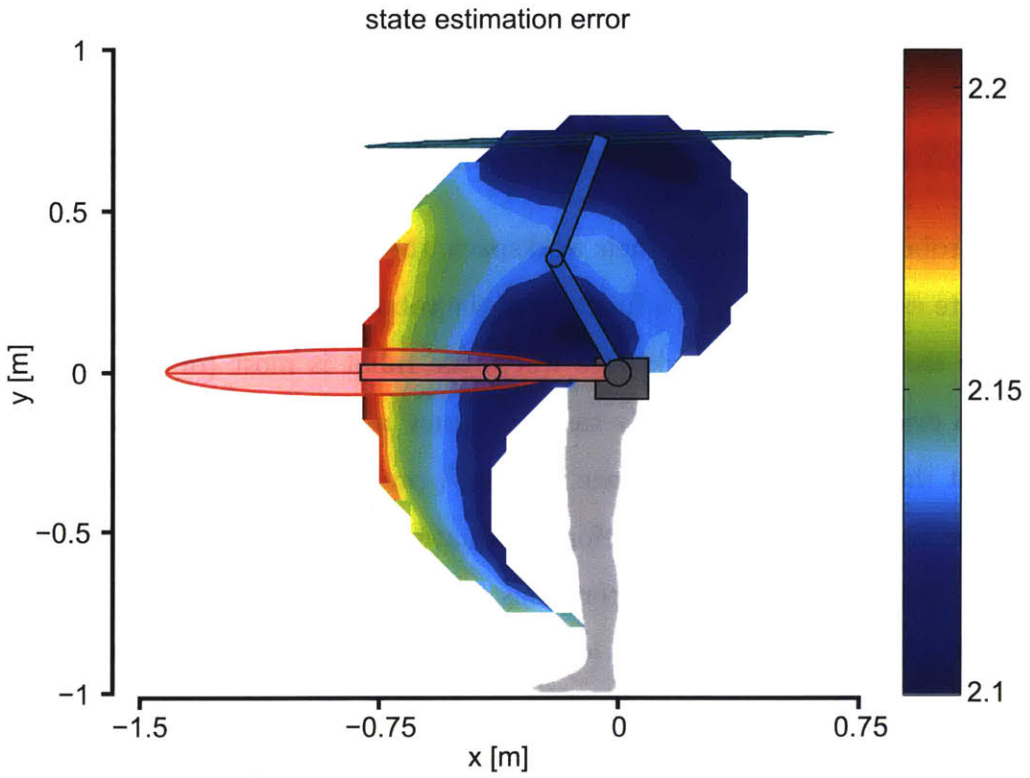

Figure 4-4: Mean squared error of a posteriori state estimation in the workspace of the SRL arm. The red ellipse represents the estimation error covariance of the end effector velocity in the configuration where the SRL is least accurate (red robotic arm). The blue ellipse represents the same error covariance, but in the configuration where the SRL is most accurate (blue robotic arm).

of the user, where it is needed the most for assembly operations. In order to improve accuracy, the bracing strategy is considered next.

4.5.4 Effect of bracing on state estimation

Securing its base to the fuselage wall, the SRL can significantly increase the stiffness with which it is suspended. Extending forward one robotic arm and grasping the structure of the aircraft will limit the SRL base motions in the horizontal direction, increasing stiffness k_x. We now consider the effects that this stiffness variation produces on state estimation error. Once again, the value of $trace(P_t)$ is calculated over the SRL workspace. In this case, though, we consider two different sets of stiffness parameters (Figure 5). In the first set, the value of k_x is increased to 10,000 N/m.

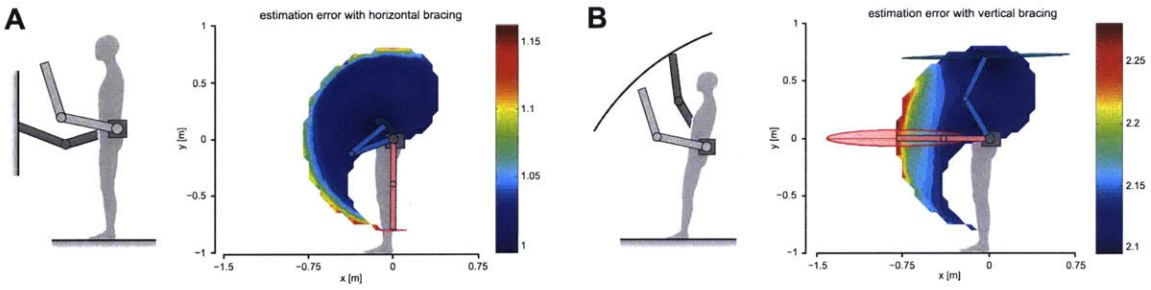

Figure 4-5: Mean squared error of a posteriori state estimation in horizontal bracing (A) and vertical bracing (B).

This is equivalent to one robotic arm grasping the environment in front of the user. Figure 5.A shows that this increased horizontal stiffness allows the other robotic arm - which is still free - to significantly reduce its state estimation error. Moreover, the area in front of the worker is now optimal in terms of accuracy, satisfying the requirements of precise assembly tasks. If the user has to operate on an elevated area of the aircraft hull (Figure 5.B), the SRL can grasp the roof with one robotic arm. This will result in an increase of the vertical stiffness k_y, which in turn will improve state estimation in the upper zone of the workspace.

4.5.5 Estimation of disturbances by using the augmented model

The external inputs to the SRL system can be divided into two categories: end effector forces and human-induced disturbance forces. The former can be assumed to be constant and measured with a force and torque sensor. The latter can be modeled as second order systems (see Section III), and Eq. 4.3 can be added to the state-space system. The augmented state vector will include one additional state for every end effector force and two additional states for every human-induced disturbance. The new state vector is

$$x_{aug} = [x^T, \Delta F_{b,x}, \Delta \dot{F}_{b,x}, \Delta \tau_b, \Delta \dot{\tau}_b, \Delta F_{e,x}, \Delta F_{e,y}, \Delta \tau_e]^T \tag{4.10}$$

Since the disturbances at the SRL base are now explicitly modeled, there is no need to consider them in matrix Q_t. The only process noise affecting the base of the

robot comes from physiological tremor (Appendix B). Its amplitudes are two order of magnitude smaller than postural sway, and do not vary with the stiffness parameters. Measurement matrix H_t and sensor covariance matrix R_t are extended to include the new force measurements.

The augmented system is observable, and measuring the end effector forces is essential to guarantee the convergence of all the elements of matrix P_t. The augmented system is not controllable, but this does not represent a problem since the state vector has been augmented in order to estimate the disturbances, and not to drive them to any arbitrary value. Figure 6 shows the value of $trace(P_t)$ in the robot workspace after 1,000 iterations. The state estimation error is suitably low in the area in front of the user.

The procedure described in this section can be repeated for the model of the bracing SRL (Eq. 4.2 and Figure 2, insert). Similar conclusions are found with respect to state estimation.

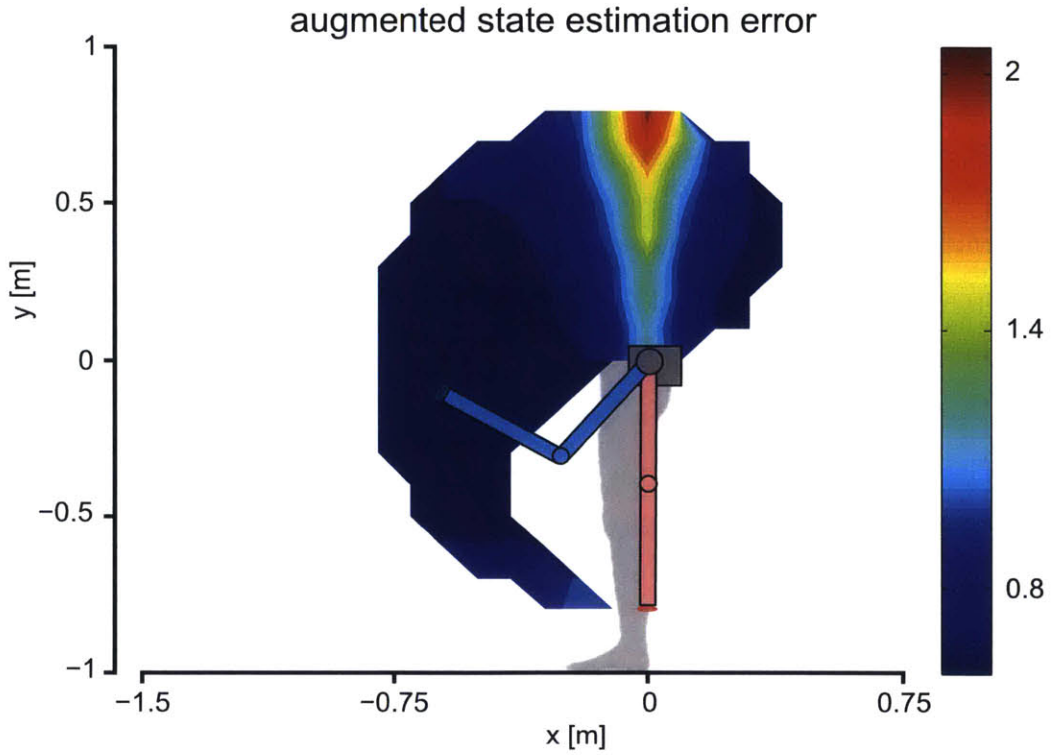

Figure 4-6: Mean squared error of a posteriori state estimation in the workspace of the SRL arm (augmented model).

4.6 Bracing strategy

It has been shown that the SRL base stiffness has significant effects on the accuracy of state estimation. The capability of shaping the base stiffness is therefore essential to maximize robot accuracy in the area of the workspace where the assembly task must be performed. The SRL can actively modulate the stiffness through bracing: utilizing the environment as a support by grasping it with a robotic arm. This section presents a method to identify the bracing configuration (the values of the robot joint angles ϑ_{r1} and ϑ_{r2}) that yields the SRL base stiffness closest to a desired value.

The endpoint stiffness matrix of a kinematic chain describes the relationship between end effector displacements Δp and applied forces F:

$$F = S \cdot \Delta p \tag{4.11}$$

, where $F = [F_x, F_y]^T$ and $p = [\Delta p_x, \Delta p_y]^T$. The endpoint compliance matrix C is the inverse of S, and both matrices are symmetric. We assume that the kinematic chain is composed by rigid bodies and elastic joints, characterized by a linear torque-displacement relationship ($\tau_i = k_i * \Delta\vartheta_i$). In this case, matrix C can be calculated as

$$C = JK^{-1}J^T + H \tag{4.12}$$

, where J is composed by the first two rows of the Jacobian matrix, K is the diagonal matrix containing the joint stiffnesses k_i and H is an Hessian term [78]. The Hessian term can be ignored if the rate of change of the Jacobian is small. The analytical expression of C in the case of a 2 links manipulator is straightforward [78]. Inverting C yields the stiffness matrix S, which is a function of the manipulator configuration. The analytical expression of S, derived in Appendix C, can be used to compute the endpoint stiffness of a 2 link kinematic chain given its dimensions, joint stiffnesses and joint angles. These values are known or can be measured for the worker legs (Figure 7), which in the sagittal plane can be approximated as a 2 link

manipulator. It is thus possible to calculate the hip stiffness matrix produced by the legs of the SRL user. This stiffness matrix, neglecting the backpack compliance, will characterize also the motion of the SRL base (the SRL is worn at the human hip).

If the SRL employ the bracing strategy, the robotic arm that grasps the environment will form a closed kinematic chain together with the user's legs. The total stiffness matrix at the human hip (or SRL base) will therefore be equal to the sum of the stiffness produced by the user legs and the stiffness produced by the bracing robotic arm

$$S_{tot} = S_{human} + S_{robot} = S_h + S_r \tag{4.13}$$

The objective of bracing is to make S_{tot} as close as possible to a given S_{des}. The component S_r varies depending on where the SRL grasp in the environment, i.e. the configuration of the robotic arm ($\vartheta_{1,r}$ and $\vartheta_{2,r}$). Rewriting the above expression yields:

$$S_{ij,r} = S_{ij,des} - S_{ij,h} = Q_{ij} \tag{4.14}$$

, where Q_{ij} are known constants. Note that $Q_{ij} = Q_{ji}$, because all the matrices are symmetric.

In order to optimize the robot configuration, we write the cost function

$$C_{ost} = \sum_{i=1}^{2}\sum_{j=1}^{2}(S_{ij,r} - Q_{ij})^2 \tag{4.15}$$

, which decreases as S_{tot} approaches the target S_{des}. The cost function C_{ost} depends only on ϑ_{r1} and ϑ_{r2}, the joint angles of the bracing robotic arms. Therefore minimizing the cost function yields the optimal robot bracing configuration, which will produce a SRL base stiffness as close as possible to the desired one. Figure 7 shows the cost function when the user is standing ($\vartheta_{h1} = 80^o$, $\vartheta_{h2} = 110^o$), and all the human and robot joints have a stiffness of 150 Nm/rad. The desired stiffness matrix is $S_{des} = diag(10,000, 10,000)$.

4.7 Conclusions

We presented the first prototype of the Supernumerary Robotic Limbs (SRL), a wearable robot designed to assist human users in complex assembly tasks. The system's mechatronic structure has been described, and a simplified dynamic model has been developed in order to study its behavior. We proposed the bracing strategy - consisting of grasping the environment - as a way for the robot to provide a firm support to the user, reducing the human-induced disturbances. We analyzed in detail the effects that sensor choice, robot configuration and bracing strategy have on state estimation.

The objective of the SRL project is to augment the skills of the human users, providing them with robot-like capabilities - such as precision, strength, endurance - and relieving them from the most tedious or fatiguing tasks. The development of wearable robotic limbs poses unique challenges, such as achieving accurate state estimation despite the unpredictability of the motion of the SRL user.

The main contributions of this chapter is the biomechanically motivated modeling of human-induced disturbances as process noise and additional state equations. Including these disturbances in the robot's dynamical model allows to identify a suitable sensor set and to develop control strategies capable of attenuating the perturbations. The bracing strategy can be used to shape the stiffness parameters at the base of the SRL, in turn reducing the state estimation error in the regions of the workspace where the user must be assisted.

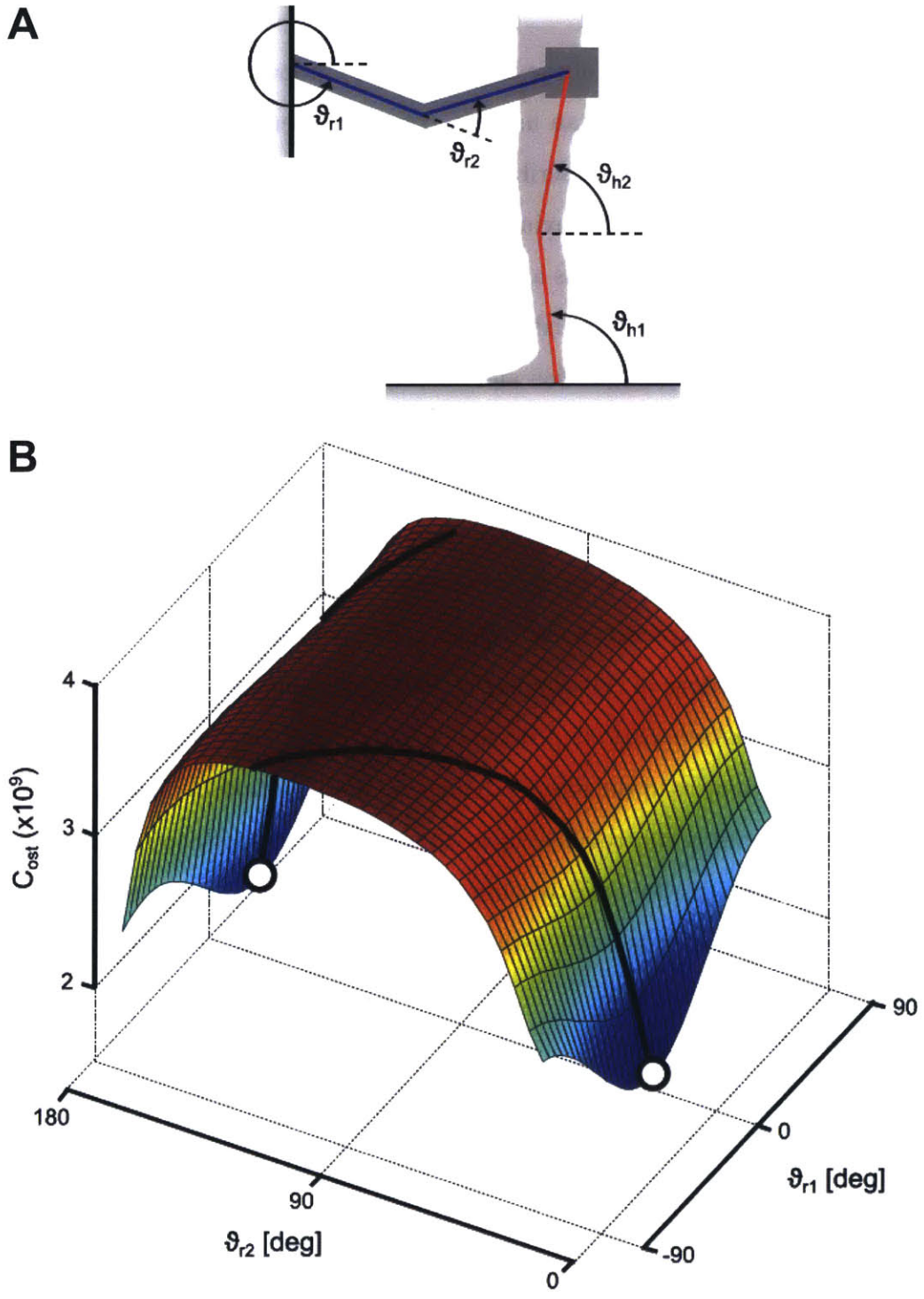

Figure 4-7: A) Scheme of the bracing strategy. B) Cost function used to find the optimal SRL bracing configuration. The cost is a function of ϑ_{r1} and ϑ_{r2}, the joint angles of the bracing SRL arm. The white dots represent the absolute minima of the cost function, while the black lines are obtained imposing ϑ_{r2} and finding the value of ϑ_{r1} that minimizes the cost.

Chapter 5

Bracing Strategy: 2D Analysis

5.1 Introduction

This chapter presents the second prototype of the Supernumerary Robotic Limbs (SRL), and its application to the support of the body weight of aircraft workers [66]. This version of the system keeps the rotational elbow joints of the previous prototype. In this case, however, these joints are actuated through a timing belt transmission. The timing belt motion is controlled by a series elastic actuator located at the base of the robotic limb. The series elastic actuators employed in this robot have been custom designed to provide high maximum torque and high torque sensing accuracy.

In the following sections we apply the âĂIJbracingâĂİ strategy - introduced in the previous chapter - for supporting the human body, compensating for its weight. We begin with a mathematical analysis of the load bearing efficiency, which proves the potential of an augmentation strategy based on additional extra limbs that are independent from the human body. The optimal SRL posture and joint torques are then obtained in order to minimize the human load. Finally, numerical and experimental results demonstrate the effectiveness of the proposed method.

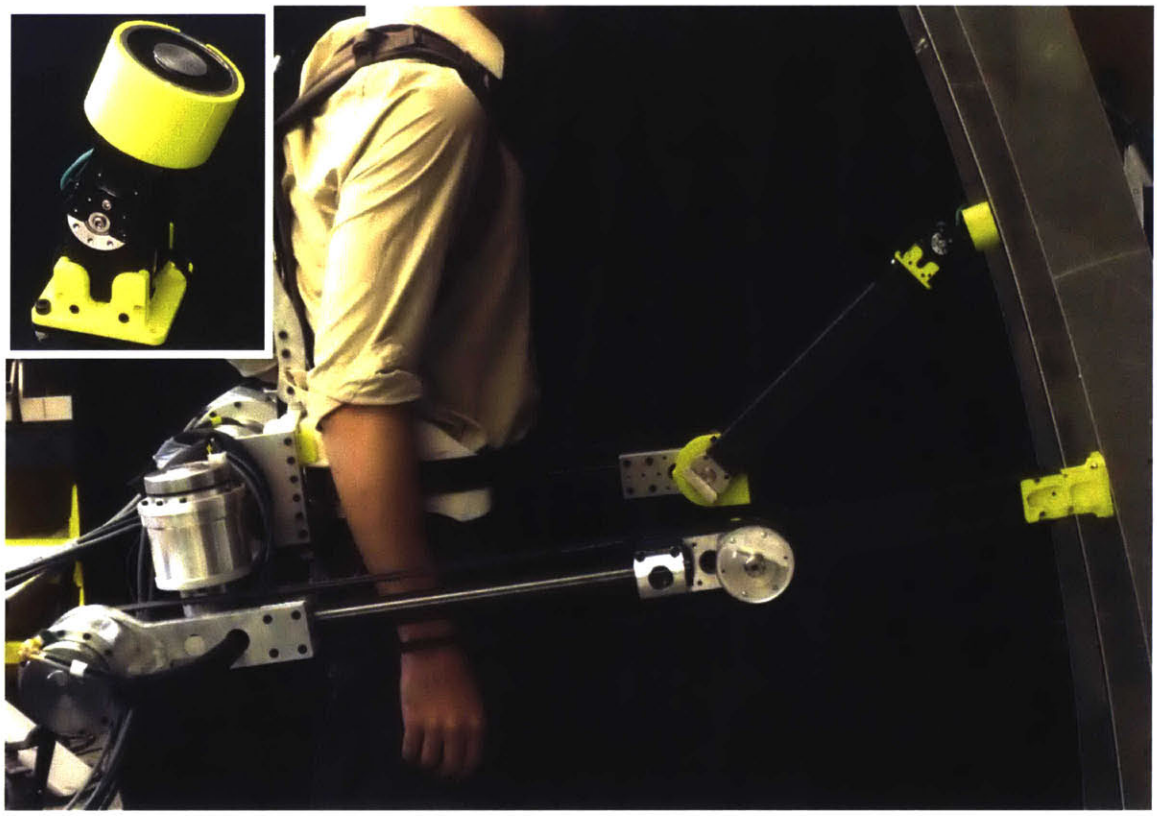

Figure 5-1: The SRL prototype. A 3D printed waist brace connects the robot to the lower back of the user. Three series viscoelastic actuators and a servo control the robotic arm degrees of freedom (two in the shoulder, one in the elbow, one in the wrist). The elbow actuator trasmits torque to its joint through two timing belts. The insert shows the model of the servo-actuated wrist, equipped with an electromagnetic gripper.

5.2 Robot design: the second SRL prototype

In this section, we present the design and implementation of the second prototype of the Supernumerary Robotic Limbs (SRL). The system consists of a pair of wearable robotic limbs that can intuitively and safely assist the human (Figure 1). A detachable 3D printed waist brace forms the interface between the human and the SRLâĂŹs base structure. Its ergonomic shape ensures that the robot rests on the iliac crest, the thick edge of the hip bone, and that the robotâĂŹs weight is directed to the legs and away from the spine [18]. Shoulder straps and a waist belt secure the SRL to the user. Each robotic limb is attached to a side of the base structure, and is provided with 4 degrees of freedom – two near the base (shoulder), one in the middle (elbow), and

one at the end effector (wrist). The range of the robot joints allows the end effectors to reach the majority of the human limbs workspace (both legs and arms) in order to provide assistance where needed.

The specifications of the joints are designed to match human performance in terms of torque and weight [49]. The shoulder flexion joint, which is the most powerful joint and has to lift objects in front of the human, has a 270-degree range of motion and a maximum torque of 69 Nm. The shoulder abduction and elbow flexion joints, which are orthogonal to the shoulder flexion joint and experience little gravity load, have a maximum torque of 39 Nm. The shoulder abduction joint has a 90-degree range of motion, while the elbow flexion joint has a 180-degree range of motion. Each joint is actuated by a brushless DC motor through a Harmonic Drive gearbox (50:1).

To minimize the robotic limbs moment of inertia and to reduce power consumption, the elbow actuator is placed immediately behind the shoulder as a counterweight. Torque is then transmitted to the elbow using two 12 mm wide, 5 mm pitch GT2 timing belts. The robotic arms are designed to allow internal routing of signal and power wires for the end effectors. A series viscoelastic element having stiffness of 153 Nm/rad is placed between each joint and its gearbox. This added elasticity a) decouples the gearbox and motor, b) provides low-cost and robust torque sensing (using encoders to measure deflection), and c) guarantees safety in case of impact [80] [65] [8]. The viscoelastic element, made of polyurethane rubber, allows the achievement of the desired joint stiffness with a significant reduction in mass and size with respect to a traditional steel coil spring [49].

One additional degree of freedom is placed at the wrist, and controlled with a servo motor. The robotic arm can be equipped with various end effectors, tailored for different tasks. For this chapter, an electromagnet (weight: 275 g, max holding force: 490.5 N) is mounted on the wrist output flange (see Figure 1, insert). The electromagnet allows the robotic arm to easily make contact with the environment. The wrist actuator is used to orient the outer surface of the magnet (a disk with D = 50 mm) so that it is parallel to the desired surface of contact. The magnetic force is then activated and guarantees a firm grip. This hoding system is faster and avoids the

extra weight and complexity of a robotic gripper or hand. If the environment does not present any ferromagnetic surfaces, a vacuum gripper (such as the Joulin FlexiGrip GS120) could replace the electromagnetic end effector. Vacuum can be created with a Venturi valve, using the compressed air system available in the aircraft factory.

5.3 Bracing and load bearing analysis

5.3.1 The Bracing Strategy

Workers in the aircraft assembly process must perform complex tasks, requiring high precision and substantial physical effort. The SRL assists the human in these demanding situations, increasing their accuracy and reducing their fatigue. In this section we present the strategy used by the SRL to provide support to the wearer, and analyze the effectiveness of load bearing in comparison to exoskeletons.

Unlike an exoskeleton, where powered joints are attached to the human joints and move together with the human, the Supernumerary Robotic Limbs can make contact with the environment at any point within their workspace. By grasping or clamping structural elements such as aircraft beams or safety scaffolds, they can secure the human body to the environment, and thereby suppress disturbances and lower the load to be borne by the human. In other words, this strategy allows the robot to brace the human body against an external structure. Therefore, we call it the "bracing strategy".

In the previous chapter, the bracing strategy has been applied to increase the equivalent stiffness at the hip of the user, thereby reducing disturbances and increasing accuracy [68]. In this chapter, we will apply the bracing strategy in order to minimize the torques that the human joints must exert to hold a weight or to keep an uncomfortable position. An exemplary case study considered in this chapter is to support an aircraft assembly worker in performing a task on the floor or at a very low position of the airplane structure. Examples of such tasks include fuselage assembly, routing wires, fastening seats, and performing quality checks. All of these operations

require holding a crouched position for extended periods of time, suppressing oscillatory movements, and stabilizing the body in order to guarantee the precision of the task execution. Maintaining uncomfortable postures may accelerate fatigue of the workers, reducing their productivity and even posing risks to their health [12]. Wearable robots such as exoskeletons or the SRL can be used to support the workers and reduce their fatigue. In this chapter, we will focus on load bearing capacity and compare the efficiency and effectiveness of SRLâĂŹs bracing strategy against leg exoskeletons. We consider the case where the worker is standing in front of the aircraft fuselage with both feet in contact with the floor, and the torso is leaning forward in order to perform the assembly task at a low position.

Figure 2 shows the kinematic model used for analyzing the load bearing characteristics of the SRL bracing strategy compared to a leg exoskeleton. Four simplifying assumptions have been adopted in the analysis of the problem. First, the model is composed by rigid links and rotational joints, and neglects the compliance of the human-robot interface. It also lumps SRL base and human torso in a single rigid body. These simplifications are possible because small deflections due to compliance do not influence the static distribution of torques between the robot and the human, which is the objective of this analysis. Second, we assume that the robot can securely grip the environment, e.g. a fuselage structure, so that no slip occurs at the contact point. This can be achieved using an electromagnet whose holding force can generate enough static friction to secure the grip (see Section II). Third, the analysis assumes that the robot links as well as the human and exoskeleton links are mass less. The effect of link mass can be included, but it makes the analysis unnecessarily complex. Finally, the model considers half of the human-robot system: it includes one human leg and one robotic limb.

As shown in Figure 2, the system consists of one SRL, human leg and torso. The position and orientation of the human torso that is aligned with the SRL base is denoted by a 3-dim vector, $p = [x_G, y_G, \beta_{torso}]^T$. The human torso combined with the SRL base link weights m kg with a center of mass above the SRL base. This creates a gravity load, $f_{x,ext} = 0$, $f_{y,ext} = -mg$, as well as a moment about the hip joint,

$\tau_{ext} = m\ g\ d_w \cos(\beta_{torso})$. Collectively, the external load to be borne by the human and the robot is expresses by a 3-dim vector, $F_{ext} = [f_{x,ext}, f_{y,ext}, \tau_{ext}]^T$.

5.3.2 Load Bearing Analysis

The basic equations that describe the static torque-force relationships of the system are as follows. For the robotic limb, the endpoint forces F_R are related to the joint

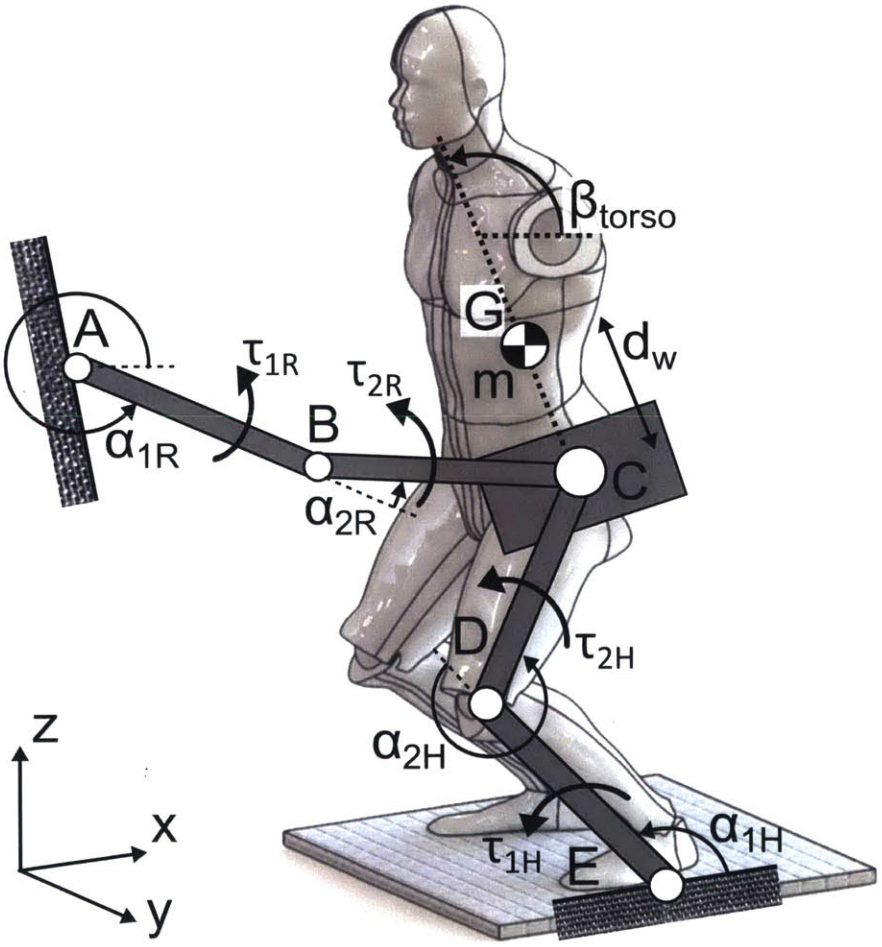

Figure 5-2: The model used to study the bracing strategy. All the angles are measured at the joints, except for β_{torso} which indicates the orientation of the human torso with respect to the x axis. Points A and B represent the SRL wrist and elbow. Points D and E represent the human knee and ankle. Point C represents both the SRL shoulder and the human hip. τ_{3R} and τ_{3H}, the torques exerted at the hip respectively by the SRL arm and the human leg, are not drawn here. Point G is the center of mass of the human torso. The general model is 3D. Its 2D projection on the xz plane is used in the computational example (Figures 3 and 4).

torques τ_R by the Jacobian matrix

$$\tau_R = J_R^T F_R \tag{5.1}$$

where the vector τ_R contains the torques at the joints of the robotic arm (wrist, elbow and shoulder). An analogous expression can be written for the human leg. In this case, the torques are referred to the ankle, knee and hip joints of the human. The expressions of the robot and human Jacobians J_R and J_H are reported in Appendix A.

Consider the total power consumed at the SRL for bearing the load. The power consumption can be written as

$$P_R = \tau_R^T W_R \tau_R \tag{5.2}$$

where W_R is a weighting matrix, which is positive-definite and symmetric. In case DC motors with torque constant K_{ti}, armature resistance R_{ti}, and gear ratio $1 : r_i$ ($r_i > 1$) are used for individual joints $i = 1, \ldots, n_R$, the weighting matrix is given by

$$W_R = diag\left(\frac{R_1}{r_1^2 K_{t1}^2}, \ldots, \frac{R_n}{r_n^2 K_{tn}^2}\right) \tag{5.3}$$

Substituting (1) into (2) yields

$$P_R = F^T J_R W_R J_R^T F \tag{5.4}$$

For comparison we consider an exoskeleton attached along the human leg, exerting joint torques on the human leg joints. The power consumption at the exoskeleton can be derived in a similar manner,

$$P_E = F^T J_E W_E J_E^T F \tag{5.5}$$

Notice that $J_E = J_H$, because the exoskeleton is constrained to follow the human leg kinematics. Our special interest is to assist the human when he/she has to squat in order to reach a very low point, as illustrated in Figure 2. At this posture, the

exoskeleton, which has to take the same posture as the human, is not advantageous; the exoskeleton must bear the load in the same way as the human. To compare the load bearing efficiency, consider the quotient between the two: P_R/P_E,

$$\eta = \frac{P_R}{P_E} = \frac{F^T J_R W_R J_R^T F}{F^T J_E W_E J_E^T F} = \frac{F^T A F}{F^T B F} \tag{5.6}$$

where A and B are real, symmetric matrices given by

$$A \triangleq J_R W_R J_R^T \ , \ B \triangleq J_E W_E J_E^T \tag{5.7}$$

It is expected that the quotient η is smaller than 1 if the SRL takes a proper posture by bracing the human body against a wall, the floor, or a structure that it can contact. It is natural to assume that the posture of the exoskeleton as well as the human leg is not singular when half way crouching, as illustrated in Figure 2. Therefore, matrix B is assumed non-singular. Since the matrix A is symmetry and the matrix B is symmetry and non-singular, the quotient can be treated as a Rayleigh Quotient. Finding the minimum of the quotient is a generalized eigenvalue problem, and is given by the smallest eigenvalue of the following matrix:

$$\eta_{min} = \lambda_{min}(B^{-1}A) \tag{5.8}$$

If the SRL is at a singular configuration, it can bear a load with zero power consumption, as long as the load vector F is in the null space of matrix A:

$$\eta_{min} = 0 \ , \ P_R = 0 \ \text{ for } \ F \in N(A) \tag{5.9}$$

The Rayleigh quotient is small even at a non-singular SRL configuration, if the SRL posture is near singular and the load vector is nearly aligned with the null space of matrix A.

The SRL can take various configurations. Finding a right posture for bracing the human body is critically important for lowering the Rayleigh quotient, i.e. efficient load bearing. The following section will address how to find the right posture that

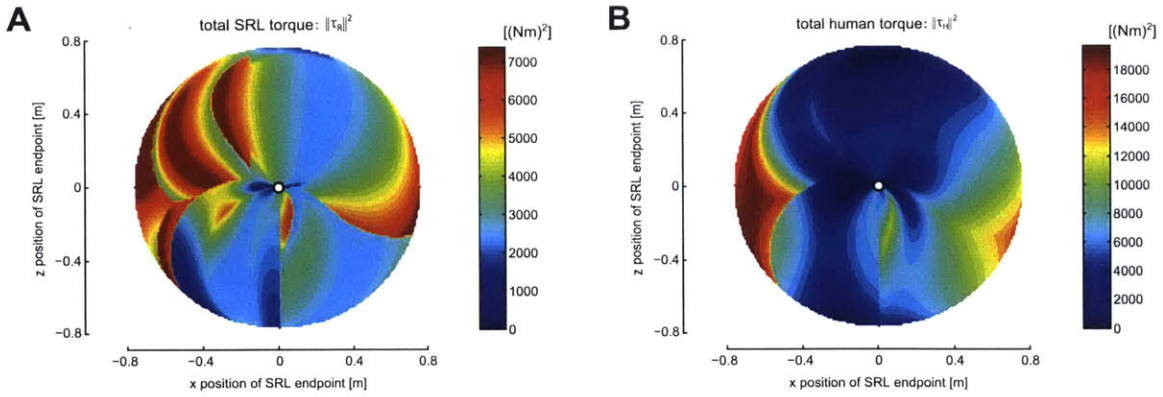

Figure 5-3: A) Squared norm of the optimal SRL torques $\|\tau_R\|^2$ and B) corresponding human workload $\|\tau_H\|^2$, plotted for every possible contact point of the SRL end with the environment. The central white dot represents the SRL shoulder (point C in Figure 2). The best bracing configurations for the SRL are the ones that lead to $\|\tau_H\|^2 = 0$ - the blue areas in B) - and also required limited robot torques - the blue areas in A). It is possible to observe that both conditions are respected when making contact the environment at either the bottom or the top of the SRL workspace (see Section V).

optimizes the metric subject to constraints on available surfaces to brace.

5.4 Optimization

5.4.1 Introduction

In order to maintain a static posture, aircraft assembly workers must compensate for their own weight and for the forces originated operating tools or moving parts. These actions generate an equivalent force and torque vector $-F_{ext}$ at the hip, which must be borne by the legs of the worker generating an equal and opposite vector F_{ext}.

When the SRL is used, F_{ext} can be provided in part or entirely by the robot, relieving the human:

$$F_{ext} = F_H + F_R \tag{5.10}$$

where F_R and F_H are the hip forces and torques generated respectively by the robot and the human. The joint torques required to originate these hip forces can be

calculated using the Jacobian matrices of the robot and of the human leg (J_R and J_H), considered as two âĂŞlink manipulators fixed to the ground at their contact points.

The total force to be generated at the hip can thus be written as

$$F_{ext} = \begin{bmatrix} J_R^{-T} & J_H^{-T} \end{bmatrix} \begin{bmatrix} \tau_R \\ \tau_H \end{bmatrix} = M\,\tau_{tot} \tag{5.11}$$

Both τ_R and τ_H are vectors with three elements, corresponding to the torques of the robot and human joints. Since the rank of M is at most 3, its null space has at least dimension 3. This means that there are infinite couples of τ_R and τ_H that originate the same F_{ext}. In other words, the human leg and the SRL arm form with the ground a closed kinematic chain that has infinite static solutions for the joint torques.

The objective of the SRL arm is to minimize the human workload. Among the infinite possible τ_R given a particular system configuration, we thus want to determine the value that minimizes τ_H. The vector of the human joint torques can be written as

$$\tau_H = J_H^T(F_{ext} - J_R^{-T}\tau_R) \tag{5.12}$$

, where $J_H^T F_{ext}$ represents the torques that the human leg should provide to generate F_{ext} without any external help, and the second term represents the torques that the action of the SRL subtracts from the human workload.

5.4.2 Problem Statement

Find an optimal posture and joint torques of the SRL that minimize the power required for the human to bear the external load, F_{ext} , subject to torque limits of the SRL and the admissible joint angles, $\theta_R \in D_R$:

$$\theta_R^{opt} = \arg \min_{\substack{\theta \in D_R \\ |\tau_R| \leq \tau_{R,max}}} P(F_R; \theta_R) \tag{5.13}$$

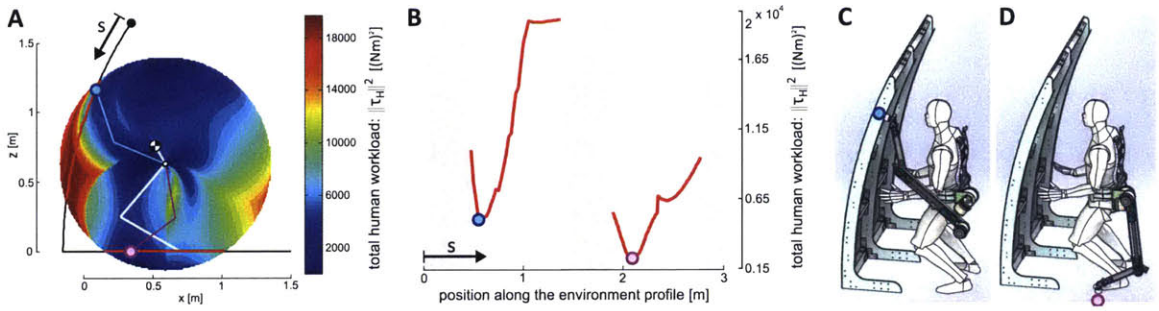

Figure 5-4: Finding the optimal SRL configuration with limited contact points. A) The human workload $\|\tau_H\|^2$ map is overlapped with the profile of an aircraft structure (black line). The human configuration is drawn with grey lines, while the optimal SRL bracing configurations are drawn with magenta and cyan lines. The red curves represent the available contact points – the intersection between the environment profile and the robot workspace. B) The value of $\|\tau_H\|^2$ in the available contact points is plotted against coordinate s (the position of the contact points along the ground profile). The grey areas represent the segments of the environment that cannot be reached by the SRL. The magenta dot is the contact point that minimizes $\|\tau_H\|^2$. The cyan dot is a local minimum of $\|\tau_H\|^2$, which can be used if it is preferable to grasp the wall instead of the floor. C) SRL bracing configuration corresponding to the local minimum on the wall (cyan point). D) SRL bracing configuration corresponding to the global minimum among the available contact points (magenta point, on the floor). Notice that the available contact points do not include the most advantageous ones (placed at the bottom and at the top of the SRL workspace, see Section V).

where

$$P(F_R;\theta_R) = \|\tau_H\|^2 = (F_{ext} - F_R)^T J_H W_H J_H^T (F_{ext} - F_R) \tag{5.14}$$

5.4.3 Optimization

The analytical expression of τ_R which minimizes $\|\tau_H\|^2 = \tau_H^T \tau_H$ can be done by finding the point where the derivative of $\|\tau_H\|^2$ is zero. The complete derivation is detailed in Appendix B.

However, this solution does not take into account the limits to the torques of the robotic arm. There might be situations in which the joint torques required to originate F_{ext} and minimize the human workload ($\|\tau_H\|^2 = 0$) exceed the maximum torques that can be provided by the SRL actuators. Moreover, the limits of the different

actuators are different (See Appendix C for the characteristics of the SRL actuators and the model parameters). In particular, the robot wrist joint is the weakest both because its actuator is the smallest and because its gripper must guarantee the no-slip condition at the base of the bracing model. In order to include these limits in the solution, we solve constrained optimization problems employing the method of the Lagrange Multipliers.

The analysis so far has been general, and holds for the general 3D problem. We will now present the analytical solution to the optimization process in the 2D case. We consider the projection of the man-machine system on the sagittal plane (plane xz, see Figure 2). Although the movements of the human and the robot are three dimensional, a planar model can adequately represent both the kinematic configuration necessary to reach a crouched position and the major joint torques required to bear gravitational loads.

The iterative procedure to find τ_R which minimizes $\|\tau_H\|^2$ and respects the SRL torque limits is as follows. The human and robot configuration (J_H and J_R) are given. We start computing the solution τ_R^* which makes $\|\tau_H\|^2$ zero (the global minimum). This solution is acceptable provided that it respects all the torque limits. If this is not true, three cases may happen.

First, one element of τ_R^* exceeds its maximum value torque $\tau_{iR,max}$. In this case we apply the Lagrange Multipliers to minimize $\|\tau_H\|^2$ with the the constraint that $\tau_{iR} <= \tau_{iR,max}$, resulting in the Lagrangian:

$$L = \|\tau_H\|^2 - \lambda(\tau_{iR}^2 - \tau_{iR,max}^2) \tag{5.15}$$

This optimization yields a new value of τ_R^*, with τ_{iR} saturated to its maximum value (for the analytical expression of the solution, see Appendix D).

Second, if two elements of τ_R^* exceed their maximum values $\tau_{iR,max}$ and $\tau_{jR,max}$, we apply the Lagrange Multipliers to minimize $\|\tau_H\|^2$ with two corresponding constraints, resulting in the Lagrangian:

$$L = \|\tau_H\|^2 - \lambda(\tau_{iR}^2 - \tau_{iR,max}^2) - \mu(\tau_{jR}^2 - \tau_{jR,max}^2) \tag{5.16}$$

This optimization yields a new value of τ_R^*, with τ_{iR} and τ_{jR} saturated to their maximum values (for the analytical expression of the solution, see Appendix D).

Third, if all three elements of τ_R^* exceed their maximum values, then we find the solution that minimizes $\|\tau_H\|^2$ among the eight triples $[\pm\tau_{1R,max}\ ,\ \pm\tau_{2R,max}\ ,\ \pm\tau_{3R,max}]^T$. This procedure is repeated until all the elements of τ_R^* are within their limits. Figure 3 shows the squared norm $\|\tau_R^*\|^2$ of the solutions obtained for every possible configuration in the workspace of the SRL. The position of the human is fixed ($\alpha_{1H} = 150°$, $\alpha_{2H} = -100°$, $\beta_{torso} = 120°$). The figure also shows the corresponding values of $\|\tau_H\|^2$.

In practice, though, it is not necessary to find τ_R^* and the corresponding $\|\tau_H\|^2$ for every point in the workspace of the robot. It suffices to intersect the SRL workspace and the available contact points with the environment. One such situation is shown in Figure 4, where the environment profile represents the floor and the wall inside an aircraft hull. For every contact point that can be reached by the robot, we compute τ_R^* and $\|\tau_H\|^2$ with the method detailed above. The optimal contact point (and robot configuration) is the one that minimizes the human workload $\|\tau_H\|^2$. If many solutions realize the same minimum workload, the one requiring minimum robot torques $\|\tau_R^*\|^2$ is selected among them. It is important to remark that this optimization method can be applied with any kind of environment profile. It is not necessary to have the contact point that yields the global minimum of $\|\tau_H\|^2$ (blue area in Figure 3B). If limited contact points are available, the algorithm selects within that subset the point that locally minimizes $\|\tau_H\|^2$.

5.5 Discussion

5.5.1 Comparison

In order to compare the performance of the SRL in reducing the human workload with that of a traditional exoskeleton, three scenarios will be analyzed. First, we consider the case of a worker without any robotic aid. We calculate the torques that the human joints must exert in order to compensate for the weight of the user.

Second, we consider the case of a worker wearing a traditional exoskeleton. In this scenario, the man-machine system must generate joint torques that compensate for the weight of both the human and the robot. The exoskeleton torques will be subtracted from the required total ankle, knee and hip torques. The goal is to minimize the absolute value of the residual torques, which must be originated by the human joints. In order to have a fair comparison, the weight and maximum torques of the exoskeleton are chosen to be the same as the ones of the SRL.

Third, we consider the case in which the worker is wearing the SRL, which employs the bracing strategy in order to minimize the workload of the user. We select for the robotic arm the optimal configuration that has been found in the previous section (configuration colored in magenta in Figure 4). In all of the three cases the position of the human is the same (joint angles equal to those considered in Section IV). This uniquely defines also the position of the exoskeleton, whose kinematics are the same as those of the weareråĂŹs leg. The SRL, conversely, is free to select the optimal bracing configuration. The results in terms of human workload are reported in Table I.

The computed human torques indicate that, although wearing an exoskeleton

Table 5.1: Human workload comparison

joint torque	only human	human and exoskeleton	human and SRL
τ_{1H} $[Nm]$	-59	-43	-10
τ_{2H} $[Nm]$	79	57	34
τ_{3H} $[Nm]$	-24	0	-29
$\|\tau_H\|^2$ $[(Nm)^2]$	10298	5098	2097

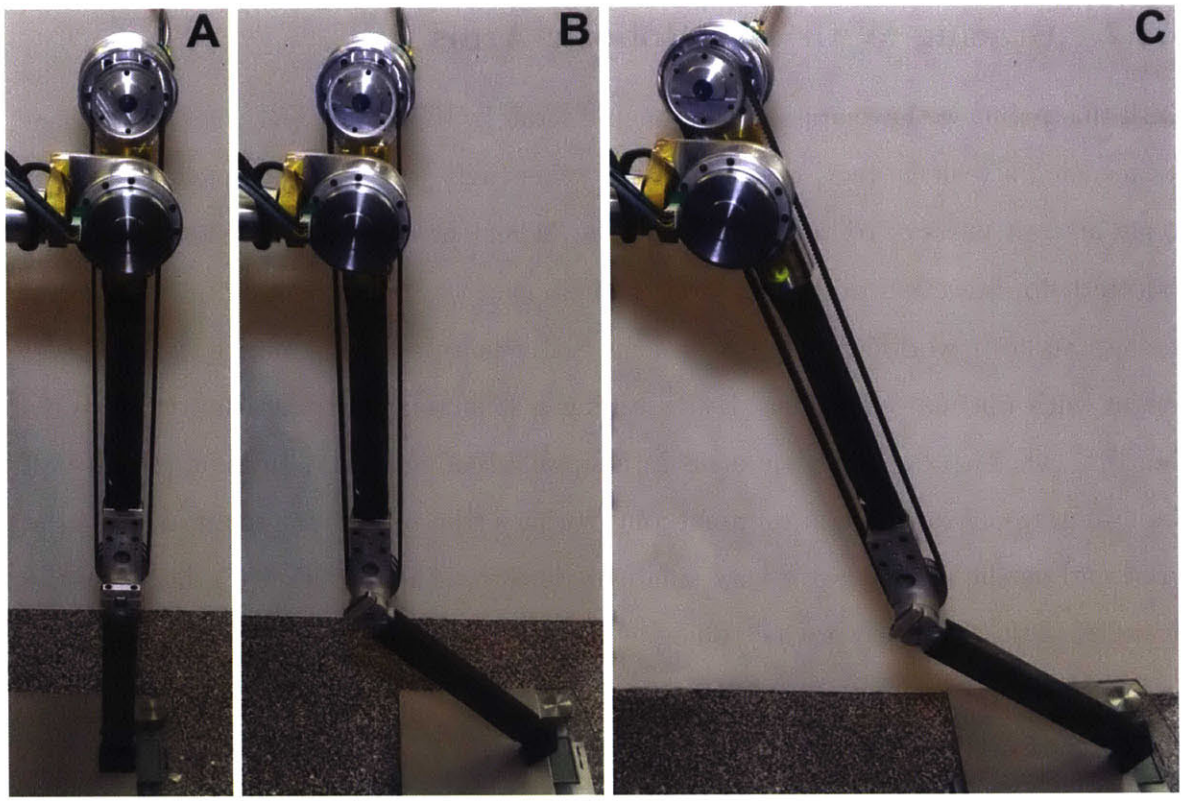

Figure 5-5: The experimental setup used to measure the power consumption of the SRL arm while bearing vertical loads. We compare three different configurations in terms of power required to bear one Newton of vertical load. In case A) the required power was 0.04 $[W/N]$, in case B) it was 0.53 $[W/N]$ and in case C) it was 0.77 $[W/N]$.

is more advantageous than not using any robotic aid, the SRL provides the best performance in terms of human workload minimization. The intuitive explanation of the advantage of the SRL in bearing the load is that, by choosing a configuration close to the singular one, the robotic arm can support the wearer without resorting to large joint torques. The load is simply discharged to the ground through the robotic structure. In the vicinity of the singularity the SRL exploits a large mechanical advantage in order to bear loads with the least effort.

The power consumption of the SRL prototype arm while bearing a vertical load has been measured in several configurations. The considered robot positions and the results in terms of required power are shown in Figure 5. These experimental results confirm that bearing a load in the vicinity of a singular configuration requires the least amount of joint torques âĂŞ and therefore of power.

5.5.2 Bracing With Two Robotic Arms

Until this point, we have applied the bracing strategy to a single SRL arm. If the user is executing a task, in fact, the help of the other SRL arm might be needed in order to get aircraft parts or to handle heavy tools. When the task does not require specific robotic help, however, both SRL arms can be used to brace the user and minimize the human body workload. In this case the SRL can always compensate the full body weight with optimal efficiency. By assuming a triangular configuration (Figure 6), the SRL can keep both robotic arms in a singular configuration and compensate all the gravitational forces with minimal joint torques (the residual moment arms at the wrist and at the shoulder are very small by design). The only limiting factor is the strength of the end effector electromagnets, whose size can be tailored to the load to be borne. This triangular bracing strategy is efficient for any COM height h (Figure 6), therefore confirming the advantage of the SRL over traditional exoskeletons.

5.6 Conclusions

This chapter presented a novel strategy for the use of the Supernumerary Robotic Limbs (SRL). Our vision for the SRL is to become a functional extension of the wearerâĂŹs body, coordinating with the user to execute complex operations and providing support during the most physically demanding tasks. In this chapter, we focus on the use of the SRL to minimize the torques required to the human joints while maintaining an uncomfortable posture or bearing a static load.

We developed the bracing strategy, which consist of the SRL making contact with the environment in order to support the user. By grasping the environment, the robot is able to reduce the static loads borne by the wearer. As a consequence, the torques required to the human joints can be minimized. We presented a method to identify the optimal SRL bracing configuration, which allows to minimize human effort while taking in account the robot torque limits and the available contact points with the environment.

Finally, we showed that the SRL can minimize user workload with a limited power

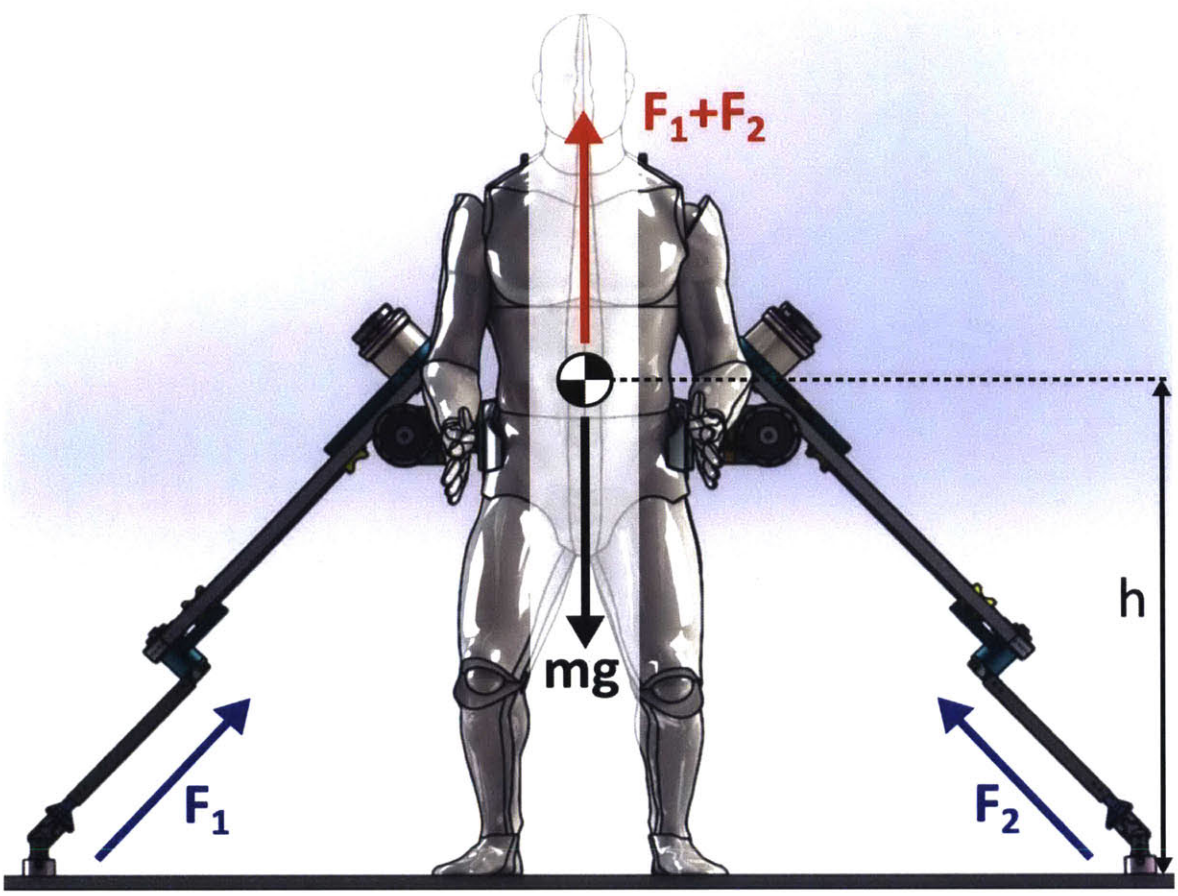

Figure 5-6: Bracing with two robotic arms. The triangular bracing strategy guarantees efficient gravitational load compensation for every h.

consumption. This can be achieved because the kinematic independence of the SRL allows it to choose the optimal available bracing point. A traditional exoskeleton, on the other hand, is constrained to follow the movements of the human leg and thus cannot select an optimal configuration, resulting in higher robot joint torques and risk of saturation. We conclude that the SRL has the potential to provide optimal support to the human user in an efficient way.

Chapter 6

Combining Bracing and Task Assistance

6.1 Introduction

This chapter explores a promising application for the SRL bracing functionality. The SRL can provide the human with positional references, jigs, and tools for assisting workers in executing tasks that require high accuracy or robustness to disturbances [69].

This chapter focuses on a class of tasks where the SRL physically interacts with the environment through contact. The SRL makes contact with a wall and thereby braces the human body against the environment. The SRL also guides the human hands by placing a drill jig over the drilling location. Bracing the human body and guiding the hands of the worker, the SRL can enhance the drilling task stability and accuracy.

We will analyze the kinematic and static properties resulting from the structural closed loops formed around the SRL, the human, and the environment. We will develop and discuss effective strategies for physical disturbance rejection and fine positioning. Finally, we will present an optimization method that identifies the SRL kinematic configuration and joint torques that stabilize the drill and at the same time minimize the human workload.

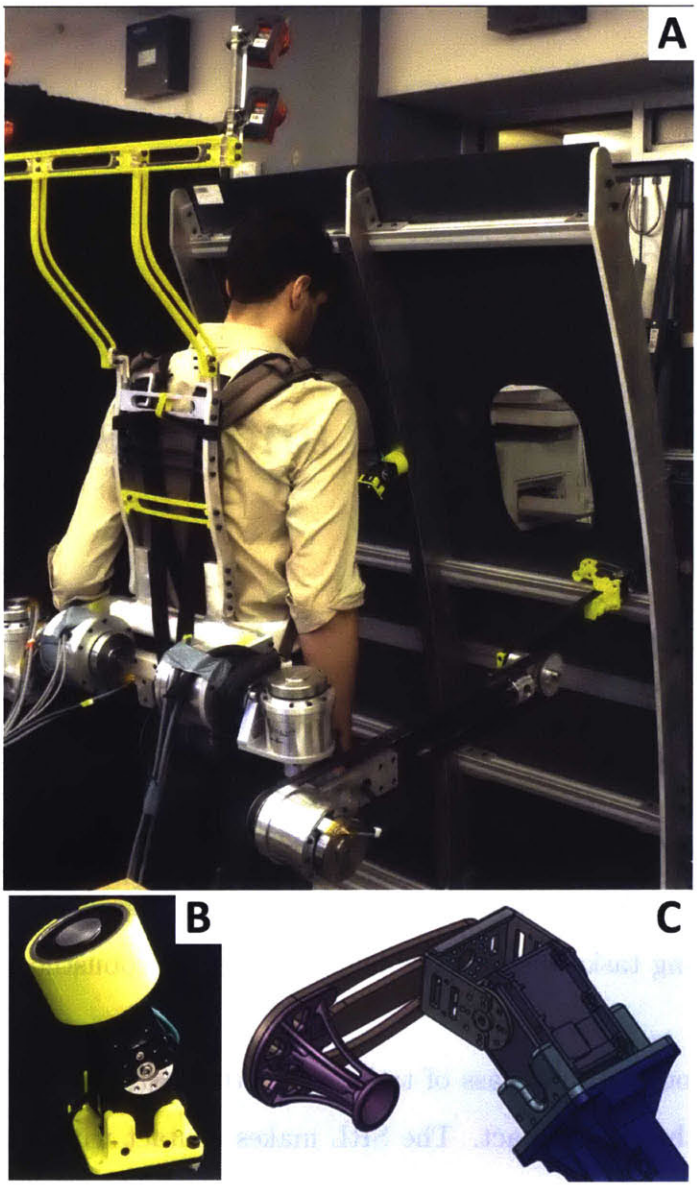

Figure 6-1: A) The SRL prototype used in a drilling task. B) The electromagnet used to establish contact with the environment. C) The drill jig end effector. In the middle of the purple element there is a hole (bushing) whose function is to guide the drill bit.

6.2 Applying the SRL to aircraft fuselage assembly

Figure 1 shows a typical assembly task inside a large aircraft fuselage. A beam, called inter-coaster, is placed between two vertical frames, and secured with special bolts. This assembly task requires many steps of operations, including picking up a workpiece, positioning it against the fuselage frame, clamping the workpiece to the

fuselage, making holes with a drill, installing bolts, and fastening the bolts. Currently, the work is executed completely by human labor. For complex installation two workers must collaborate to complete the job.

This task procedure can be streamlined with the use of the SRL. Figure 1 shows a prototype SRL system developed at the MIT d'Arbeloff Laboratory. It consists of two 4 DOF robotic limbs, a waist bracket for securing the robot around the waist, and end-effectors attached to the tip of the arms. The SRL system is equipped with a motion capture system placed above the backpack frame. One SRL may be equipped with a clamp at its end point, as shown in Figure 1, and secure the beam temporarily against the fuselage structure, rather than the human picking up and setting the clamp. Then the human can immediately move on to drilling. Another SRL can assist the human in positioning the drill against the frame. As shown in Figure 1, the second SRL may be equipped with a drilling jig at its end point, and place it precisely at a specified position by using proximity sensors at the tip or other types of sensors detecting the location of the fuselage structure. Furthermore, the drilling jig can keep the drill bit perpendicular to a beam surface and guide it to the exact location where a hole must be made. The human's work load is substantially reduced, since his/her job is simply pushing the drill towards the surface, i.e. 1 DOF motion. The SRL with the drilling jig can support the drill in other 4 DOF: x and y translations and pitch and yaw rotations.

In this example task, the first SRL clamps the beam against the fuselage structure. Note that, in turn, the human body is physically constrained by the SRL connecting the human body to the fuselage. In other words, the human body is braced against the fuselage structure. This can secure and stabilize the human body while performing the laborious task. Assembly tasks of a large aircraft fuselage are often performed in an unsecure environment with only partially covered floors. Bracing the human body will contribute to stabilizing the body and improving safety.

In the drilling task considered in this chapter, the SRL has two goals. The first one is to indicate the correct hole location to the user. This is achieved by placing the drill jig on the aircraft frame surface, so that its central bushing will guide the

drill bit towards the desired position. Using the motion capture system and endpoint feedback control, the SRL is able to position the bushing more accurately than an unaided human worker, guaranteeing also task repeatability. The second goal of the SRL is to hold the drill jig in place during the drilling process. This anchoring phase is critical, because the bushing must be fixed to the hull surface despite the presence of several potentially large disturbing forces. The main perturbations are the human-induced disturbances (involuntary movements, postural sway, breathing), the vibrations produced by the drill, and the unwanted force components (perpendicular to the dilling axis) that the worker may generate while pushing the power drill.

Since the drill jig has no gripper, it can be anchored to the hull in only one way: by pressing it on the aircraft wall with a force which is perpendicular to the contact surface. This perpendicular force will then generate static friction components which will be able to absorb disturbances parallel to the contact surface, as long as they are within the friction cone. This drill jig anchoring strategy has several advantages: first, the robot does not need any pivots or special features to hold on to. The drill jig is simply put in contact with the surface that needs to be drilled, on the desired location. Another advantage is the very fast and reliable engaging/disengaging process. The anchoring is realized by reaching the desired contact force, and is quickly released by moving the end effector away from the aircraft hull. No complicated end effector or grasping systems need to be used, making the holding system more reliable. In the following section, we will present three strategies to generate a perpendicular holding force and secure the drill jig during the drilling task.

6.3 Drill jig anchoring strategies

The main challenge presented by the drilling task is how to minimize the human effort while producing the required holding force at the drill jig. The base of the SRL is the human hip. This means that if the robotic configuration is unbalanced, the human must exert a restoring hip force in order to keep his/her position. The goal of the SRL is therefore that of generating a large drill jig contact force, while minimizing

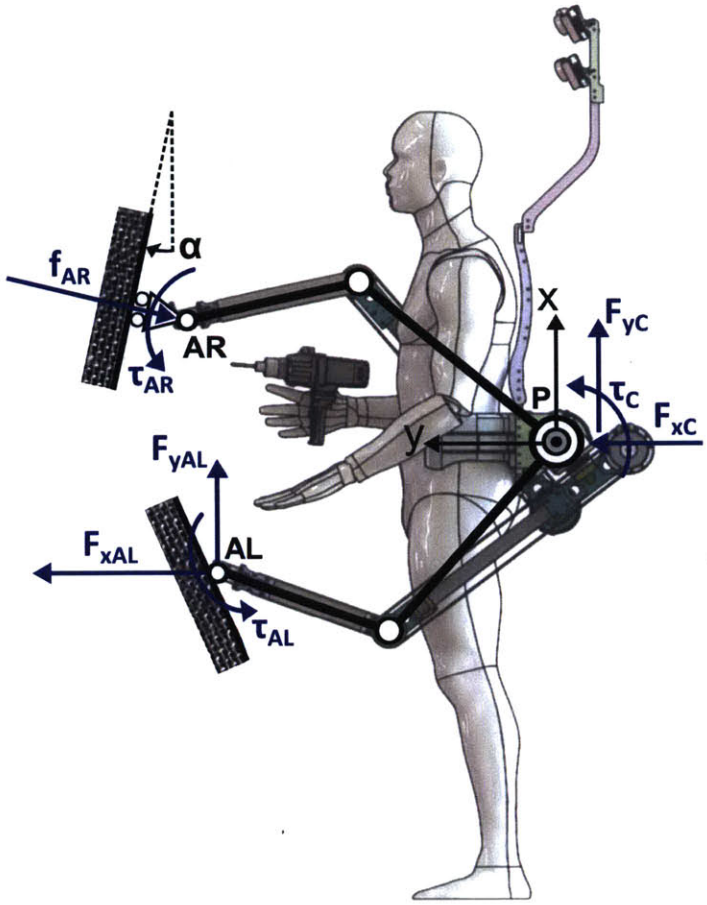

Figure 6-2: Kinematic scheme of the SRL during the drilling task, applying the General Strategy. The robotic arms are drawn in black, while the ground reaction forces (f_{AR}, τ_{AR}, F_{xAL}, F_{yAL}, τ_{AL}) and the human hip forces (F_{xC}, F_{yC}, τ_C) are drawn in blue. $f_{AR} = \sqrt{F_{xAR}^2 + F_{yAR}^2}$ is the holding force of the drill jig. It is perpendicular to the contact surface, which has orientation α.

the required human workload. This can be achieved by using the free SRL arm (the one without the drill jig) to contact the environment in a convenient location. This SRL arm can then generate ground reaction forces aimed to secure the drill jig and relieve the human.

The structure of the problem is as follows (see Figure 2 and Table 1). The position of the SRL base (human hip) and the position and orientation of the drill jig are known. They are given parameter values determined by the task (hole that must be drilled) and by the current worker position. The goal of this analysis is to determine the best point where the free SRL arm must make contact with the environment.

We also want to find the SRL joint torques that will originate the required drill jig anchoring force, while minimizing the human workload. Table I summarizes the parameters and unknowns of the problem (refer also to Figure 2).

6.3.1 Basic Strategy

The simplest drill jig anchoring strategy consists of generating with the free SRL arm a force which is equal and opposite to the holding force required at the bushing (Figure 3). In order to maintain static balance, the system needs a compensation torque τ_C.

$$\tau_C = f_{AR} \cdot d \tag{6.1}$$

This torque can be provided by the SRL wrists (they are in contact with the environment and can therefore shape the ground reaction torques). If τ_C surpasses the limits of the robot wrists, the exceeding part must be generated by the human hip.

The compensation torque τ_C depends on the magnitude of the holding force f_{AR} – which is a fixed parameter of the problem – and on the distance d between the holding force axis and the parallel axis passing through the other contact point (Figure 3). In order to reduce τ_C, this strategy requires reducing d. It is very convenient when it is possible to place f_{AR} and f_{AL} on the same axis. In most cases, however, reducing d entails decreasing the distance between the two robotic end effectors. This would place both robotic hands in the drilling area, creating unwanted obstacles to the movements of the worker. It is therefore necessary to develop an anchoring strategy that allows the SRL to generate the drill jig holding force without invading the drilling area.

Table 6.1: Variables of the problem

variables	type
f_{AR}, α, a_R, b_R	fixed parameters
F_{xC}, F_{yC}, τ_C, F_{xAL}, F_{yAL}, τ_{AL}, τ_{AR}, a_L, b_L	unknowns

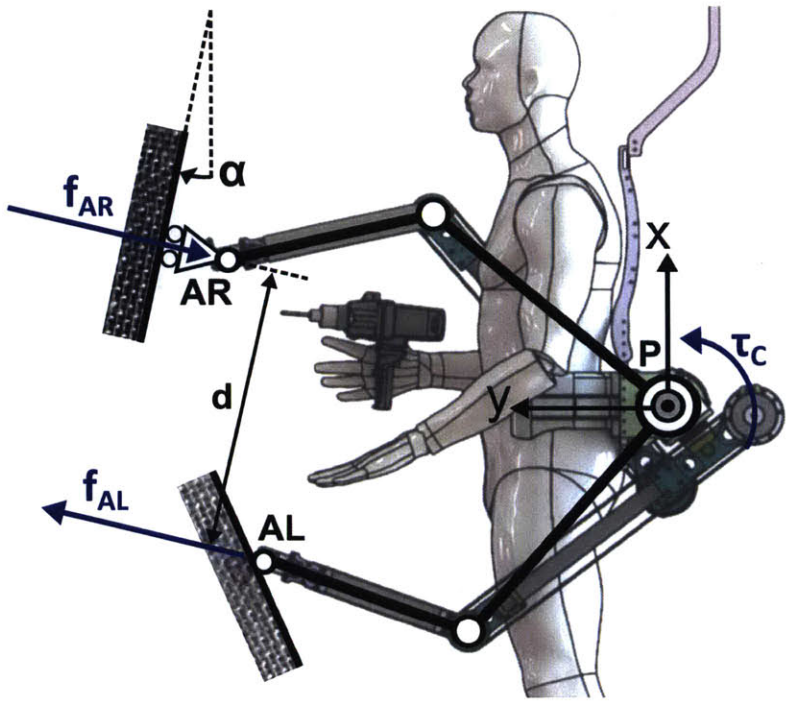

Figure 6-3: Kinematic scheme of the SRL during the drilling task, applying the Basic Strategy. $f_{AS} = \sqrt{F_{xAL}^2 + F_{yAL}^2}$ is the holding force of the SRL arm without drill jig. Its direction is parallel to that of f_{AR}, its norm is the same, and its sense is opposite.

6.3.2 Leaning Strategy

For a human, generating a strong continuous hip torque is uncomfortable and causes fatigue. In fact, this requires the constant contraction of the hip muscles. Conversely, for a standing human is simple and effortless to generate a static linear force in the horizontal plane. This can be achieved by leaning in the direction where the force must be created. Using the Linear Inverted Pendulum Model [40], this leaning force can be expressed as $F_y = mgy/L_H$, where L_H is the height of the human center of mass (COM), and deltay is the displacement from the equilibrium position in the y direction.

It is therefore possible to develop a drill jig anchoring strategy that constrains the human compensating force to be exclusively linear. The considered situation is shown in Figure 4: in order to generate the holding force f_{AR}, we want to use a robot contact force f_{AL} and a human hip force f_C in the same direction. These unknown forces can be determined writing the static equilibrium equations of the system:

$$\begin{cases} -f_{AL} + f_C - f_{AR} = 0 \\ f_C \cdot (d - d_R) - f_{AR} \cdot d = 0 \\ f_{AL} \cdot d - f_C \cdot d_R = 0 \end{cases} \tag{6.2}$$

Solving the system leads to the following solutions for the robot free contact force f_{AL} and for the human-generated force f_C:

$$\begin{cases} f_C = f_{AR} \frac{d}{d-d_R} \\ f_{AL} = f_{AR} \frac{d_R}{d-d_R} \end{cases} \tag{6.3}$$

Since d_R is fixed (it depends on the given drilling and human locations), the hip force f_C provided by the user can be reduced by increasing as much as possible the distance d between the two robotic end effectors. This is an advantage of the current strategy, because it means that the free robotic arm does not obstacle the movements of the worker in the vicinity of the drilling location. However, the limit of this strategy is that the required human force f_C is still large. In other words, the human effort is comparable (for admissible values of d and d_R) to the anchoring effect that we want to achieve. Moreover, the human can generate only the y component of f_C by effortlessly leaning forward. There is thus the need for a general drill jig anchoring strategy, able to identify the general ground reaction forces and torques that realize the desired holding force while minimizing human workload.

6.3.3 General Strategy

In the most general case, the SRL can generate 4 independent ground reaction forces in order to secure the drill jig. These free variables are F_{xAL}, F_{yAL}, τ_{AL}, τ_{AR} (see Figure 2). The human hip forces and torque F_{xC}, F_{yC}, τ_C are also unknown, and must be minimized. The location of the drill jig (a_R, b_R) is a problem input. The static equilibrium equations in this general case are:

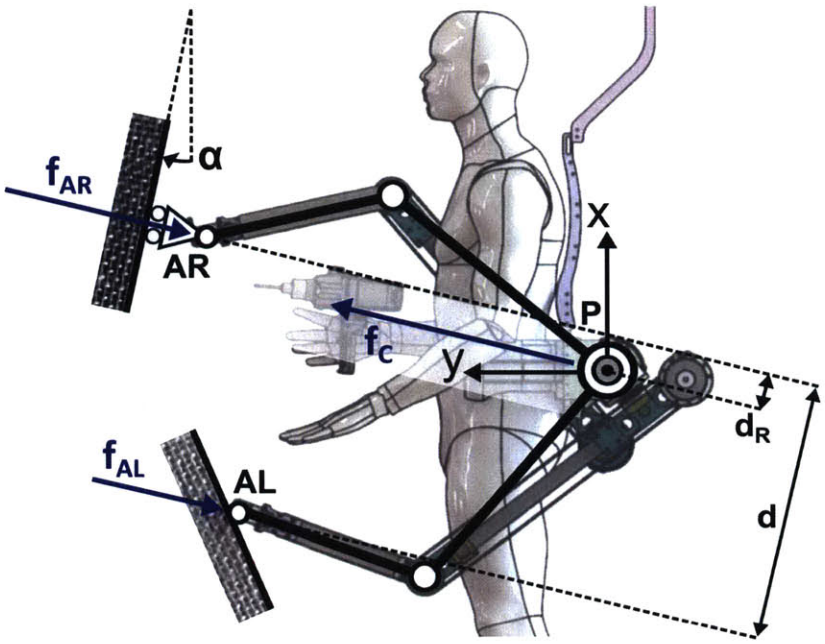

Figure 6-4: Kinematic scheme of the SRL during the drilling task, applying the Leaning Strategy. $f_C = \sqrt{F_{xC}^2 + F_{yC}^2}$ is the norm of the human hip force. f_{AR}, f_{AL} and f_C are parallel.

$$\begin{cases} -f_{AR}\sin(\alpha) + F_{xC} + F_{xAL} = 0 \\ f_{AR}\cos(\alpha) + F_{yC} + F_{yAL} = 0 \\ -F_{yC}\, a_L + F_{xC}\, b_L + f_{AR}\, \cos\alpha\, (a_R - a_L) + \\ +f_{AR}\, \sin(\alpha)\, (b_R - b_L) + \tau_C + \tau_{AR} + \tau_{AL} = 0 \end{cases} \tag{6.4}$$

If we assume that the location of the other end effector $(a_L,\ b_L)$ is known, the system is linear and can be written in matrix form as $Ax = b$, where

$$A = \begin{bmatrix} 1 & 0 & 0 & 1 & 0 & 0 & 0 \\ 0 & 1 & 0 & 0 & 1 & 0 & 0 \\ b_L & -a_L & 1 & 0 & 0 & 1 & 1 \end{bmatrix} \tag{6.5}$$

$$x = [F_{xC}\ ,\ F_{yC}\ ,\ \tau_C\ ,\ F_{xAL}\ ,\ F_{yAL}\ ,\ \tau_{AL}\ ,\ \tau_{AR}]^T \tag{6.6}$$

$$b = \begin{bmatrix} f_{AR}\ \sin(\alpha) \\ -f_{AR}\ \cos(\alpha) \\ -f_{AR}\cos(\alpha)(a_R - a_L) - f_{AL}\sin(\alpha)(b_R - b_L) \end{bmatrix} \tag{6.7}$$

Since matrix A has full row rank and $m = 3 < n = 7$, the system has infinite solutions. The solutions x represent the ground reaction forces and human forces that generate the desired holding force f_{AR}, while maintaining the system in static equilibrium. Section IV will present an optimization technique to select the most convenient solution, and use its results to identify the best robot configuration.

It is important to point out that the results of this section hold in general for any wearable robot that has two contact points with the environment. These results do not depend on the specific number of links or joint types of the wearable robot. The kinematic structure of the robot will come into play when determining the necessary joint torques (Section V).

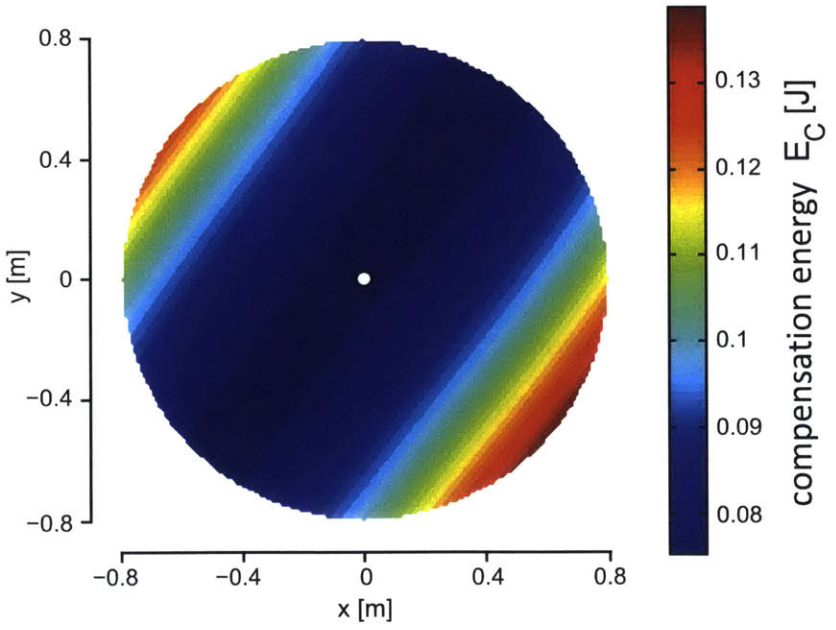

Figure 6-5: Optimal E_C for every contact point within the robot workspace. The white point represents the robot base (point P in Figure 2).

6.4 Optimization

The system found applying the general drill jig anchoring strategy has infinite solutions. The optimal solution is the one which minimizes the user workload required to anchor the drill jig. The human workload is determined by the forces and torque that the hip must exert in order to keep the system in static balance: F_{xC}, F_{yC}, τ_C. In this analysis, we include all of these values in a single scalar measure of human workload: the compensation energy E_C. This quantity is the equivalent energy that the human hip would have to provide if it was a passive element composed by three springs (two linear and one rotational). The definition of E_C is as follows

$$E_C = k_x(\Delta x)^2 + k_y(\Delta y)^2 + k_\theta(\Delta\theta)^2 \tag{6.8}$$

Since the equivalent displacements Δx, Δy, $\Delta\theta$ are linearly related to the hip forces and torque ($F_i = k_i\ x_i$), the expression of the compensation energy can be re-written as

$$E_C = \frac{F_{xC}^2}{k_x} + \frac{F_{yC}^2}{k_y} + \frac{\tau_C^2}{k_\theta} \tag{6.9}$$

The values of the three hip spring constants can be adapted from the biomechanical literature [84]. When a human is standing, the body behaves like an inverted pendulum and the equivalent stiffness at the hip is largely determined by the ankle stiffness (anterior/posterior direction: $k_{frontal}$ = 800 Nm/rad). The equivalent hip stiffness can be determined assuming small displacements (leg length L_H = 1 m): $k_y = k_{frontal}/L_H^2$. Stiffness in the x direction is higher (k_x = 1600 N/m), because the userâĂŹs legs are parallel to the x axis (Figure 2). Conversely, hip rotational stiffness is lower (k_θ = 400 N/m), because hip muscles are weaker than the leg ones. Hip stiffness parameters (k_x,k_y,k_θ) allow to determine E_C given the values of F_{xC}, F_{yC}, τ_C.

Since the goal of the optimization is to find the solution x which minimizes E_C, we select a weight matrix W that attributes a cost to the elements of x (see eq. 6).

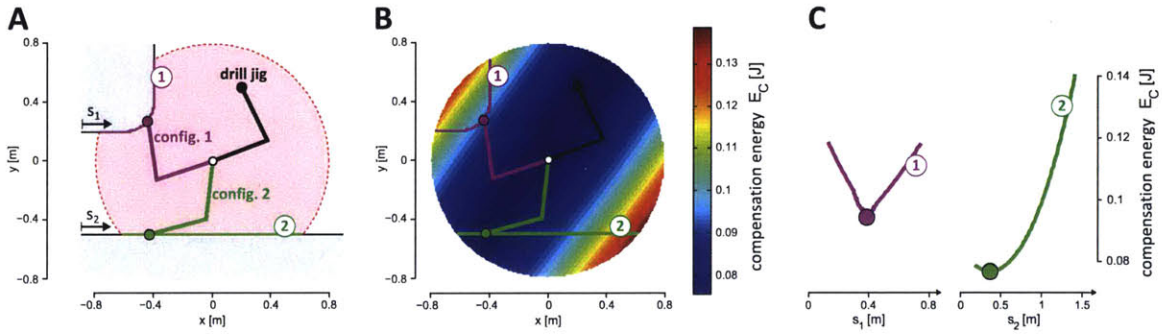

Figure 6-6: The black lines represent the SRL arm which is holding the drill bit. The green and magenta lines represent the optimal configurations of the other SRL arm. A) Intersection between the SRL workspace (red) and an arbitrary environment profile (grey). B) Plot of the available contact points (green curve (1) and magenta curve (2)) over the E_C map determined before (see Figure 5). C) Visualization of the value of E_C for the available contact points (curves (1) and (2) in the workspace). E_C is plotted along coordinates s_1 and s_2 (the position of the contact points along the environment profile). The optimal contact points, outlined with dot markers, are the ones that minimize E_C. The magenta and green SRL configurations in A) and B) correspond to these two minima.

The cost of every element is based on its weight in the expression of E_C:

$$W = diag\left(\frac{1}{k_x}, \frac{1}{k_y}, \frac{1}{k_\theta}, w_{min}, w_{min}, w_{min}, w_{min}\right) \tag{6.10}$$

where $w_{min} = min(1/k_x, 1/k_y, 1/k_\theta) \cdot 0.1$. Note that the only elements with relevant weights are the ones that determine E_C. The other elements have negligible weights (compatibly with the fact that W must be positive-definite).

The optimization problem can be solved with the Lagrange Multipliers [77]. We define the following Lagrangian function:

$$L = x^T W x + \lambda^T (b - Ax) \tag{6.11}$$

where the first term is the cost function (based on W), and the second term is the system of constraints (based on the general strategy derived in the previous section). The solution x which minimizes the cost while respecting the constraints is

$$\begin{cases} \partial L/\partial \lambda = 0 \\ \partial L/\partial x = 0 \end{cases} \tag{6.12}$$

$$\Rightarrow \; x_{opt} = W^{-1}A^T \left(AW^{-1}A^T\right)^{-1} b \tag{6.13}$$

This solution contains the ground reaction forces and human hip forces that anchor the drill jig to the ground, while minimizing the human workload. The linear system on which the solution is based (equations 4-6) was derived assuming that the contact point of the free SRL arm (a_L, b_L) was fixed. It is therefore possible to repeat the same optimization for every contact point within the workspace of the SRL. The results (optimal E_C that can be achieved given a particular contact point) are visualized in Figure 5.

In a manufacturing environment, though, the number of available contact points is limited. The free robotic arm can only make contact with the environment in the intersection between the aircraft structure surface and its workspace. Such a situation is represented in Figure 6. When limited contact points are available, the ground reaction forces (and associated optimal E_C) are calculated only for those points. The best overall ground contact is then the one that yields the smallest optimal E_C (see Figure E_C).

The general anchoring strategy, combined with the optimization method described above, is able to select the most convenient SRL configuration because it does not pose any constraints on the ground reaction forces (unlike the basic strategy and the leaning strategy). Figure 7 and Table II visualize two optimal SRL configurations, with their associated ground reaction forces and hip forces. It is evident that the anchoring force is generated by the robot with negligible human effort (small F_{xC}, F_{yC} and τ_C).

Table II reports the ground reaction forces and hip forces in the two optimal cases (see also Figure 7). It also shows the coordinates of the optimal ground contact points.

6.5 Discussion

The optimization process described in the previous section determined the SRL configuration and external forces that anchor the drill jig to the aircraft while minimizing human workload. We now find the robot joint torques that must be applied in order to realize the optimal static equilibrium. The values of the ground reaction forces and torque are known for both robotic arms. These values are either contained in the vector x_{opt} or can be determined from the problem parameters ($F_{xAR} = -f_{AR}\sin(\alpha)$, $F_{yAR} = f_{AR}\cos(\alpha)$). Knowing the ground reaction forces (equal and opposite to the end effector forces) allows us to write the following expressions for the joint torques

$$\begin{bmatrix} \tau_{1L} \\ \tau_{2L} \\ \tau_{3L} \end{bmatrix} = -J_L^T \begin{bmatrix} F_{xAL} \\ F_{yAL} \\ \tau_{AL} \end{bmatrix} \tag{6.14}$$

The same expression is applied also to the other robotic arm (with subscript R). J_L and J_R are the Jacobian matrices of the two SRL arms in the kinematic configuration that corresponds to x_{opt}.

Up to this point, we did not make any assumption on the particular structure of the wearable robot. These results hold for any wearable robot with two end effectors (the drill jig and a gripper). In the case of the SRL prototype (Figures 1 and 2), the robotic arms have 3 degrees of freedom in plane xy.

The solution for the joint torques τ_L and τ_R is unique. The SRL joint torques

Table 6.2: Optimal SRL configurations

quantities	config. 1	config. 2
$(a_L,\ b_L)$ [m]	(-0.44, 0.27)	(-0.43, -0.50)
F_{xC} [N]	7.6	6.7
F_{yC} [N]	6.8	6.3
τ_C [Nm]	0.8	0.1
F_{xAL} [N]	67.4	68.3
F_{yAL} [N]	123.1	123.6
τ_{AL} [Nm]	30.0	3.7
τ_{AR} [Nm]	30.0	3.7

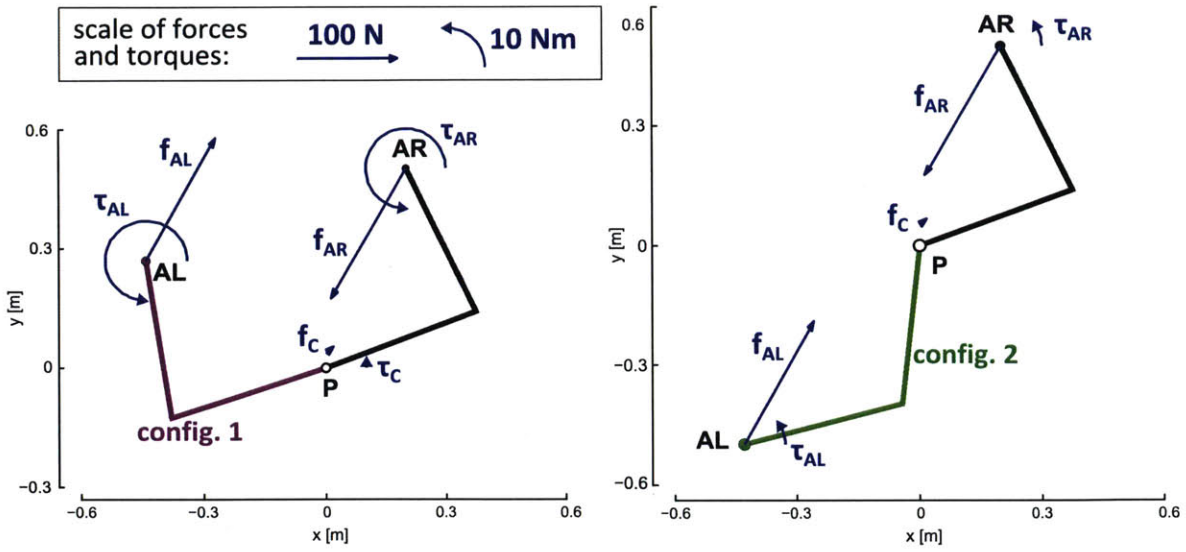

Figure 6-7: Visualization of the ground reaction forces and human hip forces in the two optimal configurations identified in Section IV (see also FIgure 6). The points and forces are defined in Figure 2. The length of the vectors is proportional to the magnitude of the forces and torques (see box for scale). Configuration 2 achieves the minimum possible E_C given the available points. It also requires smaller joint torques on the SRL joints (wrist torques plotted; for the other joints, see Table III).

for the two considered configurations (magenta (1) and green (2), see Figures 6 and 7) are reported in Table III. If the robotic arms had a different number or type of actuators, the Jacobian matrix would change accordingly.

The optimization method presented in this chapter does not take explicitly in account the limitations to the joint torques, or to the electromagnetâĂŹs gripping force. If the maximum values of these quantities are surpassed, the drill jig holding force must be decreased until all constraints are met.

The results shown in Section IV confirm that the General Strategy is superior to the Basic and Leaning Strategies. The general method always minimizes the human workload, for any environment profile. The examples reported in Table II and III show that the human workload is one order of magnitude less than the holding force exerted on the drill jig. Conversely, the other two methods are effective only in particular situations (gripper close to the drill jig for the basic strategy, and gripper far from the drill jig for the leaning strategy) and require high human workloads in the other cases. The basic and leaning strategies can be viewed as particular cases of

Table 6.3: Optimal SRL joint torques

joint torques [Nm]	config. 1	config. 2
τ_{1L}	42.3	15.3
τ_{2L}	4.0	37.1
τ_{3L}	-30.0	-3.7
τ_{1R}	-41.6	-15.2
τ_{2R}	-79.7	-53.4
τ_{3R}	-30.0	-3.7

the general strategy, which the optimization algorithm will select if their particular conditions are met. This is evident in the case of configuration 2 (Figure 7), where the optimization algorithm almost cancels out τ_C by positioning the contact point AL along the direction of f_{AR}, and requiring a ground reaction force f_{AL} which is similar in magnitude but opposite in sense (compare with section III.A).

The optimization method can also be adapted to compensate for the weight of the SRL. In this case, it suffices to modify system $Ax = b$ by imposing the value of $F_{xC} = -mg$ (F_{xC} becomes a fixed parameter). This way, the optimization algorithm will find the SRL configuration and joint torques that anchor the drill jig, compensate for the weight of the machine, and minimize the user workload.

6.6 Conclusions

In this chapter, we focused on a drilling task where the goal of the SRL is ensuring that the hole respects positional and orientation tolerances despite the presence of disturbance forces. This is achieved by using a drill jig equipped with a central hole (bushing). Once the robot has positioned and anchored the drill jig on the aircraft surface, the worker uses the bushing to guide the drill bit. The anchoring effect is achieved by pressing the drill jig on the surface of the aircraft structure.

The results presented in this chapter show that the SRL is effective in aiding the user during the considered drilling task. Our algorithm is able to select the optimal robot configuration given a limited number of available contact points with the environment. The algorithm can identify the ground reaction forces that secure

the drill jig to the aircraft structure, while minimizing the human workload. It also computes the joint torques necessary to create the desired static equilibrium.

This chapter demonstrated a novel application for wearable robotic arms that are kinematically independent from the user. The SRL is free to select the configuration and joint torques that are most effective in assisting the user during a drilling task.

Chapter 7

Bracing Strategy: 3D Analysis

7.1 Introduction

This chapter introduces the design and implementation of the third prototype of the Supernumerary Robotic Limbs (SRL). In this prototype the rotational elbow joint has bees substituted with a prismatic joint, more suitable to bear large axial loads at any point of its stroke. The main limit of the elbow joint was that it required very large torques to bear the weight of the user when the rotational joint was flexed. For the prismatic joint, on the other hand, there is no difference in bearing a force at any point of its stroke. The choice of electric linear actuators enables the SRL to support the full weight of the user.

Considering this new SRL architecture, the bracing strategy is then extended to the full 3D case. It now becomes a general method, capable of considering any possible contact point of the SRL with the environment. Quasi-static stability and compliance with which the body is supported are analyzed. Two control methods for stabilizing the body support system are considered: one is null space stabilization using Hessian matrices, and the other is joint servo stiffness based on the Jacobian [70].

7.2 Design Concept

7.2.1 Motivation for the use of a prismatic joint

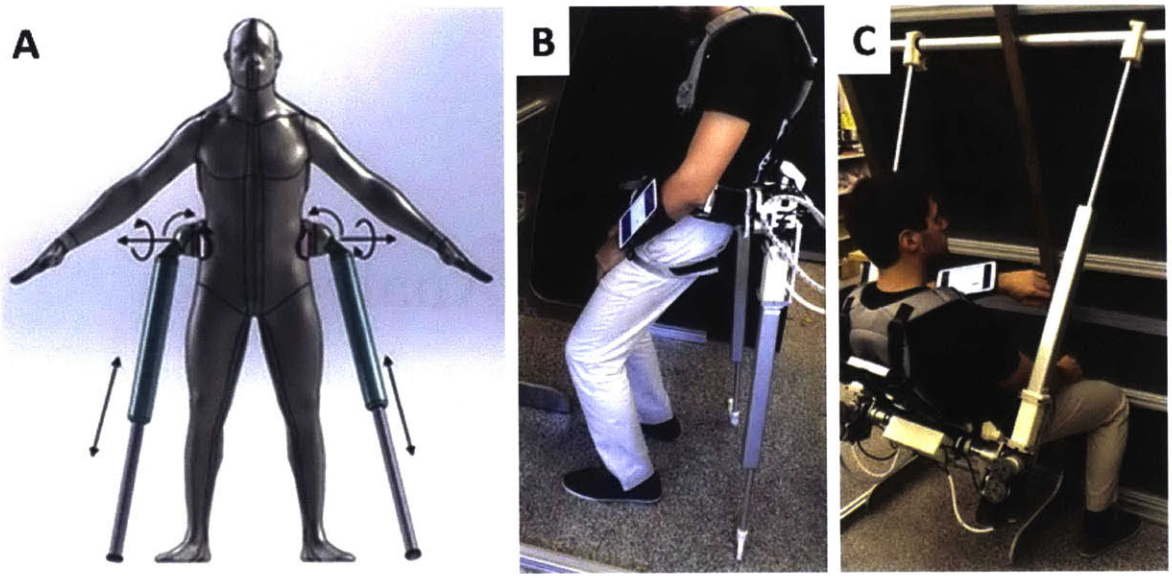

Figure 7-1: Design concept and third prototype of Supernumerary Robotic Limbs (SRL). A) The rotational elbow joint has been substituted with a prismatic joint. B,C) The prismatic joint can efficiently bear large loads.

The SRL consists of a pair of robotic limbs, a harness, and a control unit. Each robotic limb has three degrees of freedom, allowing the endpoint to reach an arbitrary position in space. One of the major functional requirements for the SRL is to bear a large load for a long time while using minimal energy. A prismatic joint with a high gear ratio is not back-drivable; hence, it can bear a load without consuming energy. The SRL in Fig. 1 exploits this feature. Once the prismatic joint is fixed at a certain length, it serves as a "stick". Consequently, most of the load is borne in the longitudinal direction of each stick, the orientation of which is varied with two revolute joints placed on the base of the robot closer to the harness.

7.2.2 Potential Uses

The SRL can be applied to various tasks to facilitate a human in performing dangerous, laborious, or difficult jobs. Fig. 2 shows a collection of potential uses of SRL. In

Fig. 2A the human wearing the SRLs is braced against a rail or a scaffold beam for safety. Here, each SRL is equipped with a gripper at the end of the stick to secure the endpoint to the rail. This type of body bracing for safety is useful for various field works, including construction, utility infrastructure maintenance, and disaster response works as well as an astronaut's Extra-Vehicular Activities (EVA). In Fig. 2B the human has to reach a low position to work on the floor or near the floor for a long period of time. The SRLs suspend the human body, so that the human does not have to crouch or take an uncomfortable posture. In Fig. 2C, the human is taking a half-crouch posture, which is laborious if the posture must be kept for a long time. The SRLs support the body from the floor to reduce the load on the knees and ankles. These body suspension applications can be found in various factory works, including aircraft fuselage assembly and automobile assembly, as well as in construction and field works.

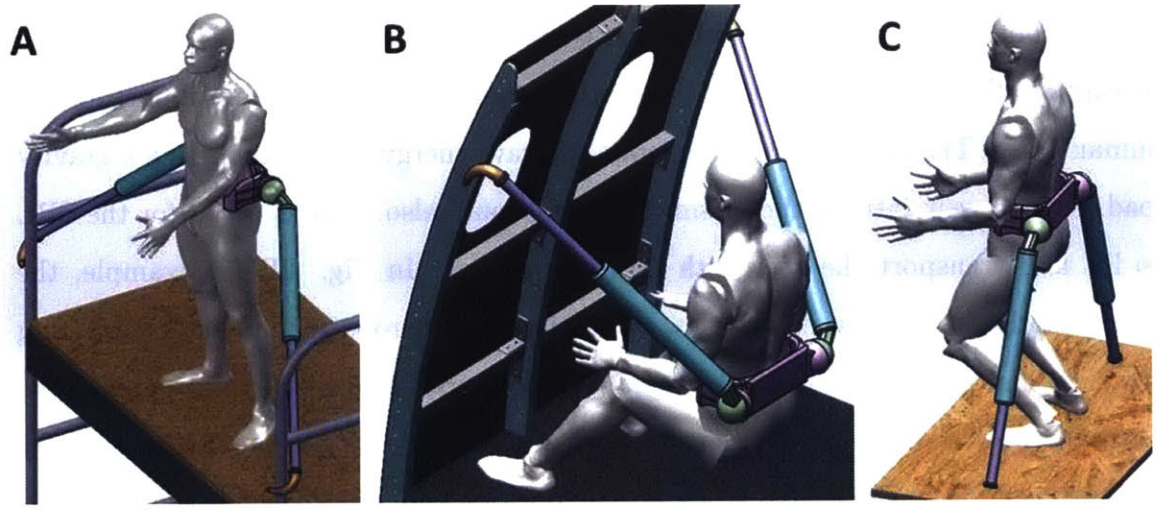

Figure 7-2: Potential uses of the SRL. A) Bracing against a scaffold for safety, B) Suspension from a wall/ceiling, C) Support from the floor.

7.2.3 Design and Control Issues

When performing a task, workers often need to change their posture and position. Examples include picking up a tool from a nearby toolbox, working at a location slightly away from the current position, and checking the side of an object. In all

of these situations, workers need to move sideways, turn, or bend down freely in the vicinity of their current position. To be a useful aid for workers, the SRL must support their weight without restraining their motion. The six active joints of the SRL can provide users with a flexible body support that aids them in the execution of a manufacturing task. The joints of the SRL can be controlled in diverse modes: pure position-control mode, compliance-control mode, torque control mode, and non-backdrivable mode. Combining these modes and assigning them to the individual joints will allow the SRL to provide the human with various types of support that can a) reduce the human gravity load, b) transport the body in a desired direction, c) stabilize the body, and d) allow the body to move freely without constraints in selected directions.

In Fig. 2B and 2C, the user is either suspended from above or supported from the floor in order to reduce the weight-bearing effort. At a desired location the prismatic joints of both SRLs may be left idle to save energy. If the gear ratio is large enough to support the gravity load with friction, no energy is required for supporting the human body. The non-backdrivable mode can save energy when supporting a gravity load. A high gear ratio in the prismatic joints would also make it easier for the SRL to lift and transport the user with position control. In Fig. 2B for example, the human body can be moved sideways; elongating the left robotic limb and contracting the right can move the user to the right and vice versa. See the supplemental video. Once the worker reaches the designed height and lateral position, the prismatic joints are switched off, and the SRL stops in that position (non-backdrivable mode).

While the two robotic limbs can support the human body, the specific SRL configuration may be at an unstable static equilibrium. In Fig. 2C, for example, the support offered by the SRL may collapse as the user rotates about the vertical axis. This instability may be eliminated or alleviated with high stiffness control of the revolute joints. More generally, the compliance with which the human body is supported may be varied by coordinating the servoed joints based on compliance control. The two revolute joints in each robotic limb are suitable for compliance control. Coordination of the four revolute joints will allow us to synthesize a desired compliance in

the task space so that the human body may be supported with a desired compliance in selected directions. In particular, the body should be supported stably and safely but should not be over-constrained.

The stability of body support and the suspension compliance depend on the configuration of the SRL, i.e. where the end effectors are secured to the surrounding environment. Among multiple locations for possible bracing, the SRL should select a desired configuration that allows it to support the human body most effectively and efficiently. Unlike lower exoskeletons, where servoed joints are attached to the human joints, the SRL is not kinematically constrained to the human limbs. The robotic limbs can take an arbitrary configuration, independent of the human limbs. This opens up the possibility of optimizing body support performance with respect to a) support stability, b) reduction of human effort, and c) reduction of energy consumption. In the following sections, we will focus on stability in supporting the human body, presenting detailed analysis and synthesis of a stiffness matrix, including null space stabilization and joint servo stiffness control.

7.3 Support Stability

7.3.1 Basic Formulation

Fig.3 shows a schematic of the SRL system with the right SRL attached to the right side of the harness (Point A) and the left SRL to the other side (Point B). The position of the center point of the harness is denoted x_h, y_h, z_h with reference to the base coordinate system, $O - xyz$. Another coordinate frame, $H - x'y'z'$, is attached to the harness, and its orientation is represented by three angular displacements: roll ϕ_x, pitch ϕ_y, and yaw ϕ_z relative to the base coordinate system. Let be the unit vectors pointing in the directions of the harness coordinate axes x', y', z', respectively. Concatenating these unit vectors in a 3x3 matrix we can write the compact expression

$$[\mathbf{n}, \mathbf{t}, \mathbf{b}] = \mathbf{R}_z(\phi_z)\mathbf{R}_y(\phi_y)\mathbf{R}_x(\phi_x) \tag{7.1}$$

where $\mathbf{R}_z(\phi_z), \mathbf{R}_y(\phi_y), \mathbf{R}_x(\phi_x)$ are 3x3 rotation matrices about the x, y, and z axes, respectively.

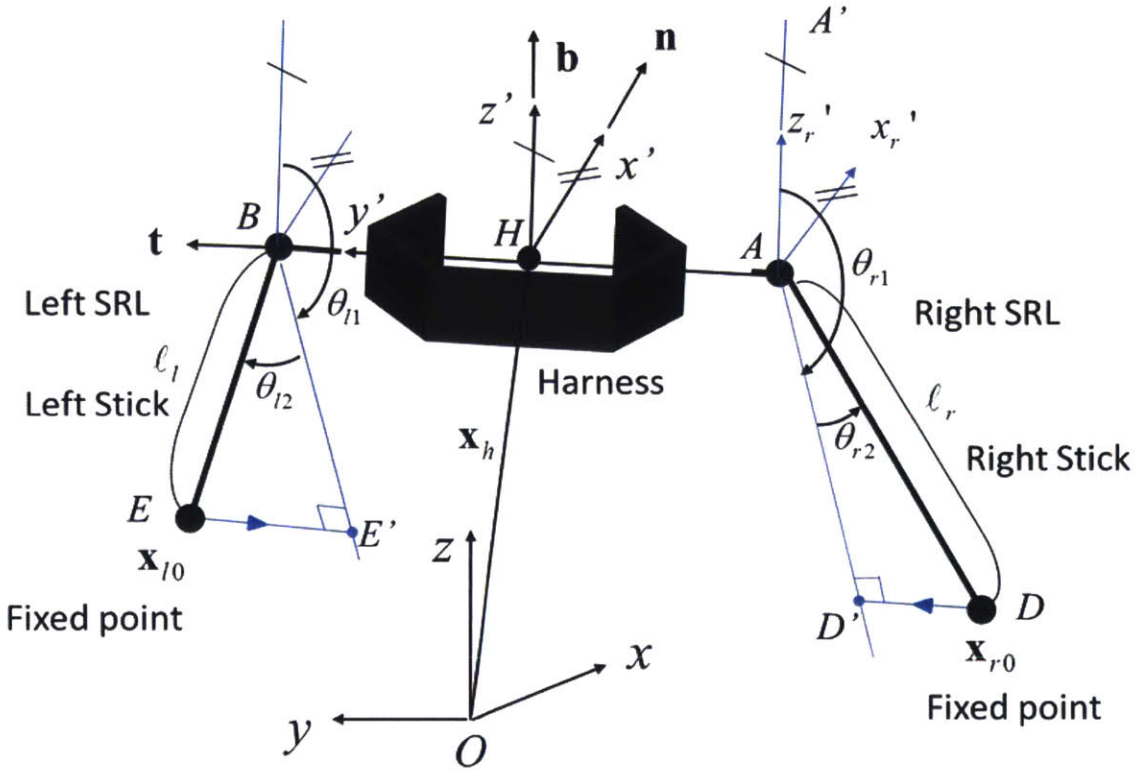

Figure 7-3: Schematic of the SRL system, coordinate frames, and joint angles. Point D' is the projection of point D, the fixed point of the right SRL, onto the $A - x'_r z'_r$ plane; the revolute joint angles are defined as $\theta_{r1} = \angle A'AD'$, $\theta_{r2} = \angle D'AD$; the left revolute angles are defined in a similar manner.

Each SRL has two revolute joints and one prismatic joint with joint displacements denoted as θ_1, θ_2, l_3, respectively. The three joint variables form a "polar coordinate system" relative to the harness coordinate frame $H - x'y'z'$ as shown in Fig.3. Each SRL has a gripper or a clamp at the tip of the stick for securing its endpoint to the surrounding environment. For a given harness position and orientation and a given location of the endpoint fixed to the environment, the joint angles of each SRL can be obtained analytically. Solving a simple inverse kinematic problem, we can write them as a vectorial function:

$$\begin{pmatrix} \theta_1 \\ \theta_2 \\ l_3 \end{pmatrix} = \mathbf{g}(x_h, y_h, z_h, \phi_x, \phi_y, \phi_z; x_0, y_0, z_0) \tag{7.2}$$

where x_0, y_0, z_0 are coordinates of the fixed point. Similar equations can be obtained for both SRLs. Denoting the right SRL with the subscript r and the left SRL by l, we can collectively write the joint displacements as a vectorial function of the harness position and orientation for given fixed points of both SRLs.

$$\mathbf{q} = \begin{pmatrix} \theta_{r1} \\ \theta_{r2} \\ l_{r3} \\ \theta_{l1} \\ \theta_{l2} \\ l_{l3} \end{pmatrix} = \begin{pmatrix} \mathbf{g}_r(x_h, y_h, z_h, \phi_x, \phi_y, \phi_z; x_{r0}, y_{r0}, z_{r0}) \\ \mathbf{g}_l(x_h, y_h, z_h, \phi_x, \phi_y, \phi_z; x_{l0}, y_{l0}, z_{l0}) \end{pmatrix} \tag{7.3}$$

Assuming that the movable range of each joint is properly limited to avoid multiple solutions to the inverse kinematic problem, the six variables of the harness position and orientation $x_h, y_h, z_h, \phi_x, \phi_y, \phi_z$ completely determine the joint displacements of both SRL limbs for given right and left fixed points, x_{r0}, y_{r0}, z_{r0} and x_{l0}, y_{l0}, z_{l0}. In other words, the six variables $x_h, y_h, z_h, \phi_x, \phi_y, \phi_z$ provide a complete and independent set of generalized coordinates that locate the system.

Differentiating the above kinematic equation yields the Jacobian matrix relating infinitesimal joint displacements to infinitesimal harness position and orientation.

$$d\mathbf{q} = \mathbf{J}d\mathbf{p} \ , \quad \mathbf{J} = \begin{pmatrix} \frac{d\mathbf{g}_r}{d\mathbf{p}} \\ \frac{d\mathbf{g}_l}{d\mathbf{p}} \end{pmatrix} \in \Re^{6x6} \tag{7.4}$$

where $d\mathbf{p} = (dx_h, dy_h, dz_h, d\phi_x, d\phi_y, d\phi_z)^T$.

Fig. 4 shows all the forces and moments acting on the SRL system that produce work. We assume that the sticks of the SRLs are massless and that the total mass of the human body and the harness is m with its center of mass at $\mathbf{x}_c = (x_c, y_c, z_c)^T$. The

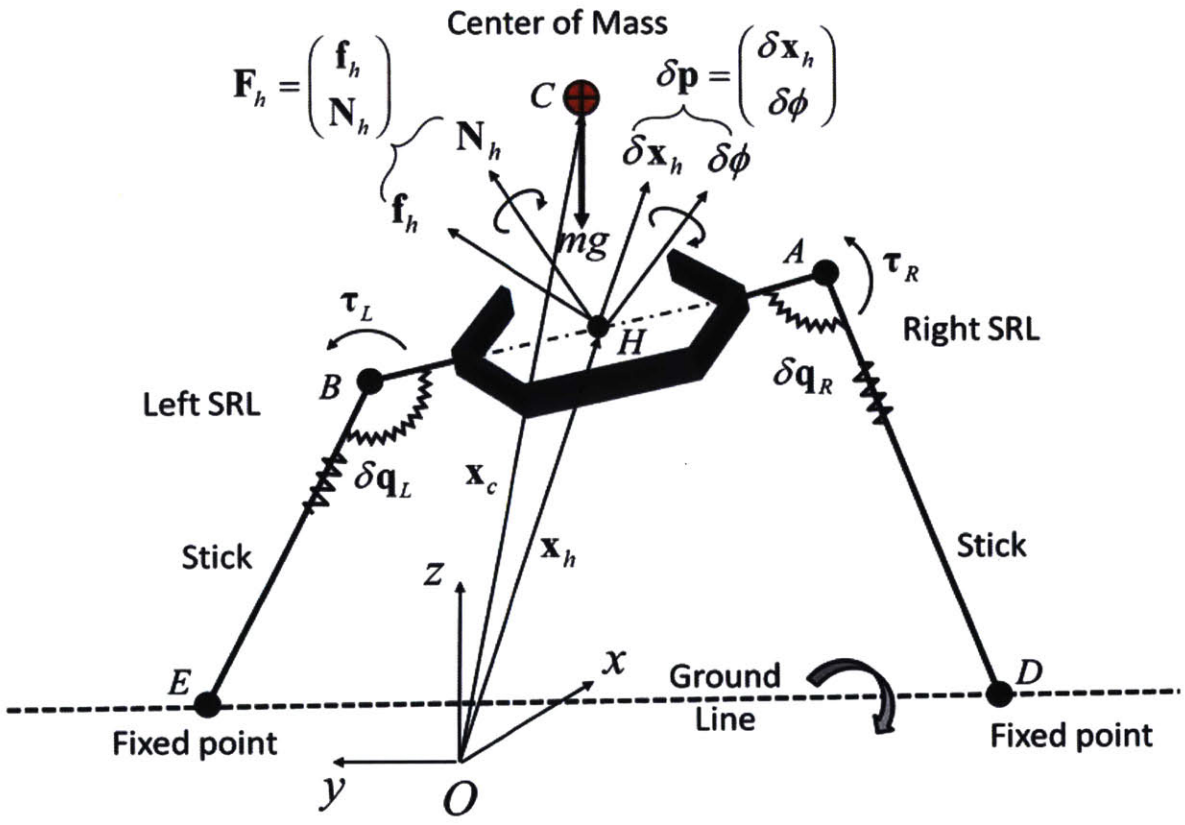

Figure 7-4: Forces and moments acting on the SRL system.

human generates force $\mathbf{f}_h$ and moment $\mathbf{N}_h$ acting on the harness, which are collectively represented as a 6-dimensional vector or wrench: $\mathbf{F}_h = (\mathbf{f}_h^T, \mathbf{N}_h^T)^T$. The two revolute and one prismatic joints of each SRL produce torques τ_1, τ_2 and force f_3, respectively. These joint torques and forces are collectively represented as a 6-dimensional vector $\tau = (\tau_{r1}, \tau_{r2}, f_{r3}, \tau_{l1}, \tau_{l2}, f_{l3})^T$. The virtual work done by these forces and moments on the SRL system with both sticks fixed to the environment is given by

$$\delta\, Work = mg\delta z_c + \mathbf{F}_h^T \delta\mathbf{p} + \tau^T \delta\mathbf{q} \tag{7.5}$$

Since the harness position and orientation $\mathbf{p}$ are generalized coordinates, it can be written as

$$\delta\, Work = (mg\mathbf{e}_z^T + \mathbf{F}_h^T + \tau^T \mathbf{J})\delta\mathbf{p} \tag{7.6}$$

where $\delta z_c = \mathbf{e}_z^T \delta \mathbf{p}$ with $\mathbf{e}_z^T = dz_c/d\mathbf{p} \in \Re^{1x6}$. The system is statically balanced if, and only if, the above virtual work vanishes for all $\delta \mathbf{p}$. That is,

$$mg\mathbf{e}_z + \mathbf{F}_h + \mathbf{J}^T \tau = 0 \tag{7.7}$$

The above equilibrium condition provides us with a basic formula for analyzing effectiveness of body bracing, human efforts, and support stability.

7.3.2 Stability Analysis

The SRLs are required to stably support the human body. In this section we will obtain the stiffness with which the body is supported, followed by its synthesis for stabilization. In analyzing the body support stiffness we assume that the human does not generate any force other than the gravity force of the body, $\mathbf{F}_h = 0$. The objective of bracing is to reduce the human effort. We consider the situation where the human is relaxed at an equilibrium point.

Let $\bar{\mathbf{p}}$ be an equilibrium harness position and orientation, and $\bar{\mathbf{q}}$ be the corresponding joint displacement vector. Consider small displacements from these equilibrium coordinates:

$$\Delta \mathbf{p} = \mathbf{p} - \bar{\mathbf{p}} \,, \quad \Delta \mathbf{q} = \mathbf{q} - \bar{\mathbf{q}} \tag{7.8}$$

Note that, at equilibrium $\bar{\mathbf{p}}, \bar{\mathbf{q}}$, the static balance conditions are satisfied with joint torques $\bar{\tau}$:

$$mg\mathbf{e}_z + \mathbf{J}^T \bar{\tau} = 0 \tag{7.9}$$

Our objective is to obtain reference inputs and feedback control law of the SRLs for stably supporting the body. To this end we consider that the joint torques are controlled according to the following vector Hookean law:

$$\tau = \bar{\tau} - \mathbf{K}_q \Delta \mathbf{q} \tag{7.10}$$

where $\mathbf{K}_q \in \Re^{6x6}$ is a real, symmetric stiffness matrix in the joint space that can be tuned with joint feedback gains. Positive feedback gains produce restoring joint torques towards the equilibrium $\bar{\mathbf{q}}$.

Consider a potential function in the vicinity of the equilibrium point:

$$U = mgz_c - \bar{\tau}^T \Delta\mathbf{q} + \frac{1}{2}\Delta\mathbf{q}^T \mathbf{K}_q \Delta\mathbf{q} \tag{7.11}$$

The quasi-static stability can be examined with the second derivative of the potential function:

$$\frac{d}{d\mathbf{p}}\left(\frac{dU}{d\mathbf{p}}\right)^T = \frac{d}{d\mathbf{p}}(mg\mathbf{e}_z + \mathbf{J}^T\mathbf{K}_q\Delta\mathbf{q} - \mathbf{J}^T\bar{\tau}) \tag{7.12}$$

To execute the second derivative we need Hessians given by

$$\mathbf{E}_z \triangleq \frac{d\mathbf{e}_z}{d\mathbf{p}} = \left\{\frac{\partial^2 z_c}{\partial p_j \partial p_k}\right\} \in \Re^{6x6} \tag{7.13}$$

$$\mathbf{H}_i \triangleq \left\{\frac{\partial^2 q_i}{\partial p_j \partial p_k}\right\} \in \Re^{6x6}\ ,\quad i = 1, ..., 6 \tag{7.14}$$

Using these Hessians and evaluating the second derivative of the potential function at the equilibrium where $\tau = \bar{\tau}$, we can find the stiffness matrix with which the body is held in equilibrium.

$$\mathbf{K}_p(\bar{\mathbf{p}}) \triangleq \frac{d}{d\mathbf{p}}\left(\tfrac{dU}{d\mathbf{p}}\right)^T\Big|_{\bar{\mathbf{p}}} = \left(mg\tfrac{d\mathbf{e}_z}{d\mathbf{p}} + \mathbf{J}^T\mathbf{K}_q\mathbf{J} - \tfrac{d}{d\mathbf{p}}(\mathbf{J}^T\tau)\right)\Big|_{\bar{\mathbf{p}}}$$

$$\mathbf{K}_p(\bar{\mathbf{p}}) = mg\bar{\mathbf{E}}_z + \bar{\mathbf{J}}^T\mathbf{K}_q\bar{\mathbf{J}} - \sum_{i=1}^{6}\bar{\tau}_i\bar{\mathbf{H}}_i \tag{7.15}$$

where $\bar{\mathbf{E}}_z = \mathbf{E}_z|_{\bar{\mathbf{p}}}$, $\bar{\mathbf{J}} = \mathbf{J}|_{\bar{\mathbf{p}}}$, and $\bar{\mathbf{H}} = \mathbf{H}|_{\bar{\mathbf{p}}}$. Note that the above stiffness matrix is represented in the $\mathbf{p}$ space, the coordinates of the harness position and orientation. If this stiffness matrix is positive definite, the equilibrium is stable in the quasi-static sense.

7.3.3 Stabilization

Based on the stiffness matrix given by (15), this section addresses how to make the SRL system quasi-statically stable. We consider two ways of making the stiffness matrix positive semi-definite. One is to exploit the Hessian term, the third term in (15), and the other is by the joint servo stiffness, the second term in (15). Combining these two methods of stabilizing the stiffness matrix will lead to an effective means of supporting the human stably.

Null Space Stabilization

The Jacobian matrix is not of full rank, i.e. $\det \mathbf{J} = 0$. This implies that there exists at least one direction in the $\mathbf{p}$ space (one screw) in which displacement $\Delta\mathbf{p}$ does not produce any joint displacement in $\mathbf{q}$. In fact a rotation of the whole SRL system about the axis connecting both fixed points D and E does not cause any displacement in the joint space. See the rotation about the broken line DE, called the Ground Line in Fig.4. Consequently, the joint compliance control cannot influence the stiffness in this particular direction, which belongs to the Jacobian null space:

$$\Delta\mathbf{p}_{null} \in N(\mathbf{J}) \tag{7.16}$$

This further implies that both the second and the third terms of the body support stiffness $\mathbf{K}_p$ in (15) are not of full rank:

$$\det\left(\bar{\mathbf{J}}^T\mathbf{K}_q\bar{\mathbf{J}} - \sum_{i=1}^{6}\bar{\tau}_i\bar{\mathbf{H}}_i\right) = 0 \tag{7.17}$$

The best we can do is to make the stiffness matrix positive-definite in the range space, which excludes the rotation about Ground Line DE.

Remark The existence of null space also implies that there exists at least one direction of joint torque vector that does not generate any force/moment (wrench) in the $\mathbf{p}$ space. Such a joint torque vector is in the null space of the Jacobian transpose [3],

$$\tau_{null} \in N(\mathbf{J}^T) = [R(\mathbf{J})]^{\perp} \tag{7.18}$$

where $R(\mathbf{J})$ is the range space of the Jacobian and $[-]^{\perp}$ represents its orthogonal complement. This joint torque vector indicates an internal force/torque that does not influence the static balance conditions. However, they do influence the body support stiffness through the third term in (15): $-\sum_{i=1}^{6} \bar{\tau}_i \bar{\mathbf{H}}_i$.

Since the rank of $\mathbf{J}$ is 5 at most configurations, the dimension of $N(\mathbf{J}^T)$ is 1. Let us write the null joint torque vector as

$$\begin{gathered} \tau_{null} = \alpha \mathbf{t}_{null} \\ |\mathbf{t}_{null}| = 1 \ , \ \ \mathbf{t}_{null} = (t_1 \ t_2 \ t_3 \ t_4 \ t_5 \ t_6) \end{gathered} \tag{7.19}$$

where α is a scalar. Substituting this into the Hessian term yields

$$\alpha \mathbf{H}_{null} \triangleq \alpha \sum_{i=1}^{6} t_i \bar{\mathbf{H}}_i \tag{7.20}$$

Note that both t_i and $\bar{\mathbf{H}}_i$ are kinematic quantities, uniquely determined at each $\mathbf{p}$, the harness position and orientation. The 6x6 matrix $\alpha \mathbf{H}_{null}$ provides the "tunable" subspace where the support stiffness can be varied by tuning the joint torques in the null space. The matrix $\mathbf{H}_{null}$ may contribute to increasing or decreasing the stability in the tunable subspace. Since parameter α may take both positive and negative values, one can always use this Hessian term to improve the stability by selecting the sign of parameter α.

Joint Servo Stiffness

The null-space stabilization with $\alpha \mathbf{H}_{null}$ may not be able to stabilize all directions. The joint servo stiffness given by the second term in (15) can be used for making the system quasi-stable in the whole range space. Let $\mathbf{K}_{p-des}$ be a desired or target stiffness in the $\mathbf{p}$ coordinate system, which is positive definite in the range space. Assuming that the null-space stabilization is in place, we can write the conditions for the joint servo stiffness to satisfy as

$$\bar{\mathbf{J}}^T \mathbf{K}_q \bar{\mathbf{J}} = \mathbf{K}_{p-des} - mg\bar{\mathbf{E}}_z + \alpha \mathbf{H}_{null} \tag{7.21}$$

Compared to the null space stabilization, the joint servo stiffness is more complex, requiring active control of joint torques. It is wise to minimize the gains of the joint servo loops, which can be obtained by using the pseudo-inverse of the Jacobian.

$$\mathbf{K}_q = (\bar{\mathbf{J}}^T)^{\#} [\mathbf{K}_{p-des} - mg\bar{\mathbf{E}}_z + \alpha \mathbf{H}_{null}] \bar{\mathbf{J}}^{\#} \tag{7.22}$$

Note that this solution minimizes the norm of the joint feedback gain matrix: $|\mathbf{K}_q|$.

7.3.4 A Special Case

Before implementing the above stabilization algorithms on a prototype SRL system, we discuss a special case which is of practical importance. One of the critical requirements for body support SRLs is to minimize the humanâĂŹs effort in keeping a body posture. An ideal case is that the SRL completely supports the human weight so that the human exerts no force and no moment, as assumed in the above analysis: $\mathbf{F}_h = 0$. This can be achieved at a particular configuration of the SRL, which turns out to be useful in most cases. This section will discuss this particular solution.

Consider the case where both SRL sticks have the same length $l_{r3} = l_{l3}$, and the center of mass C is directly above the center of the harness at a distance h in the direction of unit vector $\mathbf{b}$, so that $\mathbf{x}_c = \mathbf{x}_h + h\mathbf{b}$. When the point C is below the harness, the variable h takes a negative value. Furthermore, let us first assume that all the revolute joints of the SRLs generate no torques, $\tau_{r1} = \tau_{r2} = \tau_{l1} = \tau_{l2} = 0$, and the prismatic joints alone bear the gravity load. Under these assumptions the only possible equilibrium exists when the center lines of the right and left SRL sticks and the gravity force vector meet at a single point G, as shown in Fig. 5. At this equilibrium, the SRL configuration is symmetric, and the points A, B, C, and H as well as the fixed points of both SRLs are within the same vertical plane. Consequently, $\theta_{r1} = \theta_{r2} = 0$, $\theta_{r2} = \theta_{l2} = \theta_2$, $\phi_x = \phi_y = \phi_z = 0$ and $y_c = 0$. The prismatic joint

forces can be found as

$$\bar{f}_{r3} = \bar{f}_{r3} = -\frac{mg}{2\cos\theta_{r2}} \tag{7.23}$$

The Hessian of z_c is given by

$$\bar{\mathbf{E}}_z = \left\{\frac{\partial^2 z_c}{\partial p_j \partial p_k}\right\}\Big|_{\bar{\mathbf{p}}} = diag(0,0,0,-h,-h,0) \tag{7.24}$$

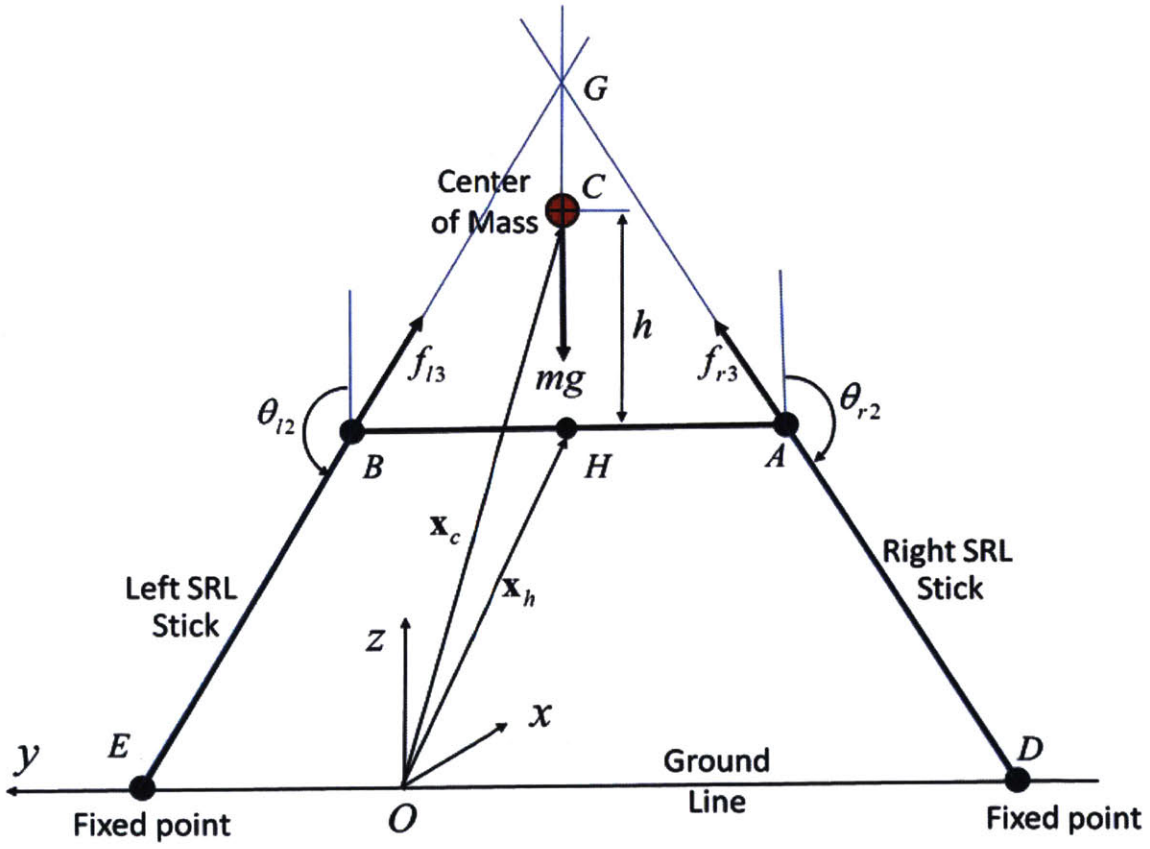

Figure 7-5: Symmetric equilibrium configuration.

Furthermore, denoting the stiffness of both prismatic joints by k_0, we can write the joint stiffness matrix as

$$\mathbf{K}_q = diag(0,0,k_0,0,0,k_0) \tag{7.25}$$

since no revolute joint torques are generated. Substituting (23) - (25) into (15)

yields

$$\mathbf{K}_p = mg\bar{\mathbf{E}}_z + k_0(\bar{\mathbf{J}}_3^T\bar{\mathbf{J}}_3 + \bar{\mathbf{J}}_6^T\bar{\mathbf{J}}_6) + \frac{mg}{2}\left(\frac{1}{\cos\theta_{r2}}\bar{\mathbf{H}}_3 + \frac{1}{\cos\theta_{l2}}\bar{\mathbf{H}}_6\right) \tag{7.26}$$

where $\mathbf{J}_3$ and $\mathbf{J}_6$ are the third and the sixth rows of the Jacobian matrix:

$$\mathbf{J}_3 = \frac{d\,l_{r3}}{d\mathbf{p}} \in \Re^{1x6}\ ,\quad \mathbf{J}_6 = \frac{d\,l_{l3}}{d\mathbf{p}} \in \Re^{1x6} \tag{7.27}$$

and the Hessians are given by

$$\mathbf{H}_3 = \frac{d}{d\mathbf{p}}\left(\frac{d\,l_{r3}}{d\mathbf{p}}\right)^T \in \Re^{6x6}\ ,\quad \mathbf{H}_6 = \frac{d}{d\mathbf{p}}\left(\frac{d\,l_{l3}}{d\mathbf{p}}\right)^T \in \Re^{6x6} \tag{7.28}$$

For $0 \leq \theta_2 < \pi/2$, the harness is suspended from a ceiling or a higher place. Therefore, the system is stable. In contrast, for $\pi/2 < \theta_2 \leq \pi$, it becomes a type of inverted pendulum, hence unstable. To stabilize the system the body support stiffness matrix (26) is compensated with joint torques exerted at the revolute joints. First, the null space stabilization is considered. The joint torques in the null space $N(\mathbf{J}^T)$ must satisfy the equilibrium conditions. At the configuration in Fig. 5, the null space joint torques meet the following conditions:

$$\begin{aligned} \tau_{r1} &= \tau_{l1} = 0 \\ \tau_{r2} &= \tau_{l2} = \tau_2 \\ f_{r3} &= f_{l3} = f_3 \\ 2f_3\cos\theta_2 + 2\tfrac{\tau}{l}\sin\theta_2 + mg &= 0 \end{aligned} \tag{7.29}$$

where $l = l_{r3} = l_{l3}$. With the joint torques of (29), the body support stiffness matrix is modified to

$$\mathbf{K}_p = mg\bar{\mathbf{E}}_z + k_0(\bar{\mathbf{J}}_3^T\bar{\mathbf{J}}_3 + \bar{\mathbf{J}}_6^T\bar{\mathbf{J}}_6) - f_3(\bar{\mathbf{H}}_3 + \bar{\mathbf{H}}_6) - \tau_2(\bar{\mathbf{H}}_2 + \bar{\mathbf{H}}_5) \tag{7.30}$$

Note that joint torque τ_2 can take both positive and negative values as long as it satisfies the last condition of (29). The positive joint torque, $\tau_2 > 0$, results in

stabilizing the body support stiffness in certain directions, as will be demonstrated with numerical examples for a prototype SRL system in the following section. The null space stabilization alone does not completely stabilize the system, but it reduces the active feedback control effort for stabilization.

7.4 Implementation and Experiment

7.4.1 Prototype

A SRL prototype (Fig. 6) has been developed in order to verify the load support strategy and control architecture that have been derived and analyzed in the previous sections. The robot is worn with a backpack-like soft structure, equipped with shoulder straps and a climbing harness. The bottom of the harness frame was shaped to fit the hip bone of a user by using 3D printing technology. This 3D-printed socket firmly secures the SRLs to the human, allowing for body support in all directions in the range space, and improves the comfort of the user. The prototype is equipped with two robotic limbs, having 3 DOF each. The locations of the revolute joints were determined such that the center of the harness would be near the center of the total mass, that is, Points C and H coincide.

Two rotational joints (actuated by Dynamixel Pro h54-100- s500-r servos, max continuous torque: 20 Nm) are placed at the base of the robotic limbs. Their axes intersect, forming an equivalent ball-and-socket joint. The third joint is prismatic (actuated by Firgelli FA-05-12-18 linear actuators, max force: 666 N, stroke: 0.46 m), and allows the robotic limbs to extend and retract in order to contact the environment and support the user. The prismatic joints are not backdrivable due to a high gear ratio, so that they can bear the human with no actuator torque. The joint control loops run on microcontrollers in the robot base, while the high-level control commands, including reference configuration, actuator reference torques, and controller gains, are computed on a desktop PC and sent to the SRL.

The total weight of the robot is 13 kg. Power reaches the actuators through a

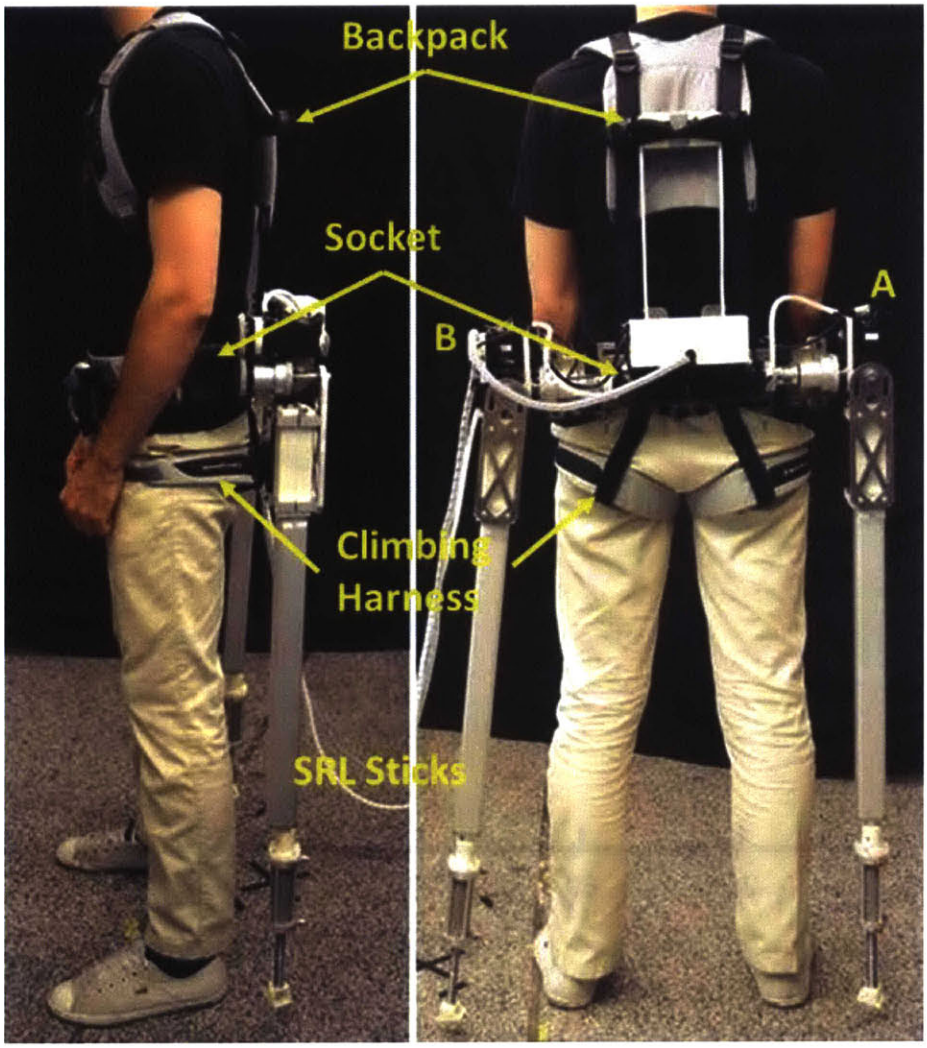

Figure 7-6: Prototype of SRL system worn by a human around the waist.

power cord. The robot can become tetherless with a wireless link and a battery pack, resulting in an additional weight of 2kg.

7.4.2 Numerical Computation

Using the parameter values and the specifications of the above prototype system, the body support stiffness is computed to verify the analytical results. Practical conditions, such as actuator torque limits, are taken into account in the following numerical examples.

First, we consider the symmetric configuration shown in Fig. 5. The eigenvalues

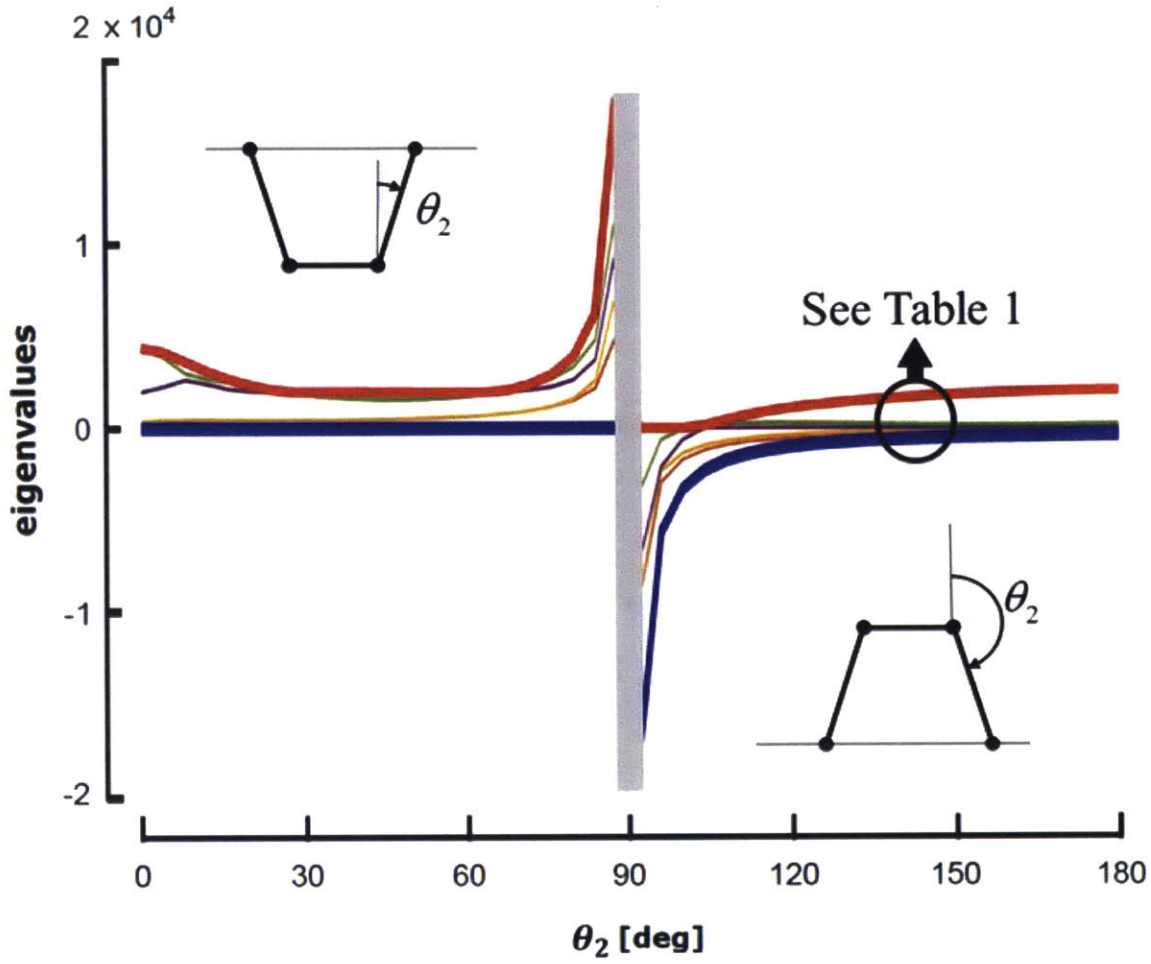

Figure 7-7: Eigenvalues of Support Stiffness Matrix K_p without stabilization control at the symmetric configuration, eq. (26). Red lines and blue lines indicate the maximal and minimal eigenvalues, respectively. At the grey zone of θ_2 near 90°, the SRL system cannot bear the human gravity load due to structural strength and actuator torque limits.

of the body support stiffness matrix given by (26) are plotted in Fig. 7 against joint angle θ_2, $(\theta_{r2} = \theta_{l2})$. In this plot, no stabilization control is considered. The sticks can bear the human load with no actuator torque because of the non-backdrivable actuators. The sticks are treated as rods with a high structural stiffness $k_0 \gg 1$, which is equivalent to a high stiffness created by high gain joint servo in a quasi-static sense. We first consider the case where the center of mass is located at the harness center, $h = 0$.

As shown in Fig. 7, one of the eigenvalues is zero for all configurations, indicating

that the support stiffness matrix K_p is singular. When the joint angle is less than 90 degrees, $0 \leq \theta_2 < \pi/2$, all eigenvalues are positive except for the zero eigenvalue. The eigenvector associated with the zero eigenvalue reveals that the rotational motion of the human body about the y-axis is not constrained. A simple joint feedback control around the axes of θ_{r1}, θ_{l1} can produce positive servo stiffness, making the entire system stable.

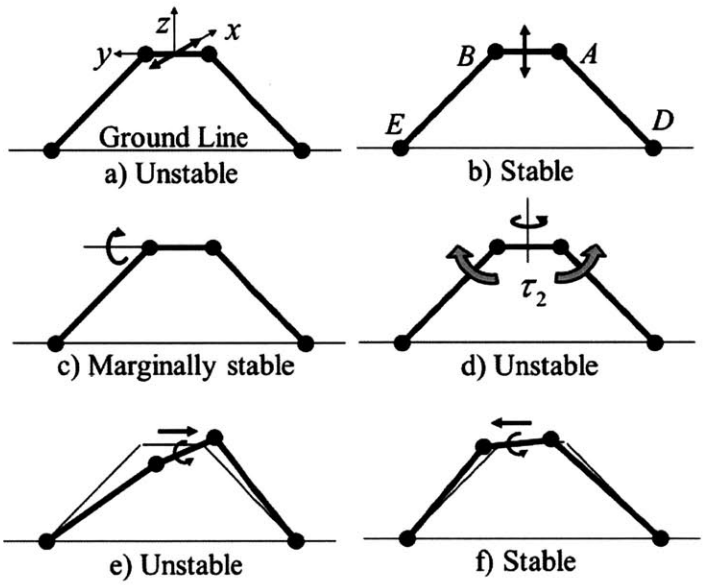

Figure 7-8: Deformation mode shapes obtained from the eigenvectors of the support stiffness matrix K_p at the symmetric configuration with no stabilization control, $h = 0$.

In contrast, the system becomes unstable for $\pi/2 < \theta_2 \leq \pi$, having some negative eigenvalues. Fig. 8 illustrates the 6 modes given by the eigenvectors associated with

Table 7.1: Eigenvalues and eigenvectors of support stiffness matrix without stabilization control at $\theta_2 = 145°$.

mode		**a**	**b**	**c**	**d**	**e**	**f**
eigenvalue		-980	133,550	0	-270	-380	77,580
eigenvector	**x**	1	0	0	0	0	0
	y	0	0	0	0	-0.3942	0.9190
	z	0	1	0	0	0	0
	ϕ_1 **(roll)**	0	0	0	0	0.9190	0.3942
	ϕ_2 **(pitch)**	0	0	1	0	0	0
	ϕ_3 **(yaw)**	0	0	0	1	0	0

the individual eigenvalues, as listed in Table 1. The mode in the x-axis translation is unstable; the SRL may fall in this direction. See Fig. 8a. The mode in the z-axis translation is stable with a large eigenvalue due to the high structural stiffness of the sticks (Fig. 8b). The mode of rotation about the y-axis is marginally stable with zero eigenvalue (Fig. 8c). The z-axis rotation, on the other hand, is unstable; the SRL tends to collapse as it rotates about the z-axis (Fig. 8d). The SRL also tends to collapse sideways, as shown in Fig. 8e. This mode is a combination of the y-axis translation and the x-axis rotation. In an orthogonal direction to the mode of Fig. 8e, the stiffness matrix possesses a positive eigenvalue (Fig. 8f). In this direction, the sticks are compressed or extended, exerting a large restoring force with the spring constant k_0. These modes are called modes a through f.

Now consider the stabilization control to stabilize some of the unstable modes. Mode a in Fig. 8 cannot be stabilized, since it is outside the range space; the SRL system is free to rotate about the ground line. The remaining 5 modes are within the range space and can be stabilized. For mode c, joint feedback control around the axes of θ_{r1}, θ_{l1} is required for generating positive servo stiffness, as in the case of $0 \leq \theta_2 < \pi/2$. Two other unstable modes d and e must be stabilized. It is interesting to note that null space stabilization can contribute to the stabilization of modes d and e.

Fig. 9 shows the eigenvalues of the support stiffness matrix with null space stabilization based on (30). Both unstable modes d and e get closer to the stable region with the null space stabilization. Comparison of the eigenvalues between Fig. 7 (without null space stabilization) and Fig. 9 (with null space stabilization) indicates that the two unstable eigenvalues in Fig.7, -270 and -380, are shifted to approximately -10 in Fig. 9 around $\theta_2 = 145°$. Positive torques applied to both θ_{r2} and θ_{l2} joints increase the internal tension that tends to expand the closed-loop linkage comprising the two sticks, the harness socket, and the ground line. See Fig. 8d. These joint torques, although kept constant, generate resistive effects against collapsing movements illustrated in Fig. 8d and 8e.

Null space stabilization alone cannot stabilize the system in the entire range space.

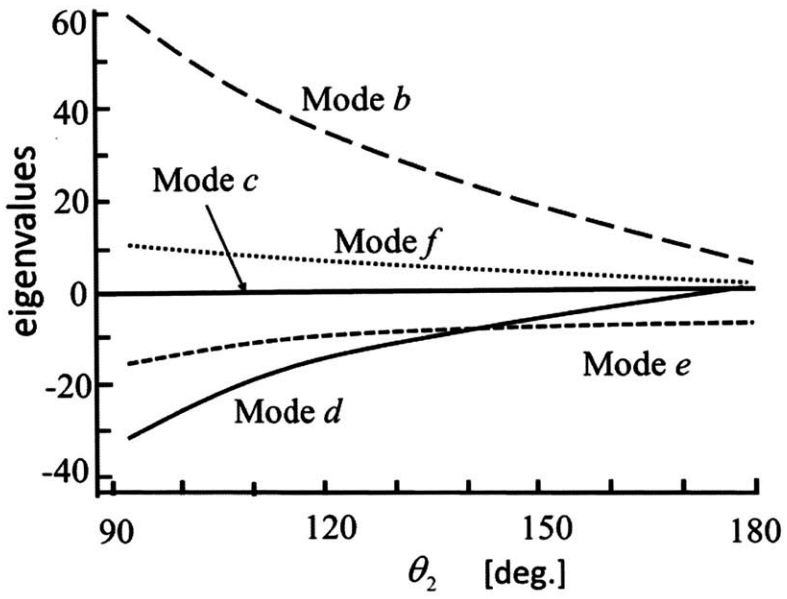

Figure 7-9: Eigenvalues of Support Stiffness Matrix K_p in the range space. The null space stabilization moves the two unstable modes towards the stable range.

We need to add joint servo stiffness with the feedback gain given by (22). Fig. 10a shows the eigenvalues of the support stiffness matrix due to the joint servo stiffness, $\bar{\mathbf{J}}^T\mathbf{K}_q\bar{\mathbf{J}}$, and Fig. 10b shows the overall stiffness including both null space stabilization and the joint servo stiffness control. All the modes were made stable except mode a, which cannot be stabilized. The eigenvalues of the six modes at $\theta_2 = 145^o$ are -546, 1695.4, 110.3, 1.4, 4.1, and 172.5, respectively.

The effectiveness of the null space stabilization varies depending on the configuration, θ_2. If it requires a large toque, it may exceed the torque limit: $0 \leq \tau_2 \leq \tau_{2,max}$. To quantify the effectiveness of the null space stabilization, the difference between the matrix norm of the gain matrix without the null space stabilization and that with the null space stabilization is evaluated for diverse configurations:

$$C = |K_{q,\ no\ null\ space}| - |K_{q,\ with\ null\ space}| \tag{7.31}$$

If this value C is positive, the null space stabilization is effective. Fig. 11 shows the value C against joint angle θ_2. Note that the null space stabilization works effectively for larger θ_2.

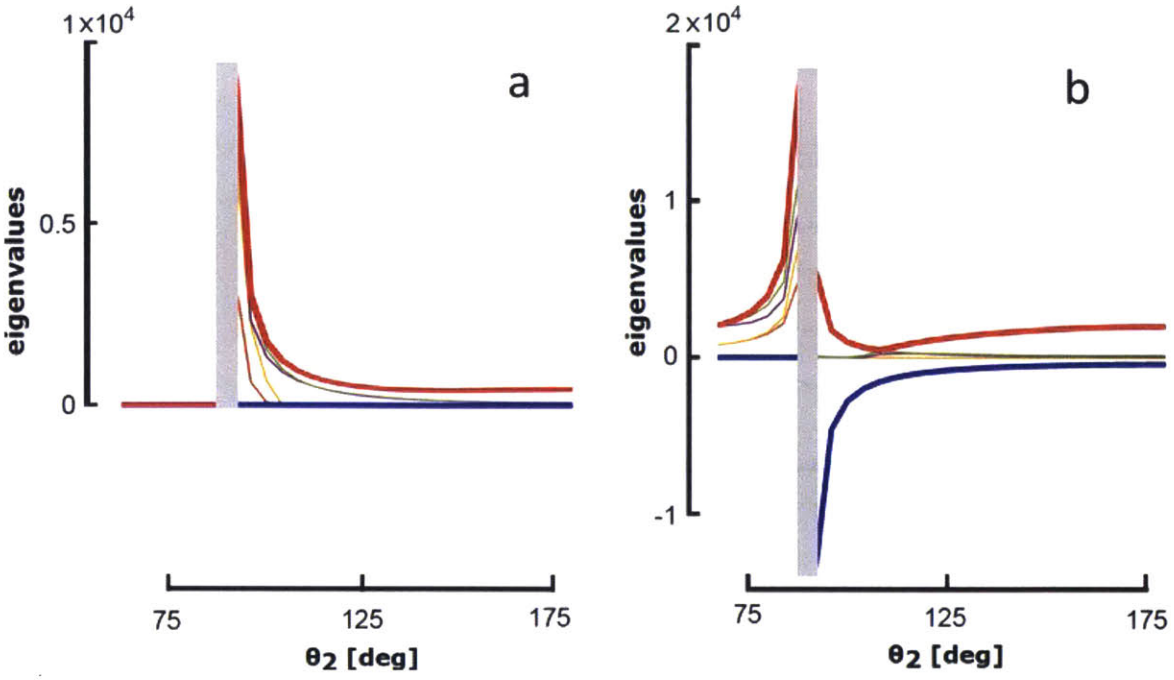

Figure 7-10: Eigenvalues of support stiffness matrix with full stabilization control. a) Contributions of the joint servo stiffness alone, b) The total stiffness with both null space stabilization and joint servo stiffness control.

The height of the total mass, h, plays an important role in stability. In particular, the system can be stabilized if the harness center can be raised higher than the total mass center, i.e. a negative h in Fig. 5. As given by (24), raising the harness center yields a positive stiffness to the fourth and fifth diagonal components of the Hessian $\bar{\mathbf{E}}_z$. These contribute to stabilizing modes c and e in Fig. 8. This arrangement of SRLs is similar to "crutches" that hold the body under the arms. It is however, cumbersome to raise the harness too high since it may interfere with the humanâĂŹs upper body motion. It is a design trade-off between stability and ease of work.

So far, we have examined a simple symmetric configuration case (Fig. 5) to illustrate the effects of the proposed stabilization techniques. However, depending on the environment, such a symmetric configuration may not be allowed, or a non-symmetric configuration may provide a better result. The analytical formulation of the problem presented in this chapter is completely general, and can be applied to any 3D configuration of the robot. As an example of 3D analysis, we now consider

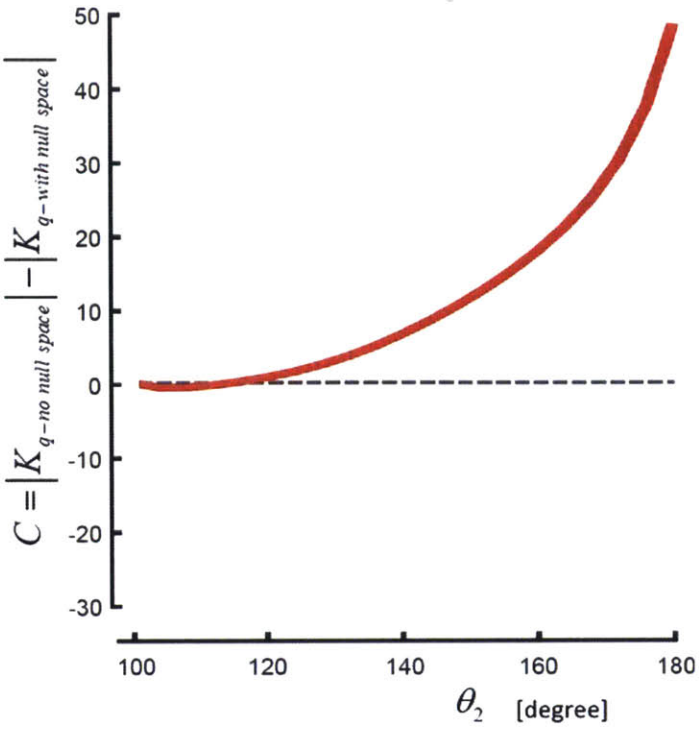

Figure 7-11: Effectiveness of combined null space stabilization and joint servo stiffness compared to joint servo alone. The gain matrix norm for the combined control is smaller.

all the possible left SRL configurations corresponding to a given right SRL position. The length of both SRLs is fixed at $l_{r3} = l_{l3} = l_{max}$. Fig. 12 plots the eigenvalues of K_p for every configuration in the workspace of the left SRL. The blue bar represents the (fixed) configuration of the right SRL. Fig.12a shows the minimum eigenvalue of K_p when no stabilization control is used. To meet the equilibrium condition it is assumed that the human exerts a necessary force $\mathbf{F}_h$. The system is unstable or marginally stable for the entire configurations of the left SRL.

7.4.3 Experimental Evaluation

The stabilization control makes the system stable in the range space. Fig.12b plots the minimum eigenvalue in the range space, which is positive for all the left SRL configurations. This plot not only shows that the system is stable but also indicates the level of stability, i.e. the stiffness in the worst direction. Note that a large

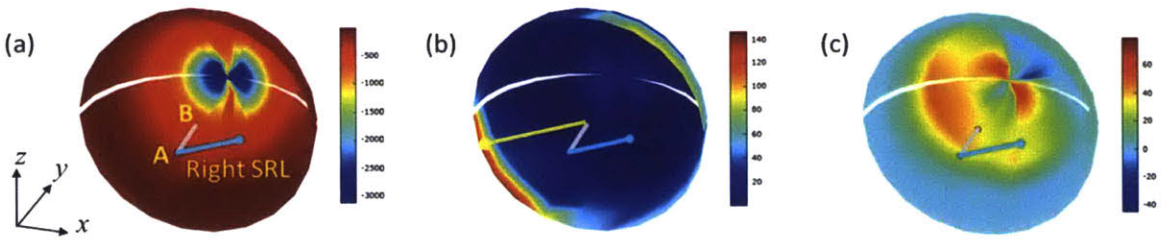

Figure 7-12: Computations for 3D SRL configurations. The right robotic limb (blue bar) is placed at $\theta_{r1} = 56°$, $\theta_{r2} = 34°$, and the left robotic limb is placed at various locations within its workspace (which has the shape of a hemisphere, since the length of the robotic limb is fixed). The base of the robot is represented by a grey bar. Plot a) shows the minimum eigenvalue of K_p when no stabilization control is used. This value is not positive in the workspace, so the system is unstable or marginally stable. Plot b) shows the minimum eigenvalue in the range space, when the stabilizing controller (null space and P control) is applied. The system has been stabilized everywhere, and the stabilization is most effective when the robot is in a symmetric configuration (left robotic limb represented by yellow bar). Plot c) shows the utility of null space stabilization, which is advantageous when the plotted C values (eq. (31)) are positive.

minimum eigenvalue is obtained for the left SRL configuration shown by the yellow bar in Fig. 12b. Fig.12c compares the feedback control effort with and without null-space stabilization. The use of null-space stabilization is beneficial when the difference in norms assumes a large positive value. It can be noticed that null-space stabilization should be used in many SRL configurations, especially when the two SRL sticks are pointing in opposite directions. In these cases, the robot is able to exert much higher internal forces without producing effects on the overall balance of the system.

The stabilization of the SRL system has been tested at the symmetric, planar configuration shown in Fig. 5 ($\theta_2 = 140°$). The experimental setup is shown in Fig. 13a. The end effectors of the robot are secured to the ground with 3D printed ball-and-socket joints, which are free to rotate.

Without stabilization control, the body support stiffness matrix K_p has three unstable (negative) eigenvalues, as shown in Fig. 13b. The x-axis translation (Fig. 13b-(1)) is unstable, and cannot be stabilized. A cable with a soft serial spring was used for preventing the SRL system from falling in the x-axis direction during experiments. The objective of experiments is to stabilize modes d and e (Fig. 13b-(2) and (3)). Restoring force and moment making these modes stable were measured to

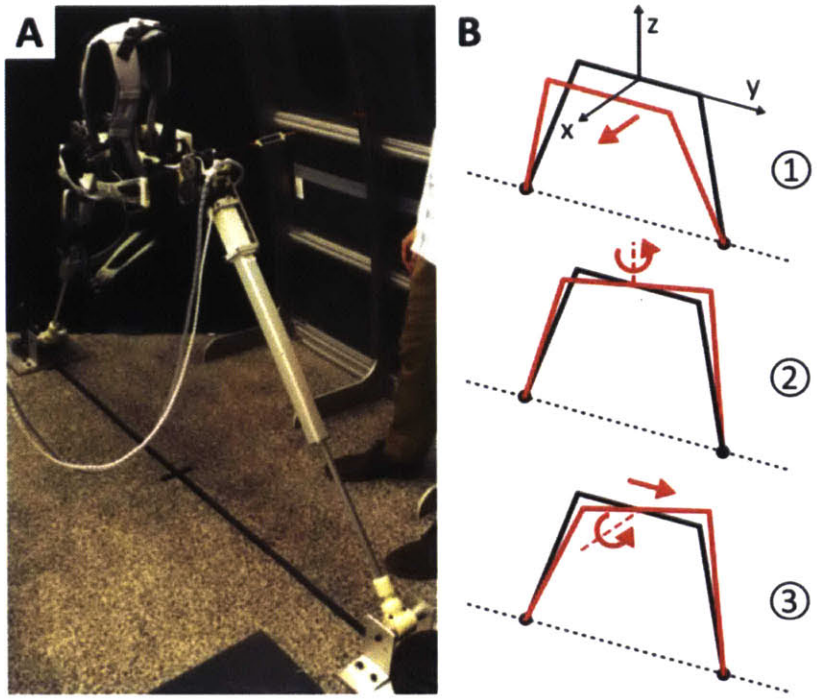

Figure 7-13: Experimental setup for stiffness tests.

evaluate the stiffness in each mode.

Two control strategies were tested. First, the SRL system was stabilized using only joint servo stiffness control. Second, the null space stabilization control was added to the joint stiffness control using the same joint feedback gains as the first case. Fig.14 shows the results. Fig.14a plots the restoring force against the y-axis displacement (mode e). The straight lines represent the theoretical prediction based on the model of the support stiffness matrix. The stiffness without null space stabilization was $6.88 \cdot 10^3$ N/m, whereas the stiffness with the null space stabilization using constant joint torques, $\tau_{r2} = \tau_{l2} = 10$ Nm, achieved $8.66 \cdot 10^3$ N/m of stiffness.

Fig.14b shows the restoring moment against rotational displacement about the z-axis. Without the null space stabilization, the rotational spring constant was $5.26 \cdot 10^2$ Nm/rad, while the one with the null space stabilization was $6.36 \cdot 10^2$ Nm/rad. The use of constant null-space torques has a stabilizing effect on the SRL base. This can be observed both for the linear stiffness in the y direction (which increases by 25% with the addition of null-space torques) and for the rotational stiffness around the z axis (which increases by 21% with the addition of null-space torques).

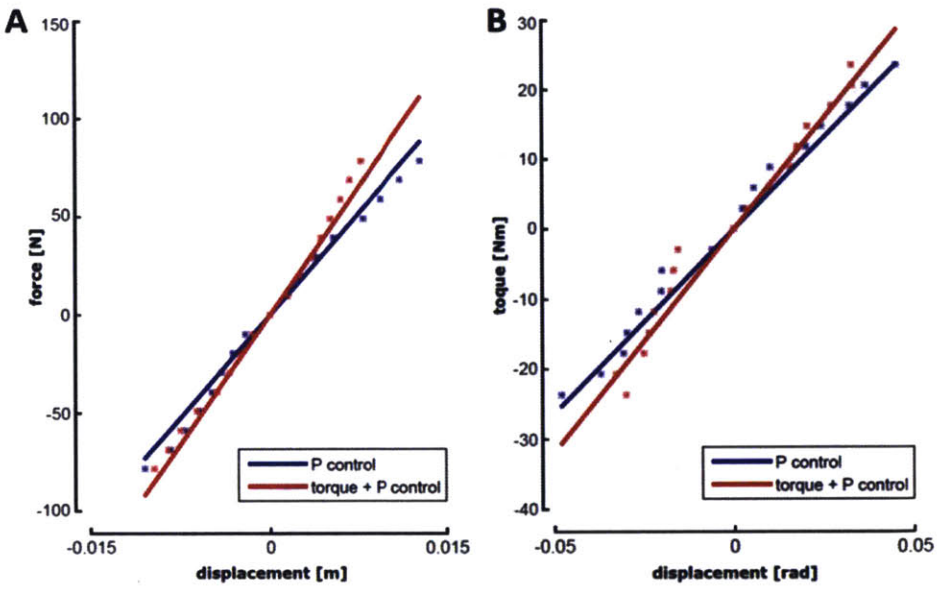

Figure 7-14: Experimental results of stiffness tests. Straight lines are theoretical prediction, while dots are experiment. Blue is joint stiffness control only, and red is combined stabilization.

The stabilization control can be incorporated into the entire SRL control system for assisting a human in practical scenarios. Fig.15 illustrates a typical application of the SRL system to aircraft assembly. The worker bends to reach a lower section of the fuselage, taking a fatiguing posture for a long time (Fig. 15a). Similar tasks can be found in many applications where workers have to work on large structures, such as a ship, a building, or plant equipment. Crouching and standing repeatedly are laborious. The SRL with two high-force prismatic joints can lift or lower the human body, while securing its grippers to the floor beams. The human body can be supported stably with the stabilization control. Although the movement in the x-direction is unstable, the human not only supports the body, but also adjusts the distance to the wall with his legs on the floor. See Fig.15b. All the other directions can be supported stably with an appropriate compliance. Often the human has to change the posture slightly, e.g. moving sideways (mode e) or rotating about the z-axis (mode d). The stiffness of modes d and e can be tuned to provide the human with sufficient stability as well as with freedom to change the posture. The stiffness demonstrated in the above experiment was found to be adequate to meet these requirements. Unlike

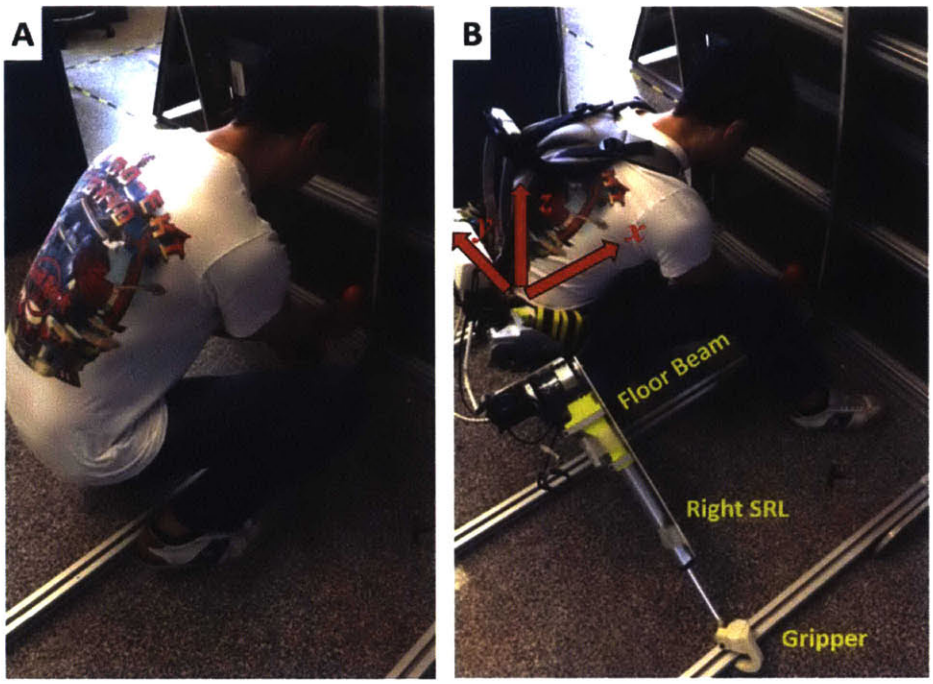

Figure 7-15: Typical application of body support with SRL system.

a passive stool, the SRL is capable of supporting the human with tunable stiffness as well as of lifting and lowering the human in crouching and standing.

7.5 Conclusion

A third prototype of Supernumerary Robotic Limbs (SRL) with high-force prismatic joints has been developed for supporting the wearerâĂŹs body in taking fatiguing postures, or working in a dangerous environment. The stiffness matrix with which the body is supported has been analyzed. Two control methods for stabilizing the body support have been presented: the null space stabilization using Hessian matrices and joint servo stiffness control based on the Jacobian. The two extra-limb structure is kinematically singular, creating a null space where a particular combination of joint torques does not disturb the balance of forces, yet influences the stiffness and quasi-static stability of the system. The joint torques in the null space can contribute to stabilizing the system without active feedback control. The control methods have been implemented on a prototype SRL system. Unlike a standard stool or a passive

body support gear, the SRL system can support a human with tunable body support stiffness, so the human can change the posture freely and stably. With the active joints the SRL can also lift or lower the body for assisting the human in crouching and standing repeatedly.

Chapter 8

Sitting/Standing Assistance

8.1 Introduction

In this chapter, we present the fourth, lightweight prototype of the SRL (Figure 1). This prototype capable of supporting the full weight of the user with a total mass of just 3.5kg. This lightweight performance has been enabled by innovative materials, joint design, and actuation choices (see Chapter 3 and Chapter 10).

We then develop a control strategy that supports the user during sitting and standing motions. The reduced mass and volume of the robot are enabled by innovative design choices including advanced materials, efficient joint structure, and high-performance pneumatic actuation. The assistive control strategy is tailored to each individual based on their motion preferences, and allows the SRL to support the user without getting in the way of his/her movements.

8.2 Technical Approach

We recorded the human motions involved in the sitting and standing process using the Kinect Motion sensing system. We then created a rigid-body 2D model (in the sagittal plane) of the human-robot system (Figure 2), and used it to compute the torques required at each joint for the sitting and standing motions (Figure 3). In the model, the human ankle, knee and hip are represented by points A, K and H

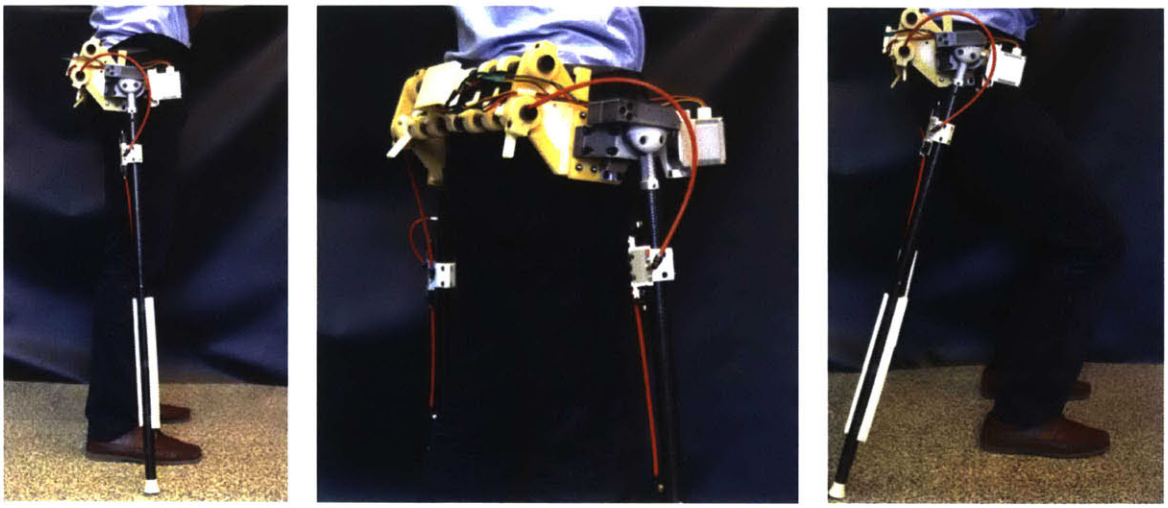

Figure 8-1: (Left, Center) Wearing the robot prototype. The SRL is a wearable robot that assists without getting in the way of the user. Kevlar parts are light yellow, while carbon fiber parts are black. (Right) The task that we consider in this chapter. The SRL assists a user while sitting and standing. Each robotic limb has two rotational degrees of freedom at its base, and a prismatic one along its length.

respectively. Since the SRL is worn through a belt-like harness, we assume that its support forces are applied to the hip of the wearer (point H).

In order to assist the user while sitting down and standing up, the robotic limbs extend backwards and make contact with the ground (at a distance d from the human ankle). The robotic limbs can only exert an axial force F_R, because the have a single

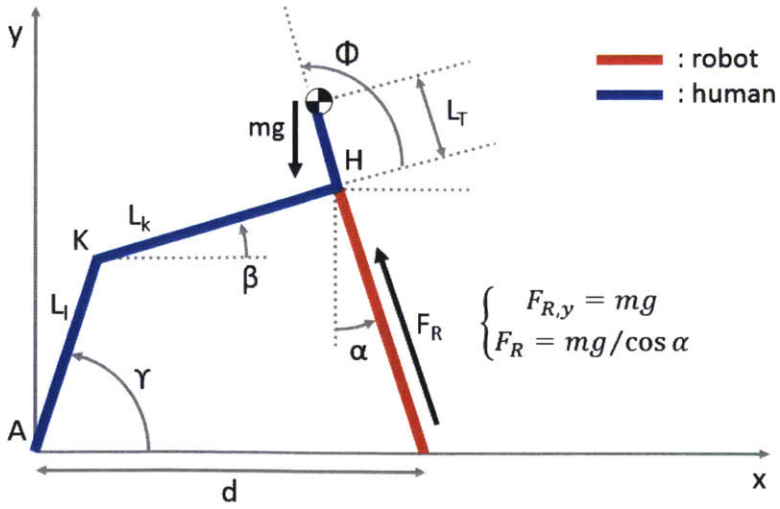

Figure 8-2: Model of the human-robot system, with length and angle parameters.

point of contact with the ground (through hemispherical end effectors realized in rubber with a high coefficient of static friction). In this model, we assume the human mass is concentrated at the Center Of Mass (COM) in the lower torso, and that the mass of the robot is negligible (its weight is 3.5kg, or about 4% of the mass of a typical user). We also assume there is no slip between the robot and its contact points with the ground, and that the motion is completed slowly enough that static laws apply. This is consistent with the slow pace of motion during manufacturing tasks, or during everyday movements for elderly or rehabilitating subjects.

In the simplest assistive approach, the robot force fully compensates for the human weight in the vertical direction (Figure 2). This allows us to determine the robot force F_R required by every user configuration. Applying the model, we find equations for the assisted and unassisted joint torques:

$$\tau_{unassisted} = J_{human}^T \begin{bmatrix} 0 \\ mg \end{bmatrix} \quad , \quad \tau_{assisted} = \tau_{unassisted} + J_{robot}^T \begin{bmatrix} mg\tan(\alpha) \\ -mg \end{bmatrix}$$

From the point of view of the design and manufacturing of the robot prototype, our approach is innovative in three main areas. First, the prototype's structure is entirely made of parts 3D printed using Kevlar and carbon fiber, with Nylon as filler between the fibers. This manufacturing process was enabled by a collaboration with MarkForged, Cambridge, MA. Second, the two rotational degrees of freedom at the base of the robot are combined into a single ball and socket joint. The ball and socket (made of carbon fiber) absorb all of the forces coming from the robotic legs, so that the servomotors actuating them do not need additional shafts or bearings. Moreover, axial forces coming from the robotic limbs pass through the center of the ball joint, and do not generate any torque. This means that the linear actuators and the structure of the robot bear the weight of the user, while the servomotors are only used to move the limbs before contact and to compensate for disturbances. Third, the prismatic degrees of freedom are actuated by pneumatic cylinders. These actuators, controlled by simple on/off valves, produce enough force and move fast enough to provide assistance on

a wide range of tasks, from weight support to balance support. Simple control laws allow us to control the position and force of the pneumatic cylinders with sufficient precision for locomotion tasks (see Figure 5).

8.3 Computing the assistive force during sitting/standing motions

Based on motion data gathered with a Kinect from 10 trials of sitting followed by standing, we can find the joint and torque trajectories as a function of time for a specific human subject (Figure 3). The mean is the red curve, while the standard deviation is shaded in yellow.

Figure 3 displays the joints' position and torque when the subject is sitting down and standing up without external help (unassisted case). In our assistive control strategy, the robot follows the natural trajectory of the human (Figure 3, left plots) but provides an assistive force - applied to the hip of the user - that compensates for the human's weight (Figure 2). We are therefore able to compute the torques that

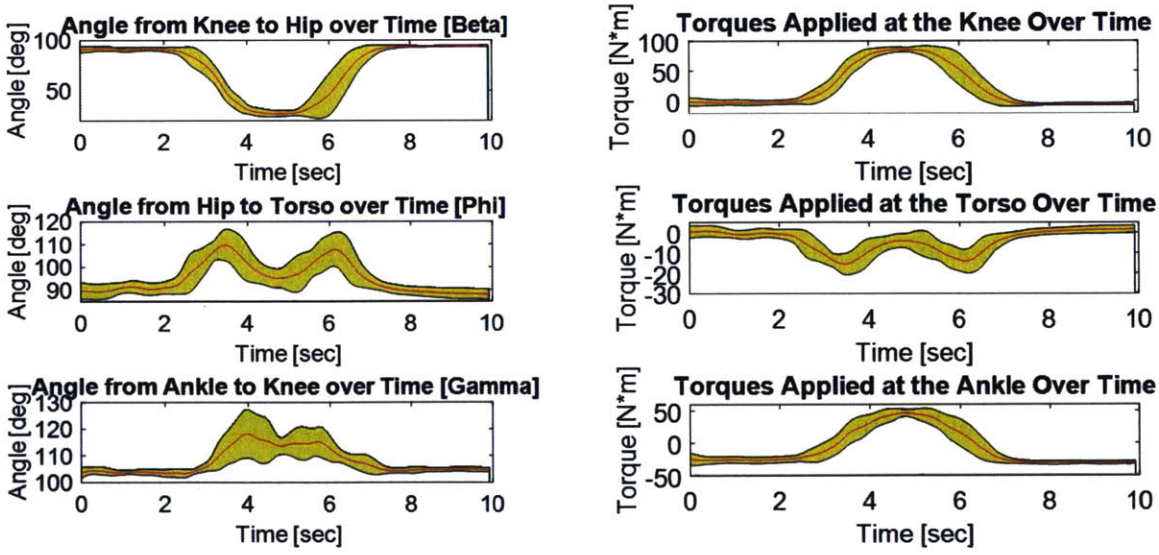

Figure 8-3: (Left) Leg angles calculated from 10 trials of the Kinect for sitting followed by standing. (Right) Torques at each joint calculated from the same Kinect data and our Jacobian model. The red line represents the mean and the shaded yellow area the standard devia-tion over the 10 trials.

the human joints have to apply when the user is supported by the robot (assisted case).

Comparing the assisted torques and the unassisted torques (Figure 4, left), it is possible to notice that in some cases the assisted values exceed the assisted ones. This happens when the robotic limbs are far from the vertical orientation (large values of α, Figure 2), and have to apply significant axial forces in order to compensate for the full weight of the user. This results in the SRL applying a large horizontal disturbance to the hip of the user, that the natural joints are then forced to absorb. We modified the force law such that the absolute value of the assisted torques never exceeds the unassisted case (Figure 4).

The goal for the robot force law outlined above is to be able to map knee angle β (measured in real time using a wearable accelerometer) to the corresponding robot force as the user wears the robot. The real-time target force generation is shown in Figure 5. Notice that since the robot's assistive force depends on the configuration of the user (angle β), the robot naturally follow any user motion without imposing any pre-defined trajectory in time. We achieved fast, robust position control with the

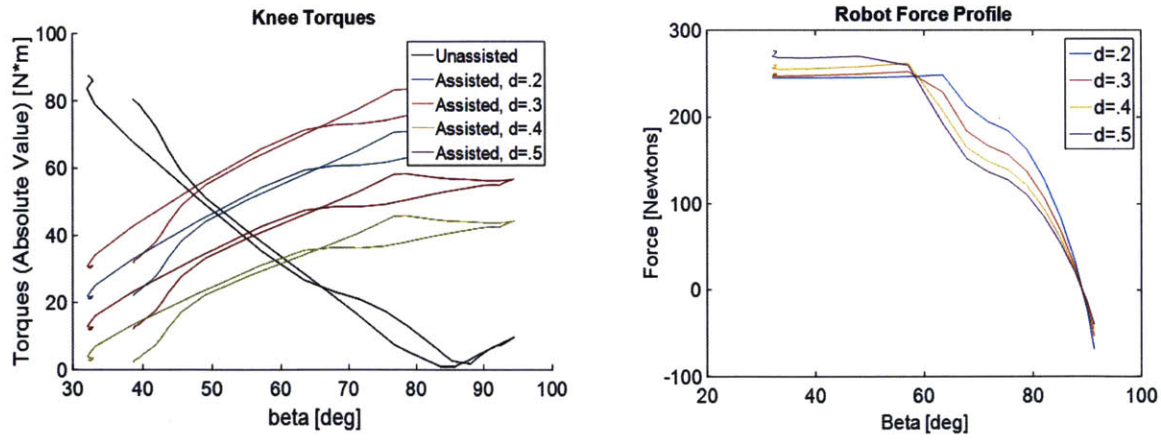

Figure 8-4: (Left) Torques at the knee, comparison of the assisted and unassisted cases. Here, in the original force law, the assisted torques exceeded the unassisted case, so we reduced the force past these crossing points such that the unassisted values are never exceeded. (Right) Optimized robot force profile, which compensates for the full weight of the user when this leads to smaller human joint torques in the assisted case. When this does not hold, the robot support force F_R is reduced until the assisted torques are smaller or equal than the unassisted ones.

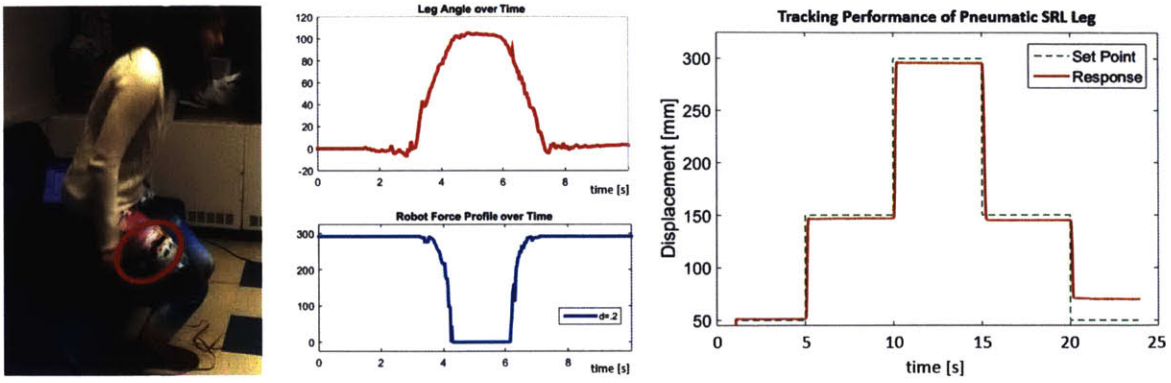

Figure 8-5: (Left) Using a wearable accelerometer (circled in red) to measure knee angle β and generate the target robot assistive force in real time. (Center) Knee angle β over time during a stand up / sit down task, and corresponding robotic assistive force F_R. (Right) Position tracking performance of the robotic legs (prismatic degree of freedom), actuated with pneumatic cylinders.

pneumatic cylinders that actuate the linear degrees of freedom of the robot (Figure 5). By measuring the difference between the desired and actual joint position (the pneumatic cylinder behaves like a spring), we can approximately control the assistive force exerted by the actuators.

8.4 Conclusions

The support strategy described in this chapter is made possible by the light weight, small volume and high comfort of our prototype. These features have been achieved with innovative choices in terms of manufacturing technologies and materials (3D printed Kevlar and carbon fiber parts), joint structure (composite ball joints absorbing linear loads instead of standard metal shafts and bearings), and actuation technologies (high-force, high-speed pneumatic cylinders with precise position control loop).

Using the Kinect sensor to analyze the sitting down/standing up motions of different individuals, we found that the optimal robot force profile varies from person to person. Our method involves recording multiple trials with for each subject to identify their individualized control law. This force profile will then be used to determine in real time the robot's assistive force F_R as we measure the user's knee angle β with an accelerometer. This approach is personalized to follow the individual's pref-

erences in terms of sitting down and standing up motions, and does not impose any pre-planned time trajectory on the human joints. In other words, the robot follows the configuration of its user by measuring the knee angle in real time. The support force is then computed based on the user's configuration, so that the assistive needs of the user are always met. This assistive approach enables the SRL to reduce the effort of the user when sitting/standing. It also exemplifies a unique feature of this novel kind of wearable robot: the ability of assisting the user without getting in the way of his/her motions.

Chapter 9

Balance Augmentation

9.1 Introduction

This paper presents a novel approach to balance assistance for human bipedal walking. To demonstrate this concept, we employ the third prototype of the SRL (introduced in Chapter 7) [67]. Unlike exoskeletons, the SRL is kinematically independent of the human skeletal structure, and can therefore take an arbitrary posture to provide optimal assistance in coordination with human motions. Furthermore, unlike crutches, canes, and other balance assistance equipment, the SRL can provide balancing support autonomously and thereby free the human arms from holding those tools.

First, the new balance assistance strategy is described, followed by kinematic and static modeling. Two gait patterns of the combined human and SRL are discussed, including optimal gait synthesis that maximizes the area of support polygon. Finally, the gait control strategies are implemented on the SRL prototype, using body motion sensors to enable real-time, seamless coordination between the user and the robot.

9.2 Balance augmentation using extra limbs

Achieving and maintaining balance is an essential requirement for bipeds. All of the modes of locomotion that bipeds can use - such as jumping, walking and running -

are statically unstable. Although dynamic stability can be achieved by employing various control strategies [83], trips, slips and unexpected disturbances can still cause falls. Losing balance is a potentially catastrophic event for a biped, given the elevated location of the center of mass.

These issues affect also human bipedal locomotion, and constitute a significant risk for large parts of the population both in professional and domestic scenarios. Data from the US Department of Labor [1], for example, show that the leading cause of death for construction site workers are falls, accounting for 36.9% of total fatalities in 2013. Another demographic subject to elevated risk of falls are the elderly. Data show that for the 80+ population, the risk of accidental death due to falls is 90 times higher than for people below 60 years of age [83]. Finally, many patients rehabilitating from leg injuries or neuromuscular disorders are in need of balance assistance devices. These patients would greatly benefit from the possibility of exercising their own leg to walk, without worrying about falls and slips.

Due to the frequency of fall-related injuries in such a wide range of situations, many approaches have been developed in order to assist and augment balance during human bipedal locomotion. In construction sites, safety regulations [62] require the presence of guardrails, personal ropes or fall protection systems whenever workers are operating at an elevation higher than 1.8m. The drawback of these systems is that they are limited to a particular area, and cannot protect workers as they change location. Moreover, none of these fall prevention systems can ensure the safety of workers operating on the ground or on slippery surfaces.

In the case of the elderly, the most common walking aid systems are canes, crutches and walkers. Canes and crutches ensure static stability if used correctly, but require subjects to dedicate one or both arms to the task of assisting balance. They also require considerable arm force, speed and dexterity, which may not be present in elderly subjects. Robotic crutches have similar limitations [34]. Operating walkers, on the other hand, does not involve fatiguing or rapid motions. Robotic walkers can intuitively follow the motions of the user [55]. All walkers, however, still need at least one user hand to guide them. Moreover, being based on wheels, they cannot follow

subjects up or down stairs, on slopes, or on irregular terrain.

Rehabilitating or disabled patients can use crutches to assist their walking balance. If leg strength is absent (in the cased of paralyzed subjects) or insufficient, subjects can also employ leg exoskeletons to generate leg walking motions [79, 61, 45]. These robots are powerful enough to achieve and maintain a correct, load-bearing nominal walking gait. However, due to their limited degrees of freedom, they cannot guarantee balance or reject disturbances such as slips and pushes. As a consequence, exoskeleton users still need to rely on crutches for balance assistance. Furthermore, exoskeletons (and particularly soft exosuits) increase loads on human leg joints [82], which could be harmful for elderly patients with joint disorders or arthritis.

This chapter proposes a novel walking balance augmentation system, based on the Supernumerary Robotic Limbs (SRL). We will present several control strategies that enable the robot to assist balance during standing and walking, increasing the surface of the region where the human-SRL system is statically stable.

This approach presents several advantages with respect to the traditional fall prevention and balance assistance systems that have been reviewed above. Unlike guardrails and ropes, the SRL is wearable and self-contained. It can therefore move with the user in every location, providing assistance without interruption. Moreover, the SRL does not require users to operate it with their arms. The whole upper part of the human body (torso, head, arms, hands) is free to move independently, while the SRL autonomously provides assistance to the legs during locomotion. This is a significant advantage of the robot over crutches, canes and walkers. Another important feature is that the SRL supports the user with additional legs, not wheels. It can therefore negotiate with all of the obstacles that are easy to deal with during legged locomotion (stairs, slopes, terrain), but would be problematic for a wheeled system such as a walker or a wheelchair. Additionally, the SRL has the potential to reduce human joint loading by supporting the user's weight. Finally, unlike exoskeletons, the SRL leaves the user's legs free to move. This means that SRL users can freely conduct their professional, domestic or rehabilitation activities, while the robot transparently assists them by preventing falls or slips.

9.3 Static balance assistance

9.3.1 System model

In order to augment human balance during walking and standing, the SRL can increase the area of the support polygon of the user-robot system. The support polygon is defined as the region on the ground where the center of mass must lie to achieve static stability. The wider the support polygon, the easier it is for the system to reach and maintain static stability. Bipedal locomotion is not statically stable, because the support polygon created by only one or two feet is so small that the center of gravity does not always lie within it. The SRL can employ the additional robotic legs to make contact with the ground, therefore enlarging the support polygon and increasing the region where the system is statically stable. In the context of dynamic walking, increasing the support polygon also leads to improved robustness with respect to unexpected disturbances. Bipeds can fall more easily if pushed in directions where they do not have any foot in contact with the ground. The presence of robotic legs in directions that cannot be reached by natural legs would prevent such falls. While increasing the support polygon, though, the SRL must avoid getting in the way of the natural motion of the user's legs. The goal of the robot is to provide assistance by seamlessly coordinating with the natural motion of the human, without modifying or influencing them.

The reference scenario considered in this chapter is a human wearing the SRL and walking on flat ground. We analyze the projection of the human-robot system on the horizontal plane xy (Figure 1). The user is modeled as a hip segment (length $2L_b$) with two legs (each L_s long) that move back and forth in the direction of walking speed v. The user's legs touch the ground at points H_R (right foot) and H_L (left foot). L_b is a constant parameter (measured to be 0.3m for the considered system), while step length L_s varies with walking speed ($0 \leq L_s \leq 0.4m$). The SRL is modeled as a base segment (coinciding with the human hip) with two legs that are able to contact the environment in the intersection between the ground and the robot workspace. Since the workspaces of the robotic legs are hemispheres, their intersections with

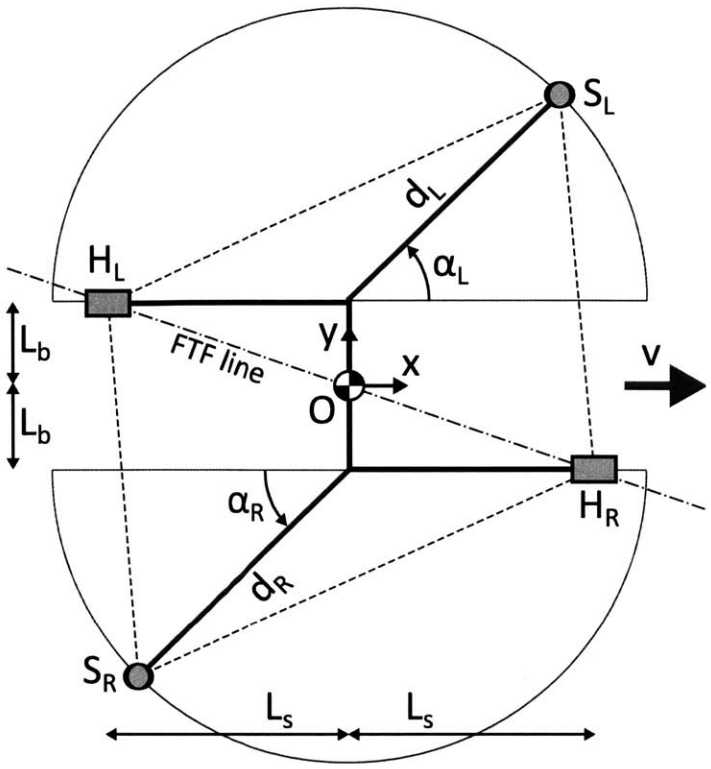

Figure 9-1: The human-SRL model for static balance assistance. The model is a 2D projection of the system on the horizontal plane xy. The thick black lines represents the human hip and legs, and the user's left and right feet are respectively in H_L and H_R. The thick grey lines represent the SRL legs, and the robotic end effectors are in S_L and S_R. The thin grey semi-circles enclose the regions of the ground that the SRL legs can reach. The dashed black line indicates the support polygon.

the ground are half circles (represented in grey in Figure 1). Point O represents the projection of the center of mass of the human-robot system on the horizontal plane. Frame xy, whose origin is O, is the mobile coordinate system that we employ to describe the configuration of the robot. The projections of the SRL legs on the ground are identified by their length (d_R, d_L) and their angle with respect to axis x (α_R, α_L). The robot end effectors contact the ground at points S_R (right) and S_L (left). The range of the SRL feet is determined by the maximum robot legs extension ($0 \leq d_R \leq d_{max}$ and $0 \leq d_L \leq d_{max}$).

9.3.2 Standing support optimization

We begin our analysis by considering the static case. The user is standing with both feet on the ground, and the goal of the SRL is to maximize the support polygon of the human-robot system (Figure 1). The SRL can achieve this objective by choosing the positions where its end effectors are in contact with the ground. The only constraint is that the configuration of the two robotic legs should be symmetric ($\alpha_R = \alpha_L$ and $d_R = d_L$). Symmetry is a desired property for the SRL configuration, because it makes the robot behavior more predictable and similar to the motion of natural legs.

In Figure 1 the support polygon is indicated with a dotted line. It can be noticed that the total support polygon is composed by two triangles ($H_L H_R S_L$ and $H_L H_R S_R$) with identical area. The base of both triangles is segment $H_L H_R$, joining the two human feet. The equation of the foot-to-foot (FTF) line passing through the user feet H_L and H_R is

$$L_b x + L_s y = 0 \tag{9.1}$$

The left end effector of the robot is touching the ground at

$$\underline{x}_{S_L} = \begin{bmatrix} x_{S_L} \\ y_{S_L} \end{bmatrix} = \begin{bmatrix} d_L \cos \alpha_L \\ L_b + d_L \sin \alpha_L \end{bmatrix} \tag{9.2}$$

Therefore, the distance between point S_L and the FTF line can be expressed as

$$d_{ftf,L} = \frac{|L_b x_{S_L} + L_s y_{S_L}|}{\sqrt{L_b^2 + L_s^2}} \tag{9.3}$$

The total area A_{static} of the support polygon is the double of the area of triangle $H_L H_R S_L$, and can be computed with the following expression

$$A_{static} = 2 \left[\frac{1}{2} \left(2\sqrt{L_b^2 + L_s^2} \right) d_{ftf,L} \right] \tag{9.4}$$

Substituting Eq. 2 and Eq. 3 into Eq. 4 yields

$$A_{static} = 2\left|L_b d_L \cos\alpha_L + L_s\left(L_b + d_L \sin\alpha_L\right)\right| \tag{9.5}$$

, which represents the relationship between support polygon area, step length L_s, SRL leg length d_L and SRL leg angle α_L.

Comparing Eq. 3 and Eq. 4, it is evident that maximizing A_{static} is equivalent to maximizing $d_{ftf,L}$. In other words, increasing the support polygon area is analogous to increasing the distance between the SRL end effectors and the FTF line. This is an important observation, because an unaided biped cannot compensate for disturbances perpendicular to the FTF line. Therefore, the presence on the ground of robotic feet not aligned with the human feet ($d_{ftf,L} > 0$) enables the system to compensate for disturbances in any direction, without the need for taking corrective steps.

Figure 2 shows the effects of parameters d_{max} (the robotic legs range) and L_s (the human step length) on the support polygon area A_{static} in the static standing configuration. It can be observed that the support polygon increases with both d_{max} and L_s. Moreover, given any particular couple of values for d_{max} and L_s, it is possible to compute the value of SRL stepping angle $\alpha_{L,max}$ that maximizes the polygon of support. The set of parameters $(d_{max}, L_s, \alpha_{L,max})$ uniquely defines an optimal configuration for the human-SRL system.

9.4 Gait sequences optimization

The goal of the SRL is to aid balance during walking by providing the user with two additional robotic legs that coordinate with the motion of the human legs. This situation is markedly different from the walking strategy of quadrupeds, because here human and robotic legs are organized hierarchically. In particular, the user legs act as "leaders" and dictate the scale and pace of the walking gait. The robotic legs, on the other hand, behave like "followers", constantly monitoring the activity of the human and adapting to it in order to augment balance and compensate for disturbances.

A full human walking cycle (Figure 3) is composed of two double support (DS) and two single support (SIS) phases [Perry]. During double support, both feet are

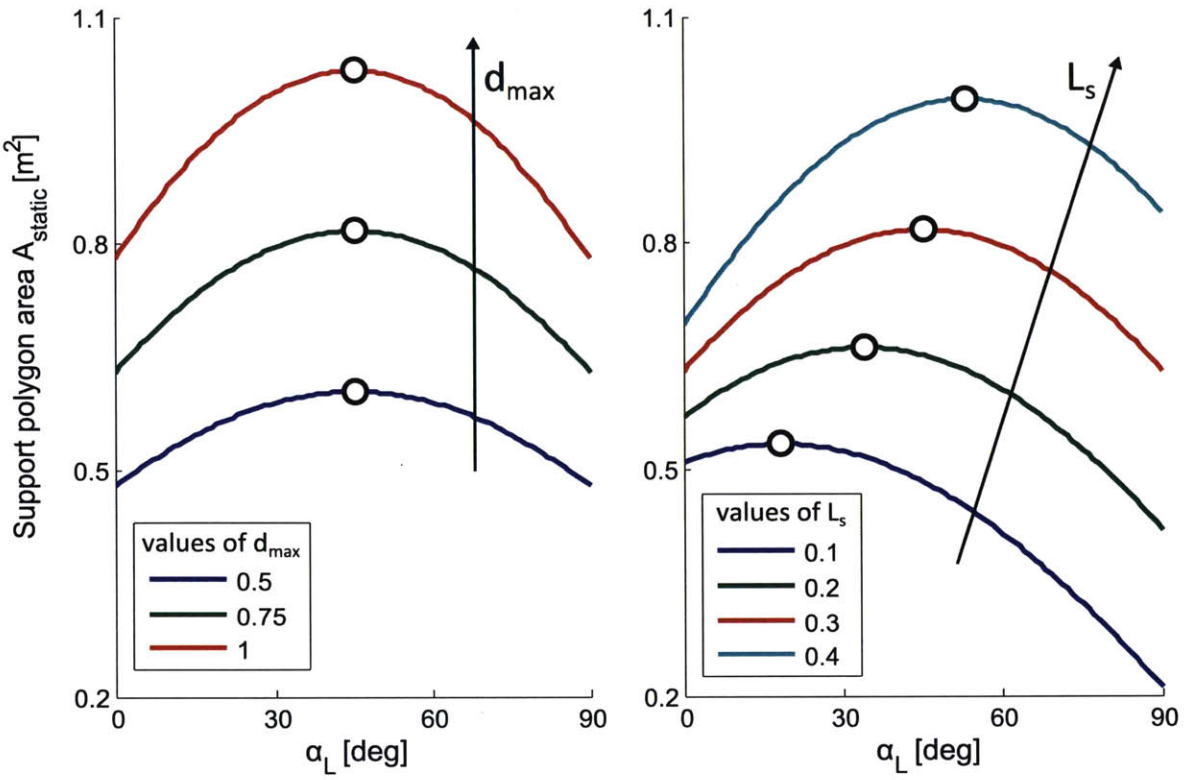

Figure 9-2: The support polygon area in the static configuration as a function of the d_{max}, L_s and α_L. In the left plot, $L_s = 0.3m$. In the right plot, $d_{max} = 0.75m$. The black circles indicate the values of α_L which maximize A_{static} once d_{max} and L_s have been fixed.

in contact with the ground. During single support, only one foot is on the ground, and the other leg swings forward to make the next step. While the human natural gait is well defined, the kinematic independence of the SRL gives us the possibility of developing new, optimal behaviors for the system. In this chapter, we will consider two different gaits for the robot. The first one creates the widest possible support polygon when both human legs are on the ground. The second gait generates smaller support polygons, but allows having three contact points with the ground in every phase of the walking gait (even when there is just one human foot on the floor). It is important to point out that these gaits concern only the SRL. The underlying human walking cycle is the same. In other words, the user is free to walk with a natural, unconstrained gait, while the robot coordinates with it in different ways according to the desired form of assistance.

9.4.1 4-2 Gait

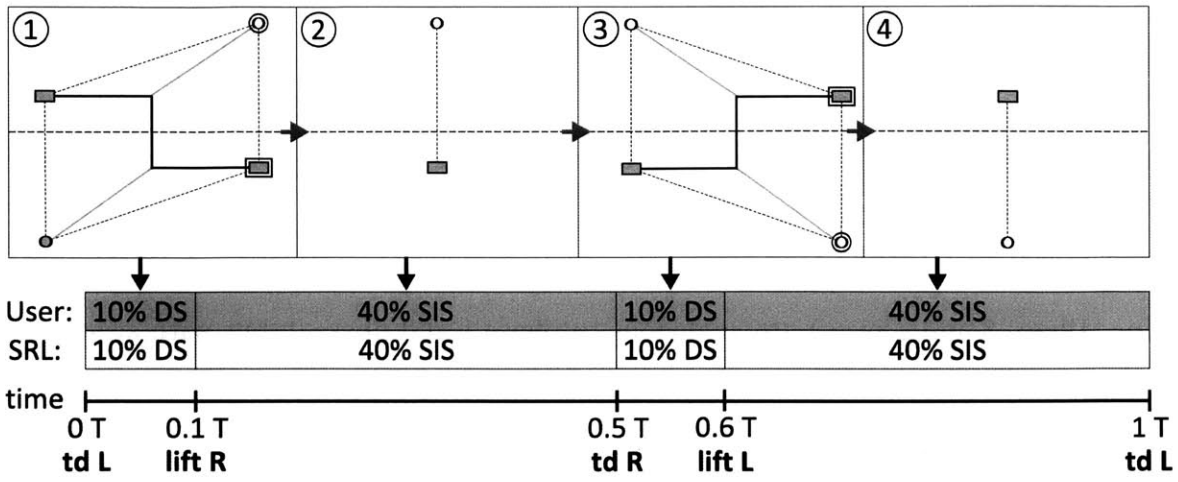

Figure 9-3: Structure of the 4-2 walking gait. The notes in bold at the bottom indicate when the SRL legs touch down (td) or are lifted from the ground.

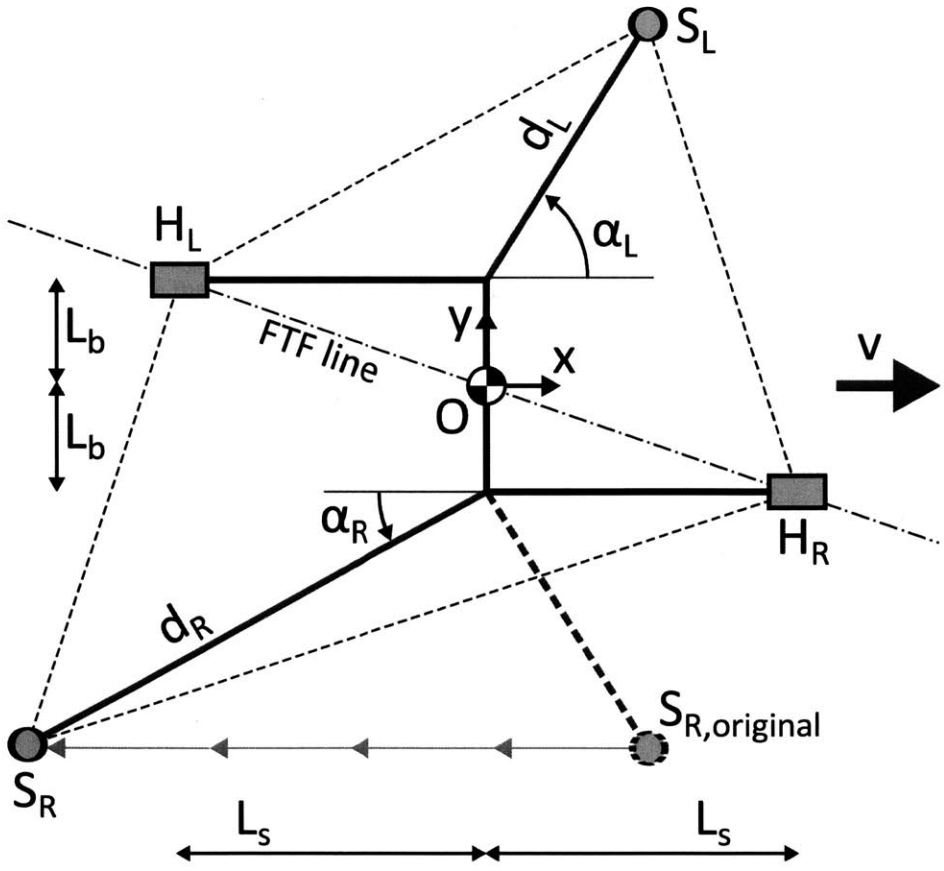

Figure 9-4: Scheme of the SRL taking a new step during the 4-2 gait.

The goal of this gait to maximize the area of the support polygon, reproducing during walking results similar to those obtained in the static case. Figure 3 shows the phases of this strategy. During phase 1, both human legs and both robot legs are on the floor. This enables the realization of the widest possible support polygon. The drawback is that, during phase 2, both a human leg and a robotic leg need to swing forward to make the next step. Therefore, in phase 2 there are only two feet on the ground (one human and one robotic), and the support polygon degenerates to a line. Phase 3 and phase 4 are analogous to phase 1 and phase 2, but with swapped sides. This gait derives its name from the total number of human and robotic legs in contact with the ground in the different phases of a walking cycle (4-2-4-2). Besides the large support polygons realized in phases 1 and 3, the benefits of this gait include its simplicity and its low speed requirements for the swing of the robot legs. The 4-2 gait is simple because the SRL mirrors the human movements, advancing with its left leg when the human puts forward the right leg and vice versa. The fact that the robot moves together with the human, moreover, means that the SRL legs must only swing as fast as the human legs. The disadvantage of this gait lies in the instability of the direction perpendicular to the degenerate support polygon (phases 2 and 4).

The timing of the robot legs motions during the 4-2 gait is straightforward (Figure 3). We now need to define the locations where the SRL feet contact the ground (Figure 4). The results derived for the static case in the previous section are not applicable here, because in general it is not possible to achieve a symmetric configuration in the x direction ($d_R = d_L$ and $\alpha_L = \alpha_R$) during walking. Let us consider an example, displayed in Figure 4. The scheme shows the configuration of the human-SRL system during phase 1. It is evident that the right SRL leg is stretched behind in a non-symmetric position.

This happens because, if the SRL makes a smaller step than the human ($x_{S_{R,original}} < x_{H_L}$, where $S_{R,original}$ is the location of the SRL foot when it touches the ground), its end effector is left behind when the human makes a new step ($x_{S_R} < x_{H_L}$, as shown in Figure 4). As a consequence, the support polygon changes its shape and area. In the situation shown in Figure 4, the left leg triangle ($H_L H_R S_L$) is the same as before,

while the right leg triangle ($H_L H_R S_R$) has been modified by the new end effector location. Assuming that left and right robotic legs touch the ground in corresponding configurations ($d_{R,original} = d_L$ and $\alpha_{R,original} = \pi - \alpha_L$), the position of point S_R is given by

$$\underline{x}_{S_R} = \begin{bmatrix} x_{S_R} \\ y_{S_R} \end{bmatrix} = \begin{bmatrix} -2L_s + d_L \cos\alpha_L \\ -L_b - d_L \sin\alpha_L \end{bmatrix} \tag{9.6}$$

The equation of the FTF line is the same as before (Eq. 1). Therefore, the

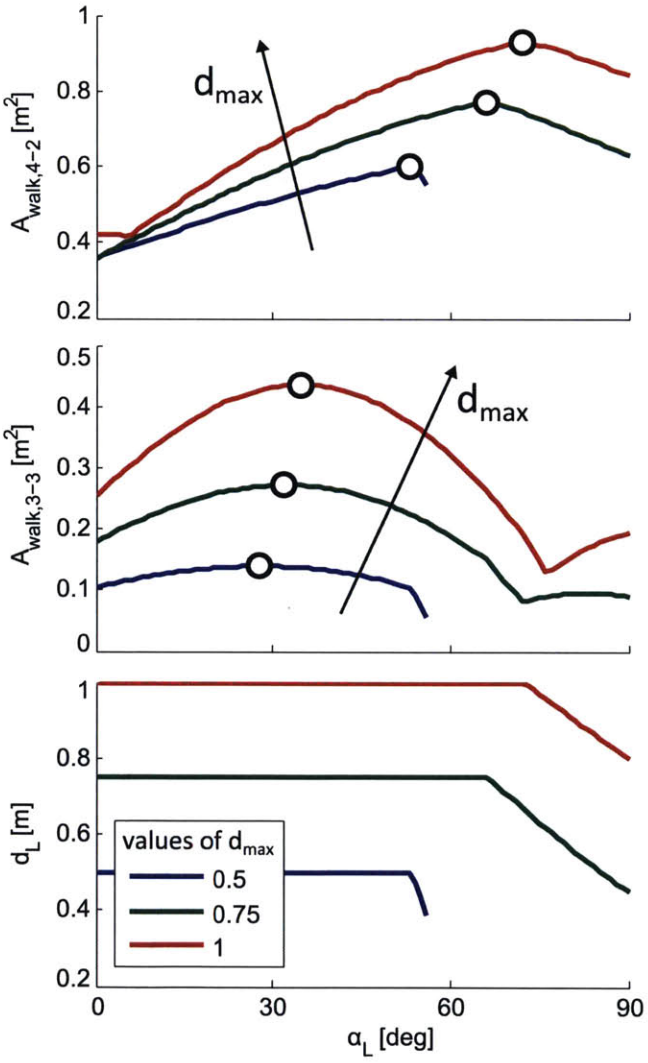

Figure 9-5: The support polygon area in walking gaits 4-2 and 3-3 as a function of d_{max} and α_L. In all of the plots, $L_s = 0.3m$. The black circles indicate the values of α_L which maximize $A_{walk,4-2}$ and $A_{walk,3-2}$ once d_{max} and L_s have been fixed.

distance between point S_R and the FTF line can be expressed as

$$d_{ftf,R} = \frac{|L_b x_{S_R} + L_s y_{S_R}|}{\sqrt{L_b^2 + L_s^2}} \tag{9.7}$$

The area A_L of the left leg triangle is half of the value in Eq. 5. Using Eq. 7, it is possible to identify also an expression for the area A_R of the right leg triangle

$$\begin{cases} A_R = |L_b(2Ls - d_L \cos\alpha_L) + L_s(L_b + d_L \sin\alpha_L)| \\ A_L = |L_b d_L \cos\alpha_L + L_s(L_b + d_L \sin\alpha_L)| \end{cases} \tag{9.8}$$

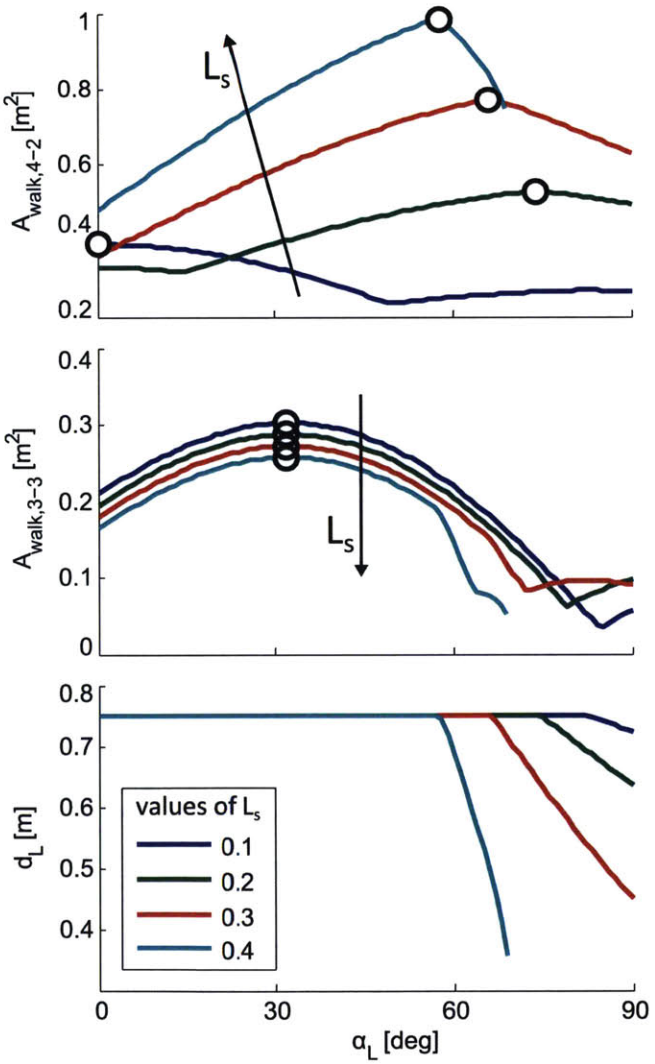

Figure 9-6: The support polygon area in walking gaits 4-2 and 3-3 as a function of L_s and α_L. In all of the plots, $d_{max} = 0.75m$. The black circles indicate the values of α_L which maximize $A_{walk,4-2}$ and $A_{walk,3-2}$ once d_{max} and L_s have been fixed.

The sum of these two areas gives the total surface of the support polygon during phase 1 and phase 4:

$$A_{walk,4-2} = A_L + A_R \tag{9.9}$$

Figure 5 and Figure 6 show how $A_{walk,4-2}$ varies with d_{max}, L_s and α_L. As in the static case, the support polygon surface increases with d_{max} and L_s. Once these two parameters are fixed, the value of angle α_L that maximizes $A_{walk,4-2}$ can be easily found numerically. However, these plots also present differences with respect to the static case. As previously discussed, during walking the lengths of the two SRL legs are generally different. Given that the length of the left robotic leg is d_L, the length of the right robotic leg (in phase 1) is

$$d_R = \sqrt{x_{S_R}^2 + (y_{S_R} + L_b)^2} \tag{9.10}$$

Which, substituting Eq. 6, leads to

$$d_R = \sqrt{(-2L_s + d_L \cos\alpha_L)^2 + (-d_L \sin\alpha_L)^2} \tag{9.11}$$

For example, in the case of Figure 4, the length of the right SRL leg is bigger than the length of the left SRL leg. This means that, if we set $d_L = d_{max}$, the right robotic leg exceeds the limit length ($d_R > d_{max}$). In these cases, the length of the longer SRL leg is clipped, and the length of the shorter leg can be computed substituting $d_R = d_{max}$ into Eq. 11 and solving for d_L:

$$a_d\, d_L^2 + b_d\, d_L + c_d = 0 \tag{9.12}$$

, where the coefficients are

$$\begin{cases} a_d = 1 \\ b_d = -4L_s \cos\alpha_L \\ c_d = 4L_s^2 - d_{max}^2 \end{cases} \tag{9.13}$$

Figure 5 and Figure 6 show the values of d_L that can be achieved for the considered values of d_{max}, L_s and α_L. The gaps correspond to solutions that cannot be geometrically achieved. The considered range for α_L is $0 \leq \alpha_L \leq \pi/2$, because the goal of the human-robot system is to step ahead in the walking direction.

9.4.2 3-3 Gait

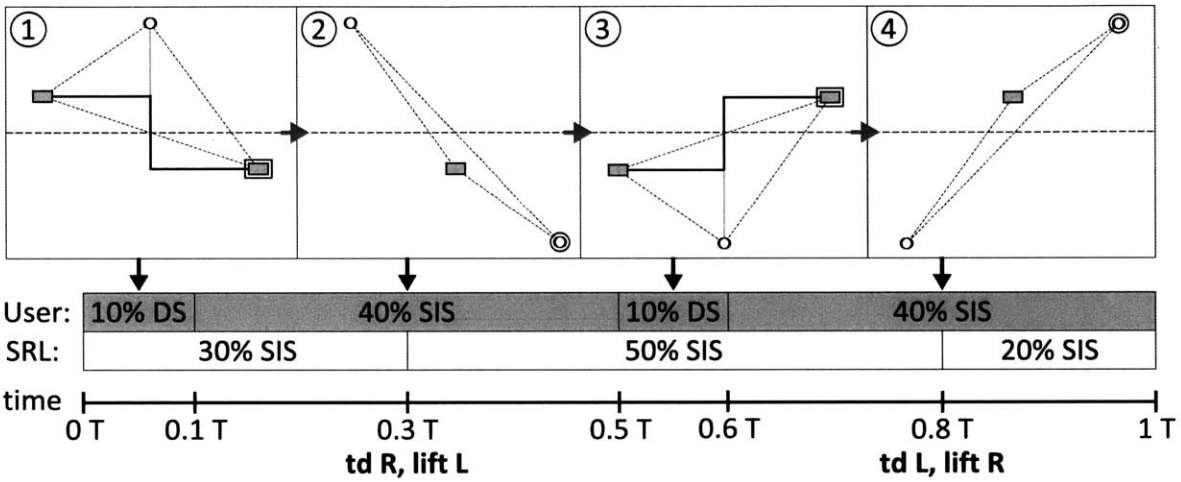

Figure 9-7: Structure of the 3-3 walking gait. The notes in bold at the bottom indicate when the SRL legs touch down (td) or are lifted from the ground.

The gait that we considered so far (4-2) is capable of realizing wide support polygons when all of the four legs of the human-SRL system are on the floor. However, when only two legs (one human and one robotic) are in contact with the ground, the support polygon degenerates to a line and the system cannot be statically stable or compensate for disturbances perpendicular to that line. In order to overcome this limitation, we developed a gait that aims to keep at least 3 points of contact with the ground at any point in the walking cycle (hence the name: 3-3). Figure 7 shows the phases of the 3-3 gait. In this new walking pattern, the robot does not act synchronously with the human anymore. Instead, the SRL swings forward in order to realize a support polygon with finite area even when only one human foot is on the ground (phases 2 and 4). The drawback is that this strategy leads to a reduction of the support polygon when both human feet are on the floor (phases 1 and 3; compare

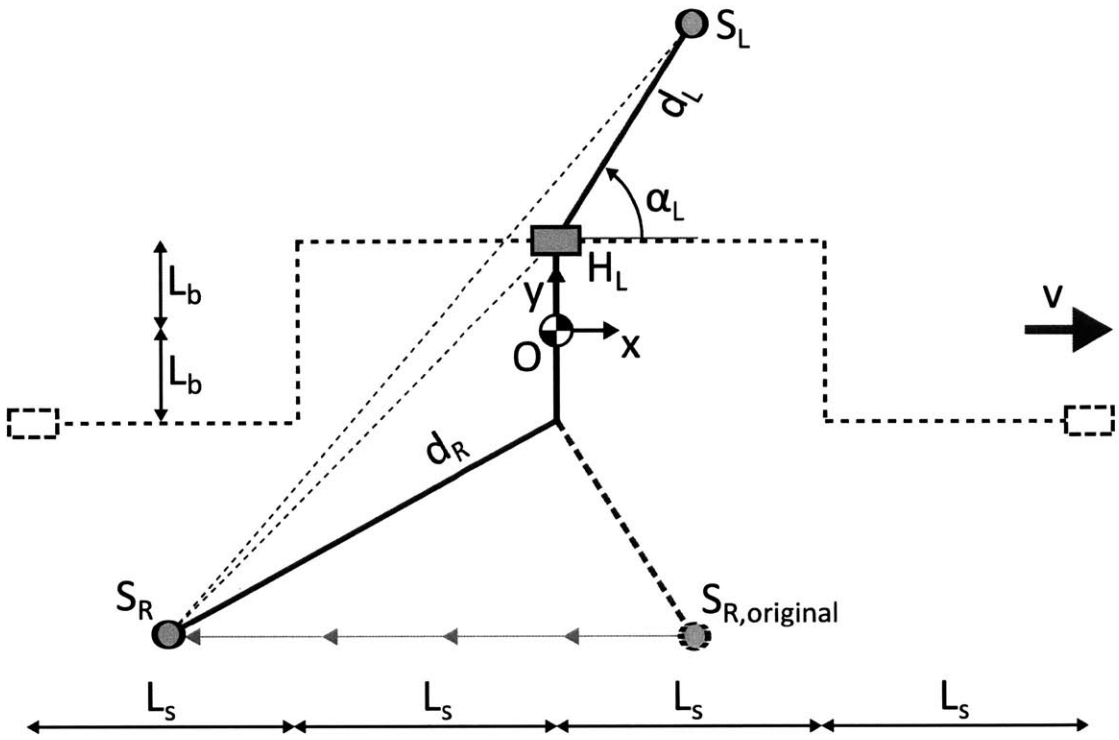

Figure 9-8: Scheme of the SRL taking a new step during the 3-3 gait.

with 4-2 gait). Note that, in Figure 7, phase 2 and phase 3 are only instantaneous (one robotic foot is lifted as soon as the other one touches the ground). The length of these phases, however, can be modified by increasing the time when both robotic legs are on the ground (this would require faster actuators, see section on implementation).

The advantage of the 3-3 gait is that, as long as 3 legs are in contact with the ground, the system can be statically stable and it can also react to disturbances (e.g. pushes, or slipping) in any direction. However, this gait is more difficult to realize than the 4-2 gait, because it requires a more complex coordination with the human (time line in Figure 7) and it needs robotic legs fast enough to swing in front of the human legs (phase 2 and 4).

In order to optimize the 3-3 gait, we need to identify the locations where the SRL end effectors must touch the ground in phases 2 and 4 (Figure 7). A scheme of this scenario is represented in Figure 8. This drawing corresponds to phase 4 in Figure 7. The left SRL leg has just touched the ground (point S_L), and defines the polygon of support together with the right SRL foot S_R and the left human foot H_L. Note that

the right SRL foot initially touched the ground at $S_{R,original}$, defined with respect to the mobile coordinate frame xy. The equation of the robot foot-to-foot (robot FTF) line, which passes through both SRL end effectors, is

$$a_{sis}\, x + b_{sis}\, y + c_{sis} = 0 \tag{9.14}$$

Where the coefficients have the following expressions

$$\begin{cases} a_{sis} = L_b + d_L \sin\alpha_L \\ b_{sis} = -L_s \\ c_{sis} = L_s L_b + L_s d_L \sin\alpha_L - (L_b + d_L \sin\alpha_L) d_L \cos\alpha_L \end{cases} \tag{9.15}$$

The position of point H_L is

$$\underline{x}_{H_L} = \begin{bmatrix} x_{H_L} \\ y_{H_L} \end{bmatrix} = \begin{bmatrix} 0 \\ L_b \end{bmatrix} \tag{9.16}$$

, and its distance from the robot FTF line can be found as

$$d_{sis} = \frac{|a_{sis}\, x_{H_L} + b_{sis}\, y_{H_L} + c_{sis}|}{\sqrt{a_{sis}^2 + b_{sis}^2}} \tag{9.17}$$

The support polygon consists of triangle $S_R S_L H_L$. Its base, segment $S_R S_L$, has magnitude

$$\left\| \overline{S_R S_L} \right\| = 2\sqrt{L_s^2 + (L_b + d_L \sin\alpha_L)^2} \tag{9.18}$$

The surface of the support polygon can be found substituting Eq. 16 into E. 17 and combining it with Eq. 18. The expression of the support polygon area in phases 2 and 4 is thus given by

$$A_{sis} = \frac{1}{2} \left\| \overline{S_R S_L} \right\| d_{sis} = |b_{sis} L_b + c_{sis}| \tag{9.19}$$

The configuration of the human-SRL system changes during phase 1 and phase 3. Both of the user's feet are on the ground, but only one SRL end effector (for example,

point S_L in phase 1) is in contact with the floor. The equation of the FTF line is the same as in the previous section (Eq. 1), while the position of the SRL foot on the ground is

$$\underline{x}_{S_L} = \begin{bmatrix} -L_s + d_L \cos\alpha_L \\ d_L \sin\alpha_L \end{bmatrix} \tag{9.20}$$

Computing as before the distance between point S_L and the FTF line, it is possible to find the following expression for the support polygon area

$$A_{ds} = |L_b(-L_s + d_L \cos\alpha_L) + L_s dL \sin\alpha_L| \tag{9.21}$$

Since in the 3-3 gait there is a non-degenerate support polygon in every phase, we chose their average area as the metric to be maximized

$$A_{walk,3-3} = \frac{A_{sis} + A_{ds}}{2} \tag{9.22}$$

Figure 5 and Figure 6 plot the behavior of $A_{avg,3-3}$ as a function of d_{max}, L_s and α_L. The same considerations as in gait 4-2 hold with respect to d_L (its length is reduced when the other SRL leg reached the limit length d_{max}). Figure 5 shows that, as expected, $A_{avg,3-3}$ increases with maximum SRL leg length d_{max}. However, it is important to point out that, unlike in gait 4-2, $A_{avg,3-3}$ decreases as L_s increases (Figure 6). In other words, smaller user steps lead to larger polygons of support when the SRL is employing gait 3-3. The intuitive reason for this result is that, with small values for L_s, the support polygon is not "stretched out" between distant points S_R and S_L, and therefore A_{sis} increases. As before, once d_{max} and L_s are defined the optimal value for α_L (the one which maximizes $A_{avg,3-3}$) can be found numerically.

9.5 Implementation

9.5.1 Space and time scaling

The relevant parameters for the calculation of the trajectories and timing of the SRL motions are L_b, d_{max}, L_s, α_L and T. Half hip width L_b is a constant defined by the size of the user and the structure of the robot. Maximum SRL leg length d_{max} (on plane xy) also depends on the design of the robot. The linear actuators in the SRL legs have a maximum length of $L_{max} = 1.25m$. Since the human hip height is $h_{human} = 1m$ in our case, the value of d_{max} can be found as $d_{max} = \sqrt{L_{max}^2 - h_{human}^2}$.

During natural human walking, step frequency f, step length L_s and walking speed v are related by

$$\begin{cases} f = C\, v^B \\ v = 2L_s\, f \end{cases} \tag{9.23}$$

, where B and C are constants [7]. The value of B is 0.58, while the value of C has been estimated to be 2.22 in our case. By attaching an accelerometer to the lower thigh of the user (see the results section), it is possible to measure the time T between to successive touch downs of the same human foot. Once the value of T is known, the walking frequency is obtained as $f = 2/T$. Substituting this value into Eq. 23 and rearranging their terms, it is possible to compute all of the other relevant walking parameters

$$\begin{cases} v = (C^{-1} f)^{1/B} \\ L_s = \frac{1}{2} C^{-1/B} f^{(1-B)/B} \end{cases} \tag{9.24}$$

At this point, it is possible to compute both the timing of the SRL motions (Figure 3 and Figure 7) and the optimal end effector placements for the robotic legs (Figure 5 and Figure 6). Note that the only value that needs to be updated is T. All the other parameters follow from T and known constants. The robot behavior is updated every time the human takes a new step. This allows for a reactive, seamless coordination of the SRL with the motion of the user.

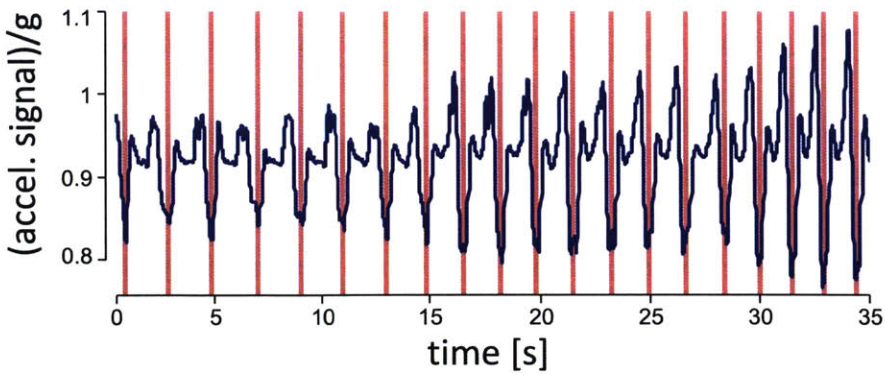

Figure 9-9: Example performance of the step detection algorithm. The blue curve is the signal measured by the accelerometer on the user's right leg (normalized dividing by g). The red vertical lines indicate the moments where a step has been detected. The algorithm works correctly on the whole walking speed range (from 0.5mph=0.22m/s at $t = 0s$ to 1.5mph=0.67m/s at $t = 35s$).

9.5.2 Experimental results

The steps of the user are detected using a simple one-axis accelerometer strapped to the lower thigh of the right leg. Figure 9 displays the filtered accelerometer signal (Butterworth filter, second order, 2Hz cutoff frequency) and the step detection results (each red star indicates a step). When the user is standing still, the accelerometer reads about 0.9g (where g is the gravitational acceleration). When the right human leg is lifted to take a new step, the accelerometer signal decreases in value. This value then increases abruptly due to the impact of the foot with the ground. It is therefore simple to detect the stepping instant as a local minimum in the accelerometer signal. Figure 9 shows correct step detection over the whole range of considered walking speeds.

Finally, the video attachment to this chapter shows the SRL coordinating with the user and providing balance assistance during walking. The robot is estimating the human walking period, and computes from this value all of the parameters that are needed to generate motion trajectories. It then realizes gait 4-2, augmenting the polygon of support of the human and improving the disturbance rejection capabilities of the human-SRL system. The robot can rapidly and seamlessly adapt to different walking speeds. The user is free to choose the walking speed and to vary it, while the

robot detects every change and adapts to them during the following walking period.

9.6 Conclusions

The SRL has been employed to enhance the balance and disturbance rejection capabilities of the user during standing and walking. We developed a model of the human-SRL system, and used it to determine the best robot configuration during locomotion. Two gaits have been identified for the robot: the first one (4-2 gait) aims to maximize the instantaneous support polygon. The second one (3-3 gait) aims to maximize the average support polygon during the whole walking period. Combining these assistive strategies with real-time detection of user motion, the SRL is able to seamlessly coordinate with the user, providing assistance without interfering with natural motion.

Chapter 10

Conclusions

10.1 Robot design

In this document we detailed the design, realization and control strategies of a fully functional Supernumerary Robotic Limbs (SRL) prototype. From the mechanical design point of view, the main challenge was to realize a system with the ability to support the full weight of an adult user, while maintaining its mass below 3.5 kg. This constraint was met with four separate innovations: the kinematic structure of the robot, the ball and socket joint design, the unconventional actuation technology chosen for the prismatic joint, and the adoption of a new manufacturing technique for the structure of the device.

The kinematic structure of the robot consists of two robotic limbs with three actuators each (two rotational ones and a prismatic one). The axes of the three actuators intersect into a single point (the center of the ball at the base of the limb). As a consequence, the linear forces coming from the robotic limb and oriented like its axis will not generate any torque on the two servomotors. If this assumption is satisfied - the control algorithms presented in Chapters 5, 6 and 7 find optimal solutions in this sense - then the required torques for the servomotors can be reduced to smaller values, and we can select lighter rotational actuators.

The ball and socket joint at the base of the robotic limbs has been designed to absorb the forces coming from the contact with the ground, without overloading the

shafts and bearings of the servomotors. The lightweight structure of the joint is simple to assemble and maintain, and avoids the use of heavy, bulky ball bearings and metal shafts. Moreover, the ball joint is directly actuated by the two servomotors through a simple bracket mechanisms. The control and maintenance of this architecture are very simple. Unlike most biomimetic ball joint designs, we do not need any nonlinear mechanisms with cables or push-pull rods to control the orientation of the sphere.

Conventional actuation technologies for prismatic joints (electric linear motors, pneumatic actuators) did not allow us to meet our strict weight, speed, force and comfort (low noise) requirements. Therefore, we selected pneumatic cylinders to extend and retract the robotic limbs. The choice of pneumatic actuation allowed us to meet all of the performance targets. Adding a lightweight, inexpensive compressed air canister to the base of the robot, the system would not need any compressor or external power source. The position of the prismatic joint is measured with a magnetic potentiometer, and controlled with a 5/3 pneumatic valve and a simple switching algorithm. The speed and accuracy of this control system are suited to provide assistance during locomotion tasks, such as dynamic walking or sitting and standing. Additionally, since the default configuration of the valve locks the cylinder in place, keeping a constant position (and providing a constant assistive force) do not require any additional power. Finally, using a pneumatic cylinder means that the prismatic joint is naturally compliant. This avoids impacts when the robotic limbs make contact with the environment, and increases the safety of the device and the comfort of the user.

The structure of the robot is entirely realized in composite materials. Where possible - in the robotic limbs and in the back of the base of the system - we employed standard carbon fiber tubes. When we needed custom parts, we used MarkForged's 3D printing technology. This manufacturing technique allows to fabricate parts using carbon and Kevlar fibers, with a nylon filler. The position and orientation of the fibers can be chosen by the designer, in order to increase the resistance of the parts in particular areas. With this technology we were able to design and manufacture parts with mechanical strength comparable to aluminum, and with a 75% weight reduction.

Besides its light weight and assistive capabilities, other features of the SRL prototype are its small volume and its wearing comfort. Because of the simplicity of its harness - there are only three buckles to tighten - the robot can be worn in a few seconds, without any external assistance. Moreover, the extensive padding and the weight distribution of the system (the COM of the robot is located just below the COM of the user) make it comfortable to wear for extended periods of time. These features enable users to wear the SRL over their regular clothing, and benefit from its assistive capabilities. In particular, the SRL has been designed to help manufacturing and construction workers, elderly people, and rehabilitating patients.

10.2 Task-oriented assistance

The independence of the SRL enables its robotic limbs to provide optimized assistance in several situations, which can be divided into static, quasi-static and dynamic tasks. When the user is in a static configuration - maintaining a fixed position like standing, or being crouched down to work on the floor - the SRL needs to compensate for his weight, and to stabilize his posture. In order to achieve these results, we developed the bracing strategy. The robotic limbs make contact with the environment, and use it as a support in order to provide assistive forces to the user. If the sum of the forces exerted by the robotic limbs on the user is a vector equal and opposite to his weight, the robot is effectively supporting the human body by pushing or pulling on the available contact points with the surrounding environment. The bracing strategy can also be used to provide assistance in delicate or dangerous manufacturing tasks. For example, the SRL can firmly hold a drill bit support against a surface, indicating to the user where to drill a hole and at the same time stabilizing and supporting the drilling operation. While one robotic arm positions and hold the drill bit support, the other one employs the bracing strategy to increase the force that holds it in place. This process does not require any active force generated by the user, who is free to concentrate on the drilling operation without worrying about the positioning or the stability of the drill bit. Finally, the bracing strategy can be employed to generate a

custom virtual stiffness matrix at the hip of the user. By making contact with the ground and using a combination of reaction forces and null-space forces, the SRL is able to stabilize the user along some directions of motion, while leaving him free to move along other directions. This is very useful in the manufacturing tasks that require workers to focus on a particular movement - for example, pushing the power drill forward in order to drill a hole - and suppress all of the others - in the example, any deviation from the linear pushing movement would break the drill bit or ruin the hole. In this case, the custom impedance generated by the SRL can constrain the unwanted body movements, while leaving the user free to perform the intended action.

The second category of tasks that can be assisted by the SRL are quasi-static operations. In these tasks, the configuration of the body changes slowly. Therefore, accelerations are small and the task can be modeled as if it was a sequence of static snapshots. We used this approach to model the sitting down and standing up movements. In this case, the goal of the SRL is to compensate for the weight of the user as he/she switches from a sitting to a standing configuration and vice versa. Because the configuration of the user is continuously varying between the initial and final positions, the robot must adapt its support force to the movements of the human. For this adaptation to be seamless, we need wearable sensors that can robustly measure the configuration of the user. We employed an IMU worn on the thigh of the user, and measuring the inclination of that body segment with respect to gravity. This piece of information is enough for the robot to reconstruct the configuration of the user and - under static equilibrium assumptions - to compute the desired assistive force for that configuration. The robot also computes the torques at the natural joints of the user, and decreases its pushing force if these torques exceed the normal values recording during sitting and standing. This way, the robot is able to modulate its action so that its effect is always beneficial to the user.

The third category of tasks for which we developed assistive control strategies are dynamic movements. In particular, we focused on dynamic walking because it is one of the most common and useful human activities, and it presents significant

risks of falls for the elderly population. In this case, we developed an innovative balance assistance strategy that makes use of the unique feature of the SRL - having two independent robotic limbs - in order to increase the support polygon of the user. The support polygon is the area defined by the points of contact of the user with the ground. Normally, this is just the area between the user's feet. If the projection of the human COM on the ground falls outside of this area, the person falls (under static assumptions). Therefore, a larger support polygon means that the user is more stable and more robust to disturbances while walking. We developed optimal gaits in which the robotic limbs coordinate with the human legs with the goal of maximizing the support polygon during walking. This new solution to the problem of balance assistance is enabled by the independence of the robotic limbs. The user wears an IMU just above the knee. This sensor is employed to measure the stepping frequency of the human. Therefore, the robot knows when the human is stepping - and which natural leg is touching the ground. With this method, the SRL is able to seamlessly coordinate with the user, adapting to different walking speeds.

10.3 Voluntary control

Is it possible for a human to learn to control additional limbs as if they were part of his own body? This is the fundamental question that guided the research presented in this thesis. While the first chapters of this document focused on the design of the prototype and on the development of task-specific strategies, the final chapter analyzes a human-machine interface that is able to achieve voluntary, independent control of the robotic limbs. In order to control extra limbs, we first needed to identify suitable independent signals that could be used as inputs to the robot. The methods usually employed to control robotic systems - buttons, levers, speech, motions, etc. - are not suitable for the SRL, because they require users to âĂIJre-assignâĂİ one or more natural degrees of freedom to the control of the wearable device. For example, if we used arm motions to control the movements of the SRL, then users would have to sacrifice one or more degrees of freedom in their natural arms in order to govern the

behavior of the artificial limbs. Such a trade-off would clearly miss the point of using a wearable system like the SRL, whose goal is to increase the number of available degrees of freedom rather than reducing or re-routing them. For this reason, we chose to employ electromyographic (EMG) signals from the torso muscles to control the robot.

Torso muscles present several advantages that make them suitable to generate independent control signals for the SRL. First, torso muscles can be co-activated in combinations that do not generate any motions of the body (they belong to its null space). This is analogous to the co-contraction of the biceps and triceps muscles at the elbow joint (their co-contraction does not generate any motion), but in a higher-dimensional muscle space. Moreover, torso muscles can be activated without moving the natural limbs. This enables the user to control the robotic limbs independently, without influencing the posture of the rest of the body. We implemented this control strategy by using the activation of the pectoral and abdominal muscles to generate movement commands for the SRL in a simple velocity control architecture. All of the subjects of the experiment learned to control the additional robotic limbs within minutes, and achieved high tracking performance. Additionally, the subjects were able to perform a complex tracking task using four limbs simultaneously -two natural arms and two robotic limbs. Their performance in this complex task was superior to the results that they would have obtained simply by activating one limb after the other, sequentially. This means that subjects learned to coordinate the motion of the natural and artificial limbs, mastering a new motor skill that would not have been possible using exclusively the natural body. These results were achieved without influencing the other degrees of freedom of the body: during the experiment, subjects were standing (they did not move their legs) and they kept their torso and heads relaxed. Therefore, the motion of the robotic limbs was controlled in a voluntary and independent fashion.

The main limit of this approach is that tracking performance decreases as the number of additional limbs increases. However, subjects also show faster learning rates and performance improvements when they are asked to control the robotic

limbs and the natural arms simultaneously. This learning process is similar to the motor skill acquisition process that takes place every time a human learns to perform a new task or to use a new tool. This indicates that if we provide SRL users with a simple control interface that enables them to effortlessly generate independent control signals, they can quickly learn to control the additional limbs in the same way they learn new motor skills.

10.4 Future research directions

The SRL project presents several promising future research opportunities. In terms of task-specific control strategies, we need to increase the number and variety of situations for which the robot has optimal behaviors. For example, in dynamic locomotion, it would be very interesting to make the SRL able to follow turning motions, or to assist users when walking up or down the stairs. Another promising research direction focuses on finding a robust way for the robot to decide which of the optimal behaviors in its library is best suited to assist the user in a particular situation. The grand vision for this control architecture is to realize a robotic system that is able to adapt to the user, providing optimal assistance without any kind of explicit human effort or command.

At the other hand of the spectrum, it would be interesting to continue the development of voluntary control strategies for the robotic limbs. In particular, increasing the number of active degrees of freedom controlled by the subjects would enable us to test their performance in more complicated tracking and manipulation tasks. The main challenge associated with controlling additional degrees of freedom with torso EMG muscles is that there is a limited number of independent input signals - the muscle combinations that belong to the torso null space and do not overlap with the muscles used to move the natural limbs.

Finally, it would be extremely interesting to test the control strategies presented in this thesis on the factory floor and in a clinical environment, to see how the target users - manufacturing workers, elderly people, rehabilitating patients - make use of the

additional capabilities brought to them by this new human augmentation technology.

Bibliography

[1] Revisions to the 2012 census of fatal occupational injuries (cfoi) counts. Technical report, Office of Occupational Safety and Health Statistics, U.S. Bureau of Labor Statistics, 2013.

[2] J Adamson, K Hunt, and S Ebrahim. Socioeconomic position, occupational exposures, and gender: the relation with locomotor disability in early old age. *Journal of epidemiology and community health*, 57(6):453–455, 2003.

[3] Haruhiko Asada and J-JE Slotine. *Robot analysis and control.* John Wiley & Sons, 1986.

[4] Samuel K Au, Paolo Bonato, and Hugh Herr. An emg-position controlled system for an active ankle-foot prosthesis: an initial experimental study. In *Rehabilitation robotics, 2005. ICORR 2005. 9th international conference on*, pages 375–379. IEEE, 2005.

[5] Peter G Bain. The management of tremor. *Journal of Neurology, Neurosurgery & Psychiatry*, 72:i3–i9, 2002.

[6] Marco Barbero, Roberto Merletti, and Alberto Rainoldi. *Atlas of muscle innervation zones: understanding surface electromyography and its applications*. Springer Science & Business Media, 2012.

[7] John EA Bertram and Andy Ruina. Multiple walking speed–frequency relations are predicted by constrained optimization. *Journal of theoretical Biology*, 209(4):445–453, 2001.

[8] A. Bicchi, M. Bavaro, G. Boccadamo, D. De Carli, R. Filippini, G. Grioli, M. Piccigallo, A. Rosi, R. Schiavi, S. Sen, and G. Tonietti. Physical human-robot interaction: Dependability, safety, and performance. In *Advanced Motion Control, 2008. AMC '08. 10th IEEE International Workshop on*, pages 9 –14, march 2008.

[9] Robert Bogue. Exoskeletons and robotic prosthetics: a review of recent developments. *Industrial Robot: An International Journal*, 36(5):421–427, 2009.

[10] Matthew Botvinick. Probing the neural basis of body ownership. *Science*, pages 782–782, 2004.

[11] Matthew Botvinick, Jonathan Cohen, et al. Rubber hands' feel'touch that eyes see. *Nature*, 391(6669):756–756, 1998.

[12] Tiffany M. Brown. Injuries, illnesses and fatalities in manufacturing, 2005. Bureau of Labor Statistics, July 2007.

[13] Raymond C Browning, Jesse R Modica, Rodger Kram, Ambarish Goswami, et al. The effects of adding mass to the legs on the energetics and biomechanics of walking. *Medicine and science in sports and exercise*, 39(3):515, 2007.

[14] GA Cavagna and P Franzetti. The determinants of the step frequency in walking in humans. *The Journal of physiology*, 373:235, 1986.

[15] Kai-Jung Chi and Daniel Schmitt. Mechanical energy and effective foot mass during impact loading of walking and running. *Journal of biomechanics*, 38(7):1387–1395, 2005.

[16] Kaare Christensen, Gabriele Doblhammer, Roland Rau, and James W Vaupel. Ageing populations: the challenges ahead. *The Lancet*, 374(9696):1196–1208, 2009.

[17] Steven H Collins, M Bruce Wiggin, and Gregory S Sawicki. Reducing the energy cost of human walking using an unpowered exoskeleton. *Nature*, 522(7555):212–215, 2015.

[18] C. Davenport, F. Parietti, and H. Asada. Design and biomechanical analysis of supernumerary robotic limbs. In *ASME Dynamic Systems and Control Conference*, 2012.

[19] Eran Dayan and Leonardo G Cohen. Neuroplasticity subserving motor skill learning. *Neuron*, 72(3):443–454, 2011.

[20] Carlo J De Luca. The use of surface electromyography in biomechanics. *Journal of applied biomechanics*, 13:135–163, 1997.

[21] Carlo J De Luca. Surface electromyography: Detection and recording. *DelSys Incorporated*, 10:2011, 2002.

[22] Ye Ding, Ignacio Galiana, Alan T Asbeck, Brendan Quinlivan, Stefano MM De Rossi, and Conor Walsh. Multi-joint actuation platform for lower extremity soft exosuits. In *Robotics and automation (ICRA), 2014 IEEE international conference on*, pages 1327–1334. IEEE, 2014.

[23] A.M. Dollar and H. Herr. Lower extremity exoskeletons and active orthoses: Challenges and state-of-the-art. *Robotics, IEEE Transactions on*, 24(1):144–158, 2008.

[24] Julien Doyon and Habib Benali. Reorganization and plasticity in the adult brain during learning of motor skills. *Current opinion in neurobiology*, 15(2):161–167, 2005.

[25] Julien Doyon, Leslie G Ungerleider, LR Squire, and DL Schacter. Functional anatomy of motor skill learning. *Neuropsychology of memory*, 3:225–238, 2002.

[26] H Henrik Ehrsson, Nicholas P Holmes, and Richard E Passingham. Touching a rubber hand: feeling of body ownership is associated with activity in multisensory brain areas. *The Journal of Neuroscience*, 25(45):10564–10573, 2005.

[27] Daniel P Ferris, Joseph M Czerniecki, Blake Hannaford, and University of Washington. An ankle-foot orthosis powered by artificial pneumatic muscles. *Journal of applied biomechanics*, 21(2):189, 2005.

[28] Drew B Fineberg, Pierre Asselin, Noam Y Harel, Irina Agranova-Breyter, Stephen D Kornfeld, William A Bauman, and Ann M Spungen. Vertical ground reaction force-based analysis of powered exoskeleton-assisted walking in persons with motor-complete paraplegia. *The journal of spinal cord medicine*, 36(4):313–321, 2013.

[29] Hartmut Geyer and Hugh Herr. A muscle-reflex model that encodes principles of legged mechanics produces human walking dynamics and muscle activities. *Neural Systems and Rehabilitation Engineering, IEEE Transactions on*, 18(3):263–273, 2010.

[30] Arvid Guterstam, Valeria I Petkova, and H Henrik Ehrsson. The illusion of owning a third arm. *PloS one*, 6(2):e17208, 2011.

[31] Hermie J Hermens, Bart Freriks, Catherine Disselhorst-Klug, and Günter Rau. Development of recommendations for semg sensors and sensor placement procedures. *Journal of electromyography and Kinesiology*, 10(5):361–374, 2000.

[32] Hugh Herr. Exoskeletons and orthoses: classification, design challenges and future directions. *Journal of neuroengineering and rehabilitation*, 6(1):1, 2009.

[33] Hugh M Herr and Alena M Grabowski. Bionic ankle–foot prosthesis normalizes walking gait for persons with leg amputation. *Proceedings of the Royal Society of London: Biological Sciences*, 279(1728):457–464, 2012.

[34] Masaru Higuchi, Makoto Ogata, Shuta Sato, and Yukio Takeda. Development of a walking assist machine using crutches (composition and basic experiments). *Journal of mechanical science and technology*, 24(1):245–248, 2010.

[35] D.O. Ibanez, F.P. Baquerin, D.Y. Choi, and C.N. Riviere. Performance envelope and physiological tremor in microsurgery. In *Bioengineering Conference, 2006. Proceedings of the IEEE 32nd Annual Northeast*, pages 121 –122, 2006.

[36] Atsushi Iriki, Michio Tanaka, and Yoshiaki Iwamura. Coding of modified body schema during tool use by macaque postcentral neurones. *Neuroreport*, 7(14):2325–2330, 1996.

[37] M. Ison, I. Vujaklija, B. Whitsell, D. Farina, and P. Artemiadis. Simultaneous myoelectric control of a robot arm using muscle synergy-inspired inputs from high-density electrode grids. In *Robotics and Automation (ICRA), 2014 IEEE International Conference on*, May 2015.

[38] Wim GM Janssen, Hans BJ Bussmann, and Henk J Stam. Determinants of the sit-to-stand movement: a review. *Physical therapy*, 82(9):866–879, 2002.

[39] Henrik S Jørgensen, Hirofumi Nakayama, Hans O Raaschou, and Tom S Olsen. Recovery of walking function in stroke patients: the copenhagen stroke study. *Archives of physical medicine and rehabilitation*, 76(1):27–32, 1995.

[40] S. Kajita and K. Tani. Study of dynamic biped locomotion on rugged terrain-derivation and application of the linear inverted pendulum mode. In *Robotics and Automation, 1991. Proceedings., 1991 IEEE International Conference on*, pages 1405–1411 vol.2, 1991.

[41] Avi Karni, Gundela Meyer, Christine Rey-Hipolito, Peter Jezzard, Michelle M Adams, Robert Turner, and Leslie G Ungerleider. The acquisition of skilled motor performance: fast and slow experience-driven changes in primary motor cortex. *Proceedings of the National Academy of Sciences*, 95(3):861–868, 1998.

[42] Hiroaki Kawamoto and Yoshiyuki Sankai. Power assist system hal-3 for gait disorder person. In Klaus Miesenberger, Joachim Klaus, and Wolfgang Zagler, editors, *Computers Helping People with Special Needs*, volume 2398 of *Lecture Notes in Computer Science*, pages 196–203. Springer Berlin Heidelberg, 2002.

[43] H. Kazerooni, J.-L. Racine, Lihua Huang, and R. Steger. On the control of the berkeley lower extremity exoskeleton (bleex). In *Robotics and Automation, 2005. ICRA 2005. Proceedings of the 2005 IEEE International Conference on*, pages 4353–4360, 2005.

[44] Keehoon Kim and JEdward Colgate. Haptic feedback enhances grip force control of semg-controlled prosthetic hands in targeted reinnervation amputees. *Neural Systems and Rehabilitation Engineering, IEEE Transactions on*, 20(6):798–805, 2012.

[45] Kyoungchul Kong and Doyoung Jeon. Design and control of an exoskeleton for the elderly and patients. *Mechatronics, IEEE/ASME Transactions on*, 11(4):428–432, 2006.

[46] John W Krakauer and Pietro Mazzoni. Human sensorimotor learning: adaptation, skill, and beyond. *Current opinion in neurobiology*, 21(4):636–644, 2011.

[47] Todd A Kuiken, Guanglin Li, Blair A Lock, Robert D Lipschutz, Laura A Miller, Kathy A Stubblefield, and Kevin B Englehart. Targeted muscle reinnervation for real-time myoelectric control of multifunction artificial arms. *Jama*, 301(6):619–628, 2009.

[48] James W Lewis. Cortical networks related to human use of tools. *The Neuroscientist*, 12(3):211–231, 2006.

[49] B. Llorens-Bonilla, F. Parietti, and H. Asada. Demonstration-based control of supernumerary robotic limbs. In *Proc. IEEE Int. Conference on Intelligent Robots and Systems*, 2012.

[50] Lenny Lucas, Matthew DiCicco, and Yoky Matsuoka. An emg-controlled hand exoskeleton for natural pinching. *Journal of Robotics and Mechatronics*, 16:482–488, 2004.

[51] Andreas R Luft and Manuel M Buitrago. Stages of motor skill learning. *Molecular neurobiology*, 32(3):205–216, 2005.

[52] Angelo Maravita and Atsushi Iriki. Tools for the body (schema). *Trends in cognitive sciences*, 8(2):79–86, 2004.

[53] Gregory Thomas Mark and Antoni S Gozdz. Apparatus for fiber reinforced additive manufacturing, July 17 2014. US Patent App. 14/333,947.

[54] Lockheed Martin. Relief for the daily grind: Industrial exoskeletons at work. Press Release, November 2014.

[55] Maria M Martins, Cristina P Santos, Anselmo Frizera-Neto, and Ramón Ceres. Assistive mobility devices focusing on smart walkers: Classification and review. *Robotics and Autonomous Systems*, 60(4):548–562, 2012.

[56] J. H. McAuley and C. D. Marsden. Physiological and pathological tremors and rhythmic central motor control. *Brain*, 123(8):1545–1567, 2000.

[57] Luke M Mooney and Hugh M Herr. Biomechanical walking mechanisms underlying the metabolic reduction caused by an autonomous exoskeleton. *Journal of neuroengineering and rehabilitation*, 13(1):1, 2016.

[58] A. Mosisa and S. Hipple. Trends in labor force participation in the united states. *Monthly Labor Review*, 129(10):35–57, 2006.

[59] France Mourey, Thierry Pozzo, Ines Rouhier-Marcer, and JEAN-PIERRE DIDIER. A kinematic comparison between elderly and young subjects standing up from and sitting down in a chair. *Age and ageing*, 27(2):137–146, 1998.

[60] Tobias Nef, Marco Guidali, and Robert Riener. Armin iii–arm therapy exoskeleton with an ergonomic shoulder actuation. *Applied Bionics and Biomechanics*, 6(2):127–142, 2009.

[61] Peter D Neuhaus, Jerryll H Noorden, Travis J Craig, Tecalote Torres, Justin Kirschbaum, and Jerry E Pratt. Design and evaluation of mina: A robotic orthosis for paraplegics. In *Rehabilitation Robotics (ICORR), 2011 IEEE International Conference on*, pages 1–8. IEEE, 2011.

[62] United States Department of Labor Occupational Safety & Health Administration. Safety and health regulations for construction, fall protection, 2013.

[63] Bureau of Labor Statistics. Census of fatal occupational injuries summary. Technical report, US Department of Labor, 2013.

[64] Fausto A Panizzolo, Ignacio Galiana, Alan T Asbeck, Christopher Siviy, Kai Schmidt, Kenneth G Holt, and Conor J Walsh. A biologically-inspired multi-joint soft exosuit that can reduce the energy cost of loaded walking. *Journal of neuroengineering and rehabilitation*, 13(1):1, 2016.

[65] F. Parietti, G. Baud-Bovy, E. Gatti, R. Riener, L. Guzzella, and H. Vallery. Series viscoelastic actuators can match human force perception. *Mechatronics, IEEE/ASME Transactions on*, 16(5):853 –860, oct. 2011.

[66] F. Parietti, K. Chan, and H.H. Asada. Bracing the human body with supernumerary robotic limbs for physical assistance and load reduction. In *Robotics and Automation (ICRA), 2014 IEEE International Conference on*, pages 141–148, May 2014.

[67] F. Parietti, K. C. Chan, B. Hunter, and H.H. Asada. Design and control of supernumerary robotic limbs for balance augmentation. In *Robotics and Automation (ICRA), 2014 IEEE International Conference on*, May 2015.

[68] Federico Parietti and Harry Asada. Dynamic analysis and state estimation for wearable robotic limbs subject to human-induced disturbances. In *Proc. IEEE Int. Conference on Robotics and Automation*, 2013. in press.

[69] Federico Parietti and Harry Asada. Supernumerary robotic limbs for aircraft fuselage assembly: Body stabilization and guidance by bracing. In *Robotics and Automation (ICRA), 2014 IEEE International Conference on*, pages 1176–1183, 2014.

[70] Federico Parietti and Harry Asada. Supernumerary robotic limbs for human body support. *IEEE Transactions on Robotics*, 32(2):301–311, 2016.

[71] Constantine Pavlides, Eizo Miyashita, and Hiroshi Asanuma. Projection from the sensory to the motor cortex is important in learning motor skills in the monkey. *Journal of neurophysiology*, 70(2):733–741, 1993.

[72] Alessandra Pedrocchi, Simona Ferrante, Emilia Ambrosini, Marta Gandolla, Claudia Casellato, Thomas Schauer, Christian Klauer, Javier Pascual, Carmen Vidaurre, Margit Gföhler, et al. *MUNDUS project: MUltimodal Neuroprosthesis for daily Upper limb Support*. Technische Universität Berlin, 2015.

[73] Jacquelin Perry, Judith M Burnfield, and Lydia M Cabico. Gait analysis: normal and pathological function. 1992.

[74] José L Pons et al. Wearable robots: biomechatronic exoskeletons. 2008.

[75] JN Sanes, S Suner, and JP Donoghue. Dynamic organization of primary motor cortex output to target muscles in adult rats i. long-term patterns of reorganization following motor or mixed peripheral nerve lesions. *Experimental Brain Research*, 79(3):479–491, 1990.

[76] S.P.N. Singh and C.N. Riviere. Physiological tremor amplitude during retinal microsurgery. In *Bioengineering Conference, 2002. Proceedings of the IEEE 28th Annual Northeast*, pages 171 –172, 2002.

[77] Jean-Jacques Slotine and Weiping Li. *Applied Nonlinear Control.* Prentice Hall, October 1991.

[78] Jean-Jacques E. Slotine and H. Asada. *Robot Analysis and Control.* John Wiley & Sons, Inc., New York, NY, USA, 1st edition, 1992.

[79] Katherine A Strausser and H Kazerooni. The development and testing of a human machine interface for a mobile medical exoskeleton. In *Intelligent Robots and Systems (IROS), 2011 IEEE/RSJ International Conference on*, pages 4911–4916. IEEE, 2011.

[80] J. F. Veneman, R. Ekkelenkamp, R. Kruidhof, F. C.T. Van Der Helm, and H. Van Der Kooij. A series elastic- and bowden-cable-based actuation system for use as torque actuator in exoskeleton-type robots. *Int. J. Rob. Res.*, 25(3):261–281, March 2006.

[81] P Vieregge, H Stolze, C Klein, and I Heberlein. Gait quantitation in parkinson's diseaseÛlocomotor disability and correlation to clinical rating scales. *Journal of neural transmission*, 104(2-3):237–248, 1997.

[82] Michael Wehner, Brendan Quinlivan, Patrick M Aubin, Ernesto Martinez-Villalpando, Michael Baumann, Leia Stirling, Kenneth Holt, Robert Wood, and Conor Walsh. A lightweight soft exosuit for gait assistance. In *Robotics and Automation (ICRA), 2013 IEEE International Conference on*, pages 3362–3369. IEEE, 2013.

[83] David A Winter. Human balance and posture control during standing and walking. *Gait & posture*, 3(4):193–214, 1995.

[84] David A Winter, Aftab E Patla, Francois Prince, Milad Ishac, and Krystyna Gielo-Perczak. Stiffness control of balance in quiet standing. *Journal of Neurophysiology*, 80(3):1211–1221, 1998.

[85] Adam B Zoss, Hami Kazerooni, and Andrew Chu. Biomechanical design of the berkeley lower extremity exoskeleton (bleex). *Mechatronics, IEEE/ASME Transactions on*, 11(2):128–138, 2006.